



Please pay particular attention to the article on page 3: “**Science on La Silla in the VLT Era**” and to the “**Questionnaire to the ESO Community**” which is distributed with this issue of *The Messenger*

Current Status of ESO

Speech to the Staff at the ESO Garching Headquarters on December 6, 1994

R. GIACCONI, Director General of ESO

The past year saw a number of important developments in and around ESO. Considering all of these together makes me feel confident about the future of this organization and our ability to successfully complete the current major task, the VLT project.

I here summarize the most important issues. It is obvious that with ESO's many simultaneous and quite diverse undertakings, we are stronger in certain areas than in others. While we have done quite well in some, we must try to improve our performance in others.

1. Visiting Committee Report

Until recently, ESO was unique among large astronomy organizations in not having a “Visiting Committee” to evaluate its scientific and technological performance. Immediately after I came to ESO, I therefore established such a Committee with the following distinguished astronomers as members: A. Boksenberg

(Royal Observatories, UK), C. Fransson (Stockholm Observatory, Sweden), K. Freeman (Mt. Stromlo and Siding Spring Observatory, Australia), J. Geiss (Universität Bern, Switzerland), J. Huchra (Harvard Smithsonian Center for Astrophysics, USA), R. Kudritzki (Universitäts-Sternwarte München, Germany), G. Miley (Sterrewacht Leiden, The Netherlands; Chair), G. Monnet (Observatoire de Lyon, France).

Following intense work that included visits to ESO's installations in Europe and Chile and discussions with many staff members, the ESO Visiting Committee has now delivered its preliminary report about the scientific side of ESO. Without going into its many detailed observations and recommendations, it is satisfying to note that it agrees very well with our perceived mission of ESO. Together with the Audit report about the more programmatic side, earlier released by the Team headed by N. Lund, they form an important basis of understanding

ESO's strengths and weaknesses and provide us with a clear road map to improvement.

In particular, the report of the Visiting Committee states that *ESO should provide facilities which will enable European astronomers to carry out outstanding science that can better be done in a global European context than nationally* and that the paramount criterion in determining relative priorities should be that of *scientific excellence*. The Committee finds that several aspects of ESO have been more responsive to scientific priorities in the recent years.

The report furthermore notes that there is a severe shortage of staff both in Garching and at La Silla. An important part concentrates on the ESO staff astronomers, their functional duties and research programmes; without good astronomers it will be impossible to carry through ESO's very diverse services to the scientific communities in the member countries.

The Visiting Committee also discusses many aspects of the VLT project. It is of the opinion, and I fully concur, that a better and clearer tie-in between the VLT project and the scientific requirements is needed for the future. I certainly intend to pursue this goal with great zeal. It also stresses that the number of instruments currently being constructed is insufficient to exploit the VLT adequately.

The Committee attaches great importance to the interferometric capabilities of the VLT and states that *failure to implement the VLTI will diminish the effectiveness of the VLT investment for European science*. Finally, the La Silla Observatory receives considerable attention in the report. While the Committee is generally impressed by the quality and management of the observatory, it does comment on certain shortcomings and makes a number of suggestions for changes.

The work of the Visiting Committee has been extremely useful and this type of survey of ESO will from now on become a permanent feature to be repeated every two years. I moreover intend to stay in contact with the members of the Visiting Committee and to ask for their advice on important matters, for instance in connection with appointments of new staff in senior positions. It is very obvious that ESO needs the best astronomers and that we must take immediate steps to work towards better interaction between our geographically separate locations: in the future, ESO should become *one observatory with two observing sites*. I will mention other actions in response to this report later in this talk.

2. Chile

You are all aware that the future relations between the Republic of Chile and ESO are being discussed at this moment, most notably during the negotiations that will eventually lead to an Interpretative, Supplementary and Amending Agreement between the two.

The main points are concerned with the granting of guaranteed observing time to scientifically meritorious observing programmes proposed by Chilean astronomers, many of which will be in collaboration with astronomers from the ESO member countries, as well as incorporation of elements of Chilean labour legislation into ESO Rules and Regulations for Local Staff.

There is no doubt that both ESO and Chile will gain from this new Agreement, once it has been ratified by the Chilean Parliament and the ESO Council.

3. Council Meeting

The ESO Council met during its regular winter meeting on November 30 and

December 1, 1994. It took a number of decisions of importance for the organization and its staff.

In particular, it confirmed a 1995 budget for ESO at the level of 138 million DM and approved a planning budget for 1996–98 at 141 million DM (at 1995 cost). I note that this represents a 12 per cent increase in the ESO budget at a time when most research programmes in the member countries have difficulties; this ensures that steady progress will continue for the all-important VLT project. Still, Council also requested a 3 million DM reduction on the expenditure side for 1995 as compared to the already very tight proposal of the ESO Executive and it is now up to us to carry this out in the most efficient way. It will not be easy, but I am confident that with the active and positive involvement of all of you, it can be done in an efficient and sensible way.

Council also approved our proposal for staff salaries next year, as well as the current ESO plans for Rules on Transfer of Staff to Chile for the VLT Commissioning.

4. VLT Highlights

The VLT project has been progressing well during the past year. As a very visible demonstration of this, most of you have probably seen the two enormous scale models of the primary mirror cell, now on display in the tent outside the Headquarters building. They provide us with a dramatic impression of the real size of this enormous telescope.

We are at this moment proceeding with negotiations of the contract for this cell, and it appears that, despite some delays with the contract for the secondary mirror, first light of the first unit VLT telescope will only be delayed by a few months. It is now expected to happen at the end of 1997, possibly at the beginning of 1998.

The civil engineering work at Paranal is proceeding at very high speed. There are now twice as many people on the mountain as originally foreseen, working shifts around the clock.

The importance we attach to keeping open the interferometric option for the VLT is underlined by the recent appointment of F. Paresce as VLTI project scientist. There will be a VLTI Symposium in the spring of 1995 and the continued drive towards membership of Australia will have a major impact on this area of the VLT project.

A VLT System Group headed by T. Andersen is being created and we have produced an end-to-end VLT model.

The VLT instrumentation is on schedule and a new Instrumentation Division has been created with G. Monnet as Head. J. Beletic has been appointed Head of a new CCD Group which will

help ESO to catch up in this very important field.

We will get an overview of the future needs for VLT instrumentation when the Vigroux Committee delivers its report at the extraordinary STC Meeting in February 1995. Another Working Group has been set up that will take a close look at which telescopes and instruments will be needed at La Silla in the year 2000. I expect that in close conformity with the main goals of ESO, this organization will then only be responsible for some major instruments there which could not easily be run by individual countries.

One of the major issues now facing us is the elaboration of a Chile Operations Plan which ensures that ESO's future facilities in that country can be optimally exploited in the new century. A provisional document was prepared by D. Baade and J. Crocker. It was presented at the recent meetings of STC and Council, both of which expressed agreement to the general ideas. The plan shows that it will in principle be possible to bring down the costs of operating the VLT, as compared to earlier estimates. The important aspect is that by building all the right features into the operation from the very beginning, there will be no need to make expensive adjustments afterwards.

It is the overall aim to ensure that the best possible science will be done with the VLT. The plan therefore foresees that ESO will become responsible for the scientific quality of the observations, that is, by putting a lot of emphasis on calibration and monitoring and improvement of instrumental performance. This can be done with less staff than originally foreseen and with a significant amount of service observing as the central feature.

I take great personal interest in these matters and look forward to learn the experience with the NTT during the next years when parts of the concepts for the VLT will be tried out.

Also in this connection, we are now taking the necessary steps to set up a VLT Assembly-Verification-Integration (AVI) group.

5. Scientific Activities

J. Bergeron was appointed Associate Director for Science. Regular Faculty Meetings are now taking place with the participation of ESO senior scientific staff. At the same time, the new internal Scientific Policy Committee (SPC) has worked very successfully.

There have been a number of scientific meetings during the past year, including the very successful Workshops on the Use of the VLT in June and Quasar Absorption Lines in November. The comet impact on Jupiter in July provided ESO with an opportunity to interact in a very

positive way with the media and the public. Educational issues were discussed during the joint EU/ESO Workshop on Teaching of Astronomy in Europe's Secondary Schools.

In Chile, the ESO staff astronomers were re-located to the Vitacura office in Santiago. From now on they will work here when they are not at La Silla. This will probably also result in better contacts with their Chilean colleagues.

6. Administrative Matters

Mr. W. Buschmeier took over as Head of Administration and among many other tasks is responsible for the imple-

mentation of the Work Package Structure (WPS); the Management Information System (MIS) is still to come. These changes must be accompanied by a very careful scrutiny of the way ESO spends its money. Although the budget of our organization may seem large, we also have many tasks to carry out. We must set strict priorities and avoid all unnecessary expenses.

7. Basic Themes for 1995

Finally, I state here some of the basic themes for 1995:

- Excellence in science

- Scientific priorities in VLTI, VLT and La Silla operations
- Scientific methodology
- VLT Execution
- VLTI Design and Planning
- La Silla reduction in quantity and improvement in quality
- Shift from development to operations
- Improvement in efficiency
- Better fiscal and management control

We want ESO to be one of the best observatories in the world, if possible the best one. This can be done, but it will not be easy! Let us work together towards this common goal!

Science on La Silla in the VLT Era

J. ANDERSEN, Chairman, ESO-STC

Over the next 6–8 years, the VLT will enter full operation on Paranal. Construction is going ahead full blast on all telescopes and the instruments for UT1 and 2, while instrumentation plans for UT 3–4 are in the definition phase. The recent ESO Workshop on "Science with the VLT" was one of the ways in which ESO is involving its user community in the process of defining the final VLT instrumentation programme.

In the VLT era, the functions and boundary conditions of the La Silla observatory will no doubt see drastic changes, for two main reasons:

1. Many of the highest priority scientific programmes will move to the VLT. Experience shows that new tasks for medium-size telescopes will also appear.

2. In making large investments in our unique new research tool in times of financial hardship, our governments expect, in return, that we trim all ESO operations and optimize the scientific output of our resources.

The VLT project is proceeding vigorously on a credible schedule. Modern management tools are going into place which will allow rational cost/benefit analyses. Thus the time is ripe to prepare specific plans for the long-term future of La Silla.

A New Working Group

The Director General has appointed a small Working Group to address the title subject of this article. Its task is to propose a long-term plan for the equipment and operation of La Silla, consistent with the scientific priorities of the community and with the available resources.

Members of the Working Group are,

from ESO: Jacqueline Bergeron, Associate Director for Science; Jim Crocker, Head of Programme Office; and Jorge Melnick, Head of Operations, La Silla; from the Users Committee: Michel Deneffeld and Hans Schild; and from the STC: Johannes Andersen (Chair) and Sergio Ortolani. The Working Group may co-opt additional members later, but stresses from the outset that one of its most important tasks is to organize the widest possible consultation with the ESO user community.

The first full-day formal meeting was held on October 27. The Working Group set up a schedule for its work, defined its strategy for consulting the community, and identified and structured the main questions to address. Some first recommendations will be needed for the 1996 budget proposal.

A Call to the Community

Clearly, no credible planning can start before the scientific plans and priorities of the user community are known. Hence, the first action of the Working Group is to issue a call to the community for advice, direction and help in our further work, through this article and accompanying questionnaire (also distributed directly by mail).

To avoid misunderstanding we emphasize that, at this time, there is no a priori limit on the number, size or instrumentation of ESO telescopes to be operated on La Silla in the future, nor on the operational costs.

Clearly, the final plan must conform to the realities of our limited resources, but no idea or suggestion should be withheld at this time because rumours sug-

gest that some specific cut has *de facto* been decided already: it has not.

The Key Questions

In order to facilitate a structured discussion, the Working Group has defined a few main programme categories within which needs can be assessed:

Stand-alone programmes for La Silla

Which programmes will continue to be done best (only?) from La Silla?

Preparations for VLT programmes

Which (new) programmes will be needed to prepare VLT projects?

Follow-up of VLT programmes

Which (new) programmes for La Silla will be generated by the VLT?

VLT programme off-loading

Which (new) programmes can be done most efficiently in tandem between the VLT and La Silla?

In all of these types of programme, your scientific needs will translate into requirements for La Silla and its instrumentation. Some of these derived questions are listed below; please consider them, but by no means feel limited to these topics:

- Scientific goals and requirements: Field, limiting magnitude, wavelength range. Are your needs met by present instruments? If not, what are the highest-priority future needs, taking into account facilities elsewhere?

- Wavelength coverage: Are there serious (if perhaps temporary) gaps in

wavelength coverage of the planned VLT instruments?

- For wide-field imaging: Field size, $m_{l,m}$, wavelength, detector type.
- For wide-field spectroscopy: Same questions, plus requirement on sky subtraction (fibres or multi-slits).
- Spatial resolution: What are the needs for tip-tilt corrected images or full adaptive optics?
- Spectral resolution: Where is high-resolution spectroscopy done most efficiently? If on the VLT, is an interim solution needed on La Silla?
- Continuous, long-term monitoring: What is the need for La Silla-size telescopes? Dedicated telescopes run by independent teams?

• Simultaneous observations: What is the need?

Educational aspects of La Silla

As a somewhat separate, but significant issue, is La Silla important in training the new generation of European observational astronomers? If so, how should it be organized?

All Hands on Deck!

This article and the questionnaire was sent in early November 1994 to Institute Directors and individual scientists throughout the ESO Member States. The Working Group strongly encourages the

widest possible distribution to colleagues of all ranks – not least the younger ones who will be the most affected by the result.

The Working Group will consider all replies with equal interest and attention. Our draft conclusions and proposals will be discussed with the community in several iterations, possibly including some form of Workshop.

Please send your reply to the ESO Headquarters in Garching (*Attention: La Silla 2000 W.G., c/o S. Teupke*) **before February 1, 1995.**

ESO's planning must continue. In your own interest, take this opportunity to help us make the best of it!

TELESCOPES AND INSTRUMENTATION

N-Band Long-Slit Grism Spectroscopy with TIMMI at the 3.6-m Telescope

H.U. KÄUFL, ESO-Garching

Careful readers of *The Messenger* may remember that the acronym TIMMI stands for Thermal Infrared Multimode Instrument. So far, however, TIMMI could be offered as a monomode instrument (i.e. imaging) only. This has now changed and TIMMI has become a true multimode instrument, combining imaging and longslit spectroscopy with $\frac{\lambda}{\Delta\lambda} \approx 200$ for the $10\ \mu\text{m}$ atmospheric window. The long-slit spectroscopic mode is now implemented utilizing grisms. Rather encouraging tests and scientific exposures on astronomical objects have been possible. The grisms in TIMMI have been manufactured utilizing anisotropic etching of mono-crystalline silicon which has a refractive index of ≈ 3.4 . While grisms are widely used in optical and near infrared instrumentation, TIMMI is probably the first astronomical instrument for the $10\ \mu\text{m}$ atmospheric window ever using grisms manufactured from such high-index materials.

1. Short Description of TIMMI¹

Like all infrared instruments TIMMI is a cryogenic instrument. It is mounted in-

side a Solid Nitrogen/Liquid Helium cryostat. Its optical principle is best described as an 'infrared EFOSC'. For technical details see e.g. Käufl et al. 1992 or 1994. The telescope focal plane is located inside of the dewar. In the focal plane there is a mechanism to exchange the cryogenic field mask with a cryogenic slit

assembly (slit-width ≈ 0.9 arcsec). Behind an $f = 103$ mm collimator there is a 3.6 mm \varnothing pupil stop. A filter wheel is located behind that pupil stop in the collimated beam. The grisms are mounted to the filter wheel. This is followed by a lens wheel. All three mechanical functions of TIMMI are operated remotely under com-



Figure 1: *The rare but essential ingredients are shown. The three grisms are mounted in one fixture to the filter wheel. For each grism the order sorting filter, the base prism and the silicon wafer carrying the diffractive structure had to be mounted in a space of less than $1\ \text{cm}^3$. The mount needed to be designed compatible with operation at 60 K. The silicon wafer is mounted in direct optical contact to the prism, and great care was required during assembly to avoid contamination of the optical surfaces. It was also required to carefully adjust the orientation of the grooves parallel to the apex of the prism.*

¹The TIMMI project started in July 1990 when ESO signed a contract with the Service d'Astrophysique of the Commissariat à l'Energie Atomique (Principal Investigator: P.O. Lagage). The instrument was then built by the SAP according to ESO's specification in a period of two years.

puter control. TIMMI is mounted at ESO's 3.6-m telescope in the $f/35$ configuration. The camera features a 64×64 element Gallium doped Silicon photo-conductor array bonded to a silicon Direct Voltage Read-out (DVR) circuit². Various magnifications can be chosen (at present 0.3 arcsec/pix, 0.46 arcsec/pix and 0.6 arcsec/pix). For the long-slit spectroscopic mode the 0.6 arcsec/pix scale is used which allows for a useful slit length of TIMMI on the sky of ≈ 35 arcsec.

Because of the strong background radiation emitted by atmosphere and telescope in this part of the spectrum the observations need to be done in chopping and nodding mode.

While TIMMI provides new and fairly unique observational possibilities for the ESO users community, it was also supposed to be a test-bed to gain experience for similar instrumentation at the VLT.

2. The Silicon/Germanium Grisms³

The standard technology to produce grisms for visible and near infrared applications is to replicate ruled gratings with resins to the back of glass prisms. Unfortunately, this technology cannot be applied to the spectral domain relevant for TIMMI because of the strong internal absorption of these resins at $\lambda \approx 10 \mu\text{m}$. Moreover, for a given diameter of the collimated beam in a spectrograph, a grism made from material with refractive indices n of order 1.5 has roughly a factor of 4 less dispersive power than a standard reflection grating.

For a given collimator size the dispersion of grisms scales with $(n-1)$. When using high-index infrared optical materials such as Silicon ($n \approx 3.4$) or Germanium ($n \approx 3.9$ at $T = 77\text{K}$) the dispersion is typically 5–6 times that of a glass/resin grism. For a given collimator size a Germanium grism then also has $\approx 50\%$ higher dispersion than a normal reflection grating. This is extremely important and beneficial for infrared instruments since it can allow to reduce the size of the cryostats typically by 33% linearly or by 70% in volume and hence

²This detector has been manufactured by Leti/LIR, Centre d'Etudes Nucléaires de Grenoble, France.

³For readers who are not entirely familiar with grisms: a grism is a transmission grating mounted to the back of a prism. Light, when passing the transmission grating, will be deflected according to its wavelength. The prism bends the light deflected by the grating back parallel to the optical axis of the incoming beam. In this way the device works like e.g. a prism of the Amici type. Inserted into a parallel beam light for a given centre-wavelength passes without deviation whereas light at other wavelengths will leave the device tilted with respect to the optical axis.

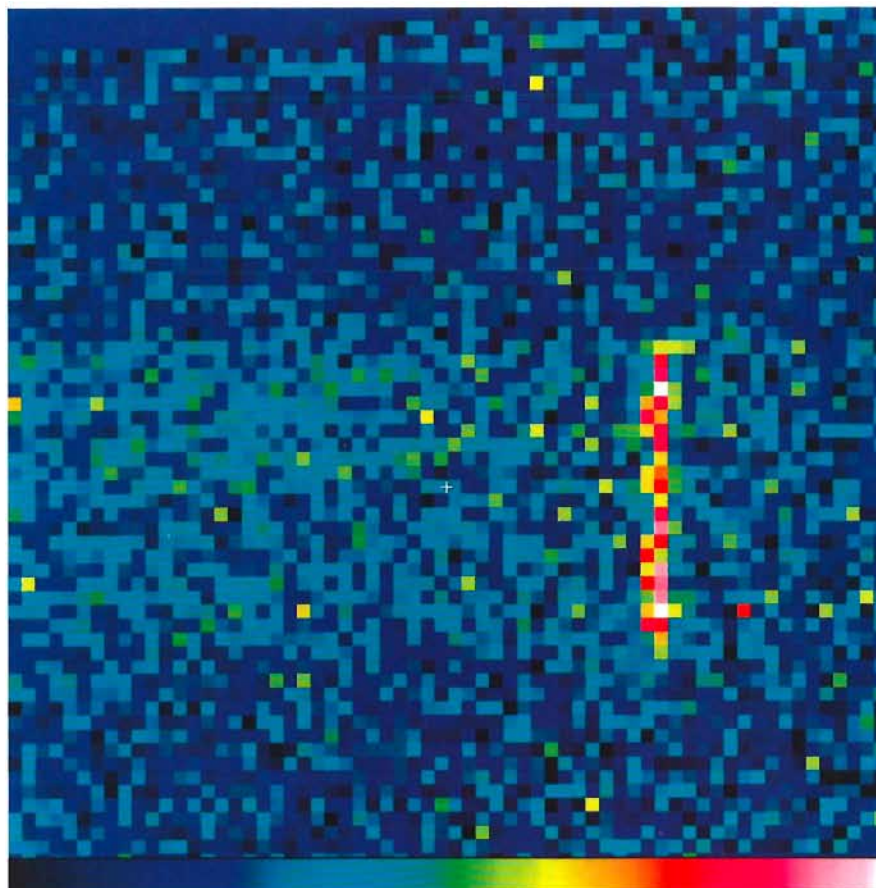


Figure 2: This shows the long slit spectrum obtained for IC 418 after 1 hour of integration. The bright emission of [Ne III] at $\lambda = 12.8 \mu\text{m}$ of the ionized gas as well as the thermal continuum radiation of the dust can clearly be seen. North is up, increasing λ to the right. The scale along the slit is 0.6 arcsec per pixel.

mass with respect to normal spectrographs.

Grisms are an extremely convenient and elegant way to convert a camera into a long slit spectrograph. Since the centre (i.e. zero deviation) wavelength is determined to first order only by the geometry of the grism itself but not by its orientation with respect to the optical axis, such a spectrograph is intrinsically very stable and rather simple from a mechanical point of view. There is no need for the delicate and complicated high-precision grating mounts (n.b. working in vacuum at 60–80 K) required in normal infrared spectrographs. This, however, also implies that grisms cannot be tuned effectively. The number of spectral elements (and hence the spectral resolution) a grism spectrograph can provide is therefore ultimately limited by the number of pixels of the camera detector in dispersion direction times the number of grisms one can afford on the exchange mechanism.

Nevertheless, all advantages described above will remain purely hypothetical unless there is a way of manufacturing these devices. In spite of major efforts which started in 1991, ESO has not been able to procure suitable

grisms from a commercial source. Standard grating ruling techniques with a diamond stylus are incompatible with the relatively large groove spacing required (of the order of $10 \mu\text{m}$) and the material properties of Germanium and Silicon (both are crystalline materials with diamond like structure). ESO therefore concluded a contract with the Fraunhofer Gesellschaft (Institut für Festkörpertechnologie, München) to produce such gratings from monocrystalline Germanium or Silicon wafers. The manufacturing of small silicon gratings is rather straightforward since it is based on standard techniques used for solid-state engineering. For a description of the underlying concept and other applications of this technology see e.g. Wiedemann et al., 1993. A similar process for Germanium, however, needed to be developed from scratch. This process is now available and can be used for second generation devices for TIMMI and all other upcoming projects in ESO, be it VLT or La Silla instrumentation.

3. First Observational Results

The grisms were mounted in TIMMI in May 1994 (Fig. 1). Special test time was

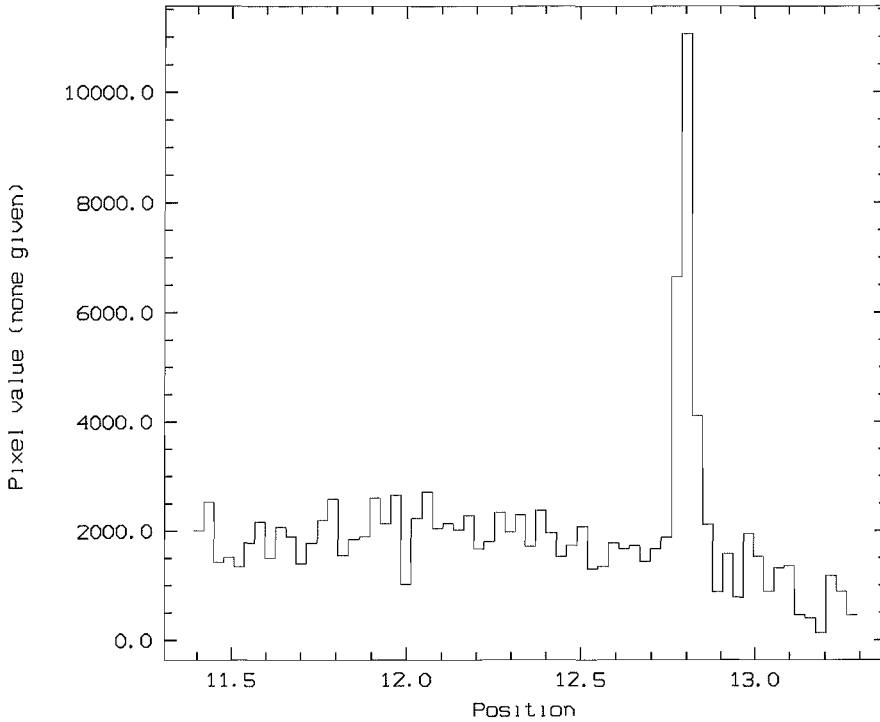


Figure 3: This is a projection of the spectrum shown in Figure 2 on the wavelength axis. As the emission of [NeIII] at $\lambda = 12.8 \mu\text{m}$ is quasi monochromatic, this line shows the instrumental profile. The spectrum is not yet corrected for atmospheric absorption or instrumental efficiency. The noise on the right side of the spectrum is caused by absorption of atmospheric CO_2 which sets the red edge of the $10 \mu\text{m}$ window. What looks like noise of the continuum left of the line are most likely features created by other infrared active atmospheric components. It needs to be demonstrated in the future by further processing of the data how well such structures can be reduced by observing reference stars.

allocated to assess the astronomical performance. This first test, however, was only marginally successful. The instrumental profile could be measured and was found to correspond exactly to the theoretical expectations. The astronomical tests, however, were severely affected by mechanical problems in TIMMI with the slit assembly. Also a major fraction of observation time was lost due to maintenance activities at the telescope and bad weather.

Most of the mechanical problems in TIMMI were resolved before the next scheduled run of TIMMI in November 1994. The grism mode was then tested in the setup night November 11–12. When observing stars it was found that in spite of the rather narrow slit (0.9 arcsec) typically 50–80% of the light reaches the detector. This depends obviously somewhat on the seeing which was between 0.6–2 arcsec as reported by the DIMM (ESO's on-site on-line seeing detector). Figure 2 shows a long-slit spectrum of IC418 covering the range from $11.5 \mu\text{m}$ to the atmospheric cut-off at $13.3 \mu\text{m}$. From these data it will e.g. be possible to get the ratio of the [NeIII] line at $12.8 \mu\text{m}$ to the thermal dust continuum along the slit with very high quality. This will allow for new insights into the excitation conditions of this dusty low excitation planetary nebula.

The grism mode was immediately used for the observing programme in the following night (*Infrared imaging of warm dust in starburst galaxies and AGNs*) to record a long slit spectrum of NGC 253. For this observation the position angle of the slit was aligned with the major axis of the galaxy by rotating TIMMI with the Cassegrain adaptor rotator.

4. Technical Data of Spectroscopy Mode

A summary of technical data of the spectroscopy mode is given in Table 1.

TABLE 1. Summary of Technical Data of Spectroscopy Mode

Spectral resolution (2 pixel sampling):	$\frac{\lambda}{\Delta\lambda} \approx 200$
Slit width (fixed):	0.9 arcsec
Slit orientation:	nominally north–south (can be changed ± 90 deg)
Slit viewing:	with TIMMI in imaging mode through slit
Tracking of objects:	with TV camera in f-35 adaptor either with optical light from the object itself (through dichroic) or with field stars
Wavelength range:	
Grism 1	8.0–9.15 μm
Grism 2	9.6–11.0 μm (not yet operational)
Grism 3	11.5–13.3 μm
The gratings operate in first order. Order sorting is done with a long-pass filter. The period of the grooves is 11.9805, 10.0551 and 8.4505 μm . The blaze angle is approximately 23 degrees.	

From the observations of IC418 the sensitivity of the spectroscopic mode can be provisionally estimated. A S/N of ≈ 10 can be expected in 1h total observing time for the [NeIII] line for $0.6 \times 10^{-14} \frac{W}{\text{m}^2 \text{arcsec}^2}$. For a continuum source a S/N of 10 can be expected for a source of 400–800 mJy/arcsec² (≈ 4.5 mag) for 1 h total observing time.

5. Conclusion and Outlook

The first results obtained with the long-slit spectroscopy mode of TIMMI are extremely encouraging. There is certainly a great variety of astronomical programmes which will benefit from the spectroscopy mode as it is implemented now. Usage of the mode is hence strongly encouraged. Nevertheless, it is also clear that a lot of improvements are possible and desirable.

In the near future a new set of gratings made from Germanium will become available. These devices can then be much better antireflection coated than the present devices in TIMMI. An increase in transmission by 30% can be expected. These gratings will then also be chosen in such a way that the entire $10 \mu\text{m}$ window is covered with some overlap. In the tests it was also obvious, that the camera shows some internal radiation background. Finding ways to reduce this background will further enhance the sensitivity of this new mode of TIMMI.

Acknowledgements

The support of all staff of the ESO infrared group in Garching and La Silla was essential to make this project successful. Specifically, however, these gratings would never have materialized without the delicate mechanical design made by A. Silber and without G. Wiedemann who brought the idea for the manufacturing process to ESO. P. van der Werf provided valuable help during the astro-

nomical tests. The author also appreciates the fruitful and pleasant collaboration with the *Fraunhofer Institut für Festkörpertechnologie*

References

- H.U. Käufel et al. 1992, *The Messenger* **70**, 67.
H.U. Käufel et al. 1994, *Infrared Phys. Technol.* **35**, 203.

G. Wiedemann, D.E. Jennings; 1993, *Applied Optics* **32**, 1176.



With this periodically compiled collection of short notes, the NTT Team intends to keep the community informed about changes in performance, configuration, and operation of the NTT and its subsystems.

EMMI and SUSI Receive Additional Attention

The NTT Team is slowly reaching its full staff complement. On September 19, Albert Zijlstra took up his duties as EMMI/SUSI instrument scientist. He will be in charge of all aspects which can be handled from Garching. A primary task will be the design and testing of standard calibration and reduction procedures for these two instruments. Besides various other assignments, he will also answer user inquiries about EMMI and SUSI (please e-mail them to ntt@eso.org) and he will organize the support for remote NTT observers. Having been in Garching for two years as a postdoctoral fellow, Albert is already well familiar with the environment of his new job.

Image Quality

The dynamical range of this subject is currently unusually extreme. On the one hand, several observers succeeded in securing images with an FWHM of 0.5 arcsec or even better (cf. *The Messenger* No. **76**, p. 21). In many of these excellent nights, the effective image quality obtained with the NTT has been slightly better than the seeing measured with DIMM, the Differential Image Motion Monitor.

On the other hand, NTT images are still often plagued by elongations. Some recent extreme cases could be quickly identified with a hardware failure of the guideprobe control. But some weaker aberrations continue to show up. Using the NTT's intrinsic image analysis capabilities, it could be shown that the zenith distance dependence of astigmatism has increased quite significantly since the commissioning. The follow-up work now concentrates on the lateral support of the primary mirror (the problem might be with the lateral support itself or due to imperfect centring of M1 in its cell).

We are grateful to Dr. S. Ortolani for granting permission to technically eval-

uate the sequence of excellent images which he obtained in May and to Dr. R. Falomo who, as a visitor to the Science Division in Garching, analysed them and several other datasets.

M1 Actuators Checked

As part of a systematic checkout of the active optics system, the currents of all 78 actuators of the M1 radial support system were measured and logged. A number of them were found to be far above the average and, in fact, out of specification, due to increased mechanical friction. These actuators were overhauled one by one in the mechanics workshop at La Silla.

TCS Computer Upgraded

The computer running the Telescope Control System (TCS) has for much of the time been working at a level of 50% or more of its capacity. In a real-time application this is dangerously high and has on a small number of occasions substantially increased the response time to TCS commands even in the case of relatively minor malfunctions of some components connected to the NTT Local Area Network. For this reason, the CPU has with the help of the HP Computer Group at La Silla been upgraded from an HP A900 to an A990 model which more than doubles the safety margin.

Slip Ring Replaced

During the technical maintenance period in August, the slip ring which is the central link for communications, including the time signal from the atomic clock, between the NTT and the outside world, was replaced. This action had become very critical because rapidly progressive corrosion had already paralysed some of the data channels. The reason had been the dripping of condensing water from the pipe through which the cooling liquid

of the air conditioning system circulates. The slip ring was fully re-designed; the manufacture of spare parts required significant help from the mechanics workshop at La Silla. At the time of the installation, which went very smoothly, the new slip ring was also properly shielded against condensation.

Instrument Rotators

The rotation of the rotator on side B (EMMI) through 360 degrees in May continues to have the effect which had been hoped for. At telescope positions where the speed of rotation of the instrument rotators changes sign, the torque no longer increases by so much that the motor can hardly, or even not at all, overcome it. However, the same measure taken on side A has not brought about any perceptible improvement. Meanwhile, F. Franza and M. Ziebell have contacted the Technical University in Munich for advice where the problem has met much interest.

By removing a so-called watch dog from the interlock chain of the control system on side A (IRSPEC), the difference in frequency between sides A and B of sudden stops of the power amplifier (a problem completely independent of the one above) could be removed. The search for the origin of the remaining failures continues. But their intermittent origin makes this a difficult task.

Additional Field Tests of New Control Software

The preparation of the new control system proceeds closely along the lines of the NTT Upgrade Plan. The field test of Work Component No. 3 was executed in October. Its objective was the control of the secondary and tertiary mirror. With the help of the Electronics Group at La Silla an adapter board had been developed to map the signals between the present and the future system so

that the changeover could be achieved very quickly. The goals of the test were achieved, and some dark time could even be used for further astronomical and optical tests of the telescope. The latter confirmed that the new control system also satisfies all quantitative requirements.

The M2/M3 application software includes position servo loops similar to the control of the telescope main axis. The experience gained during the development and the field test is becoming very valuable for the design of the VLT ALT/AZ software. In general, the NTT experiences are receiving more and more attention now when the detailed design of application programmes within the VLT Telescope Control Software is starting.

Increased Robustness of CCD Data Acquisition

In the operations log it was noted that in about 1% of all CCD readouts, the VME node concerned would time out during the transfer of the data file to the control computer. Since it was suspected that the reason is a bug in the OS-9 operating system of the VME (which would be out of reach for ESO to correct), a workaround was installed which consists of repeating the file transfer until it succeeds. This simple solution has eliminated the problem. We are grateful to A. Longinotti and P. Sinclair for their joint efforts in this matter.

New Graphical User Interface for EMMI

The software group at La Silla is responsible for developing the new control software for EMMI which will be installed together with all the rest of the new VLT compatible control system for the NTT. For the design of the graphical user in-

terface (GUI), R. Schmutzer came for an extended visit to Garching where a small group of astronomers in close interaction with him provided the user requirements. The result offers a maximum of, partly user configurable, functionality on a minimum of screen space without compromising clarity. The VLT Software Group will probably make the code available to VLT instrument consortia in order to inspire a common look and feel of the GUI's of VLT instruments.

IRSPEC

F. Gutiérrez has completed his work to enable the automatic transfer of data files to the workstation for on-line analysis with the IRSPEC package of MIDAS. After partial adaptation of the set of FITS keywords, archiving of the observations will begin (similar to what for some years now has been the practice for EMMI and SUSI).

Check Lists for Telescope Operations

We are trying to steadily improve the reliability of the NTT by upgrading our operational standards. Recent examples are the extensive check lists which the night assistants have compiled. In the afternoon, the night assistant uses these lists to record all steps to be taken to prepare the telescope for the night. This systematic check-out of various subsystems may in some cases conflict with the observer's need to calibrate the instruments. Observers have the possibility to request that the startup procedure be abbreviated. However, by doing so they also accept an increased risk of discovering a problem only after scientific observations have started.

Similar procedures are followed for the

shutdown of the telescope after the end of the observations.

MIDAS Observing Batches

The MIDAS procedures which are essential for a number of on-line operations (e.g. telescope and instrument focussing, target acquisition), have with the help of C. Levín and the MIDAS Group in Garching been included in the software configuration control scheme used also for MIDAS in general. Before every new release of MIDAS, the master-copy of the procedures will be thoroughly tested and the results compared with reference data.

Together with other colleagues at La Silla, a prioritized list with requests for enhancements of these procedures has been submitted to the MIDAS group. A number of minor improvements are expected to be implemented already in the first quarter of 1995.

Higher Throughput Expected for Remote Observers

First tests have been performed with the new roof-to-roof communication link between La Silla and Garching which has a bandwidth of 2 Mbit/sec. Early in 1995, this link will replace the 0.064 Mbit/s tie line which is currently used for observations with the NTT under remote control from Garching. This will enormously improve the throughput of the system. Especially the transfer of data files will be accelerated by nearly an order of magnitude so that sending a 2k×2k to Garching will take about 1.5–2.5 minutes. However, file transfer may for many applications no longer be needed since the display in Garching of a 1k×1k picture kept on the disk at the NTT will be much faster still.

Astrophysics on Its Shortest Timescales

D. DRAVINS, Lund Observatory, Sweden

The VLT will permit enormously more sensitive searches for high-speed phenomena in astrophysics, such as those expected from instabilities in accretion onto compact objects, or in the fine structure of photon emission. On [sub]millisecond timescales, light curves are of little use, and measurements have to be of power spectra or other statistical functions, which increase with the light collected to a power of 2 or more, making the gains very much greater than for ordinary photometry or spectroscopy.

High-Speed Astrophysics

The frontiers of astrophysics have expanded through observational breakthroughs. The Universe has turned out to be more enigmatic than even the creative fantasy of astronomers had been able to predict. It is worth recalling that many of today's 'ordinary' topics such as quasars or stellar coronae are results of discoveries enabled by improvements in technology. This mode of advance is different from the situation in e.g. particle physics, where it is often possible to make predictions of novel phenomena, and then to construct experimental apparatus to verify some specific theory. In astronomy, the discovery of quasi-periodic oscillations in accretion disks or of millisecond pulsars was not the result of theoretical predictions, but rather the inescapable revelation once the sensitivity in the relevant parameter space had been sufficiently enhanced. In the past, one major thrust in expanding the parameter envelope of astrophysics was the addition of new wavelength regions, in particular through space missions. Now, that most regions are accessible, the thrusts are moving toward other domains, such as higher spatial and temporal resolution. This article is concerned with the latter of these.

High-speed astrophysics, entering the previously unexplored domains of milli-, micro-, and nanosecond variability, has the goal to discover and explore the possible very rapid variability in astronomical objects. One aim will be to examine radiation from accretion systems around compact objects in the Galaxy where, in some cases, variability is already known to exist on timescales down to milliseconds. Highly energetic events occur in such gas flows onto white dwarfs, neutron stars or presumed black holes. The environments of such objects are promising laboratories to search for very rapid phenomena: the geometrical extent can be very small, the energy density very high, the magnetic fields enor-

mous, and a series of phenomena, ranging from magneto-hydrodynamic turbulence to stimulated synchrotron radiation might well occur. Some processes may occur over scales of only kilometers or less, and there is no immediate hope for their spatial imaging. Insights can instead be gained through studies of their small-scale instabilities, such as hydrodynamic oscillations or magneto-hydrodynamic flares. Phenomena which might be encountered on timescales of seconds, milli-, or even microseconds, include:

- Plasma instabilities and fine structure in accretion flows onto white dwarfs and neutron stars
- Small-scale [magneto-]hydrodynamic instabilities in accretion disks around compact objects
 - Radial oscillations in white dwarfs ($\approx 100\text{--}1000$ ms), and non-radial ones in neutron stars (≤ 100 μs)
 - Optical emission from millisecond pulsars (≤ 10 ms)
 - Fine structure in the emission ('photon showers') from pulsars and other compact objects
 - Photo-hydrodynamic turbulence ('photon bubbles') in extremely luminous stars
 - Stimulated emission from magnetic objects ('cosmic free-electron laser')
 - Non-equilibrium photon statistics (non-Bose-Einstein distributions) in sources far from thermodynamic equilibrium.

Parameter Domains of Astrophysics

The whole science of astronomy can be subdivided into parameter domains with respect to electromagnetic wavelength, and the timescale of study. Classical astronomy, for example, was largely confined to wavelengths accessible from the ground, and timescales between perhaps 0.1 seconds and 10 years.

Advantages of observing in the optical

Rapid astrophysical events are generally expected in accretion processes near compact objects such as white dwarfs, neutron stars or presumed black holes. A number of such sources have previously been studied in the subsecond and millisecond ranges, both in X-rays and in the optical (e.g. Motch *et al.* 1982; Beskin *et al.* 1994).

There are quasi-periodic oscillations, flashes, pulsars, and other phenomena. For best detection and visibility, X-rays could appear to be most attractive, since they often originate in high-temperature regions quite close to the compact object.

Nevertheless, the optical region may in practice be the best for the detailed study of the most rapid phenomena. The reason is that the number of photons that can be detected per second (and especially per millisecond!) is often much greater from the optical parts of the sources (as observed with large telescopes), than that from their X-ray parts, observed with current space instruments. Foreseeable satellites will not be able to collect more than typically a thousand X-ray photons per second, even from quite bright objects (Bradt *et al.* 1990). While this will be adequate to explore many exciting phenomena, it is probably not adequate in searches for very rapid fluctuations.

In contrast, optical light curves of some accretion sources showing periodicity on the scale of seconds can be quite prominent already when recorded with telescopes in the 1.5-m class (Larsson 1985; Imamura *et al.* 1990). Using an 8-metre telescope, and an instrumental efficiency improved by a factor 3, implies some 100 times more photons collected. Detailed light curves could then be seen if their periodicity was merely tens of milliseconds (with count rates on the order of a million photons per second).

Another advantage of the optical is the feasibility to ultimately detect quantum

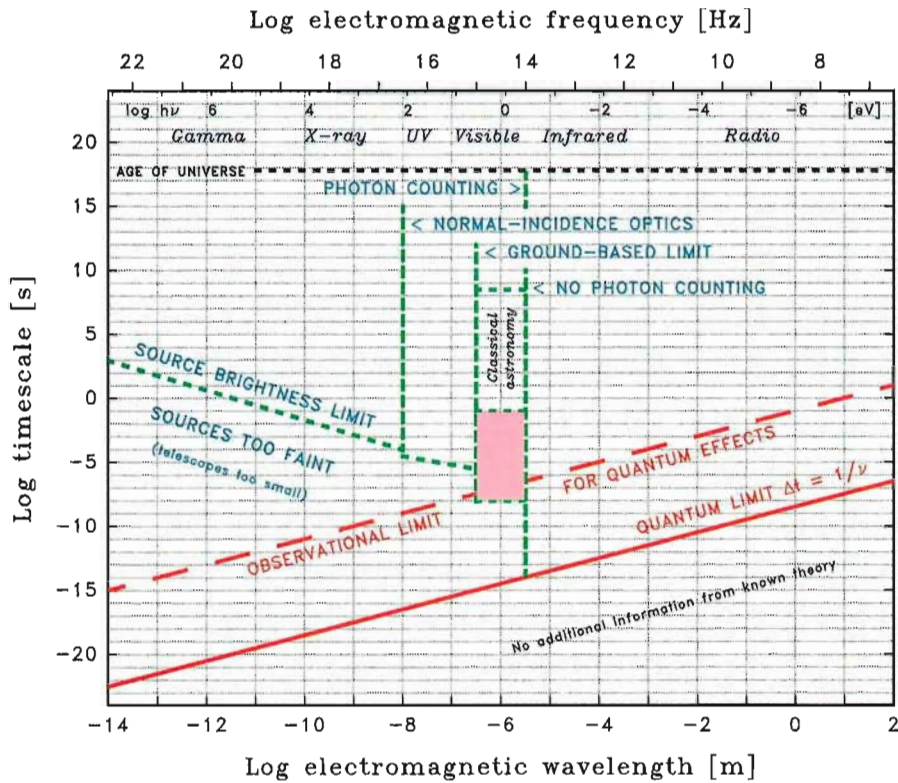


Figure 1: Parameter domains of astrophysics, subdividing electromagnetic radiation with respect to timescale of study, and the wavelength. This diagram (covering some 500 square decades in parameter space) encompasses all of astrophysics, save neutrino, gravitational, cosmic-ray, and in-situ studies. All regions are not yet accessible to observation, in particular due to insufficient observable photon fluxes for high-energy radiation. The optical high-speed domain is marked in pink.

phenomena. At present, these seem unreachable for X-rays, due to their much higher electromagnetic frequencies (Figure 1). Some quantum effects are easier

to observe in radio (e.g. the bunching of photons appears as 'wave noise'), but a limit is set by the difficulties of photon counting at wavelengths beyond the in-

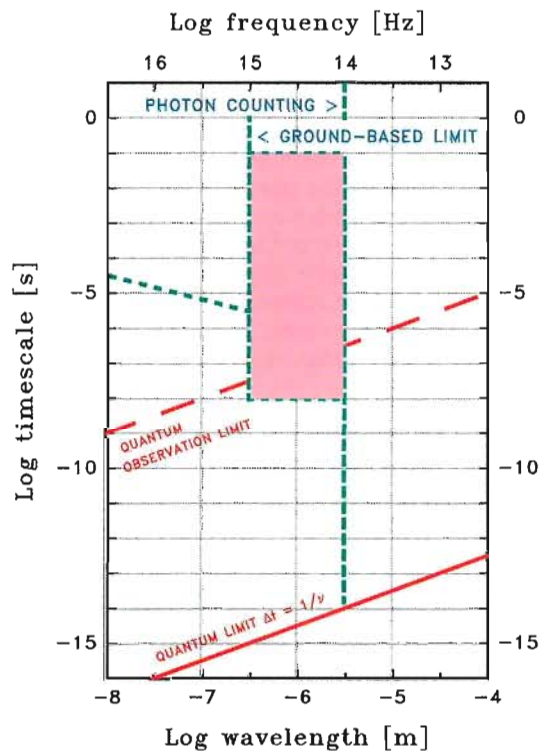


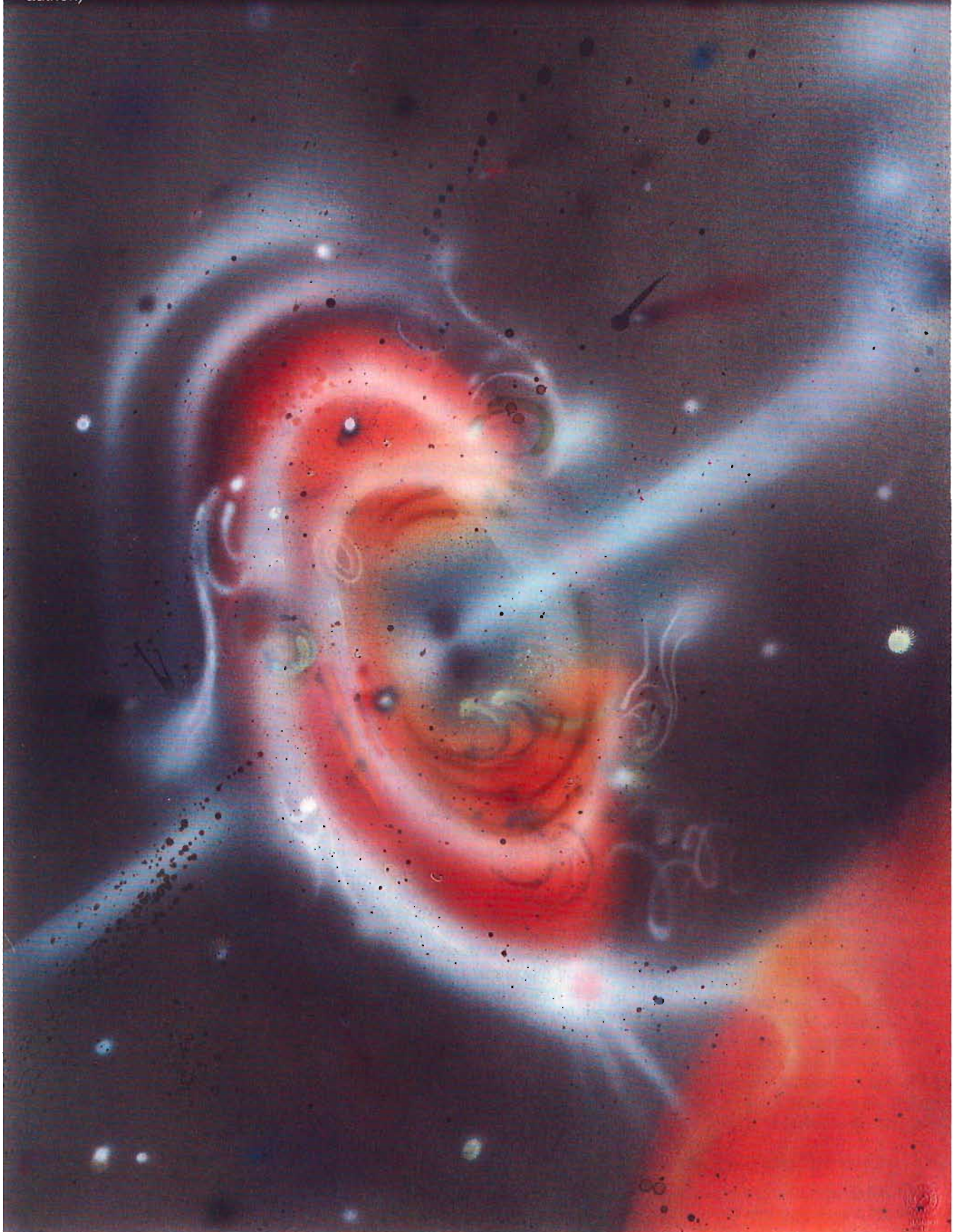
Figure 2: A subset of Figure 1, showing a region around the optical, with expected timescales for various astrophysical processes marked.

frared. While this does not hinder studies of rapid variability as such, it does preclude full studies of quantum effects in radiation.

Accretion Physics for High-Speed Studies

What novel phenomena can we expect to detect in accretion processes? An artist's vision, combining established knowledge with predicted phenomena unfolds in the painting of Figure 3. In a close binary system, matter is escaping from the dynamic and unstable outer atmosphere of an evolved red giant and impinging into an accretion disk surrounding a black hole. (For a general review of phenomena in such systems, see e.g. Livio, 1994.) Here, the accretion flow is neither smooth, nor regular. It is turbulent, and eddies can be seen on many different scales (Meglicki *et al.* 1993). The disk is asymmetric (perhaps reflecting the time history of matter flows from the giant star; Kaitchuck *et al.* 1994; Lanzafame *et al.* 1993; Marsh *et al.* 1994; Whitehurst 1994); the accretion flow is spiral shocked (Heemskerck 1994) and warped perpendicular to its main plane (perhaps due to tidal torques or differential precession; Iping & Peterson 1990). A well-collimated jet is ejected from the central portions, but after some distance it becomes unstable (due to its internal helical magnetic field?) and disintegrates after suffering a supersonic collision with the surrounding circumstellar medium. At certain distances from the centre, hydrodynamic instabilities appear as various types of waves (Chen & Taam 1992; Honma *et al.* 1992; Wallinder 1991), possibly seen by a distant observer as quasi-periodic oscillations. The angular momentum of some of the inflowing matter conspires with moving hydrodynamic shocks to form a three-dimensional structure above and around the disk (Hawley & Smarr 1986). Some of these 'walls' are very thin, their thickness perhaps reflecting electric current sheets. Differential gas motions inside and around the accretion disk feed a dynamo which generates a chaotic magnetic field on many different spatial scales (Stone & Norman 1994; Torkelson & Brandenburg 1994), whose energy is released in short and energetic flares of magnetic reconnection, accompanied by local mass ejections and high-energy radiation. Some magnetic areas are cooler than their local surroundings ('spots'; Bao 1992;), while others dissipate with magnetic heating and appear hotter (Horne & Saar 1991). Such magnetic processes also contribute to sustaining a hot chromosphere and corona surrounding the disk (Mineshige & Wood 1990). At the very centre, a glimpse of

Figure 3: Artist's vision of accretion processes in a close binary system, where matter is escaping from an evolved red giant star onto an accretion disk surrounding a black hole. This illustrates the very great complexity that may be expected in accretion flows around compact objects: numerous hydrodynamic instabilities interfere with the dynamo generation of chaotic magnetic fields, with relativistic effects visible near the centre. While there is no hope to obtain any detailed images of these phenomena in the near future, such small-scale physics of accretion processes can nevertheless be studied from analyses of rapid temporal fluctuations in their radiation. (Artwork by Catrina Liljegren, Bild & Form, Lund; copyright by the author.)



processes very near the black hole can be seen: the appearance is asymmetric because the flux (and wavelength) of light is altered by both the gravitational field and by the Doppler effect in the rotating gas (the side approaching the observer is brighter; Fukue & Yokoyama 1988). Further, relativistic ray-bending permits us to view also the 'back' side of the central region. All this is accompanied by infalling planetisimals and crashing comets, possibly remnants of a former planetary system (Pineault & Landry 1994), local hydromagnetic instabilities seen as vortices in the gas streams ('tornados'; Abramowicz *et al.* 1992), gas ejections collimated by local magnetic fields, and many other small-scale instability phenomena (Mineshige & Kusunose 1993). On larger scales, the whole disk is undergoing acoustic oscillations (Nowak & Wagoner 1992).

How much could be reality and what is fantasy? Of course, nobody *knows* exactly what an accretion disk looks like (and, arguably, none has ever been *directly* observed). However, all the phenomena depicted in Figure 3 were inspired by predictions in the literature. Some of the processes hinted at occur over very small dimensions, and it will not be possible to image them with any presently foreseen interferometer (although some features could be made visible through Doppler imaging or similar techniques). In order to learn more, we are driven toward high time resolution. Even if there is no [immediate] hope for the spatial imaging, signatures of many events may be observable in the time domain, on timescales of seconds, milli-, or even microseconds. A resolution of $1 \mu\text{s}$ translates to a light travel distance (and thus 'resolution' along the line of sight) of 300 metres, irrespective of distance to the source.

How Rapid A Variability Can Be Detected?

Increasing the temporal resolution to microseconds, one should encounter successively more rapid events, on timescales such as those expected for magnetic instabilities in accretion systems, or for non-radial oscillations in neutron stars. However, there do not yet appear to exist any predicted *macroscopic* processes in the nanosecond domain. Such resolutions, however, lead into the *microscopic* realm of quantum optics, and the quantum-mechanical statistics of photon counts. To understand what information they carry, we have to examine the physical properties of light.

Nanoseconds and quantum optics

Classical physics merges all radiation of a certain wavelength into the quantity

'intensity'. When instead treating radiation as a three-dimensional *photon gas*, other effects also become significant, e.g. higher-order coherence and the temporal correlation between photons. The best known non-classical property of light is the *bunching of photons*, first measured by Hanbury Brown and Twiss in those experiments that led to the astronomical intensity interferometer, used to measure stellar sizes (Hanbury Brown 1974). Different physical processes in the generation of light may cause quantum-statistical differences (different amounts of photon bunching in time) between light with otherwise identical spectrum, polarization, intensity, etc., and studies of such non-classical properties of light are actively pursued in laboratory optics.

Such quantum correlation effects are fully developed over timescales equal to the inverse bandwidth of light. For example, the use of a 1 nm bandpass optical filter gives a frequency bandwidth of $\simeq 10^{12}$ Hz, and the effects are then fully developed on timescales of $\simeq 10^{-12}$ seconds. Instrumentation with continuous data processing facilities of such resolutions is not yet available, but it is possible to detect these effects, albeit with a decreased amplitude, also over more manageable nanosecond intervals.

Beyond Imaging, Photometry and Spectroscopy

Conventional optical instruments, like photometers, spectrometers, polarimeters or interferometers, are capable of measuring properties of light such as its intensity, spectrum, polarization or coherence. However, such properties are generally insufficient to determine the physical conditions under which light has been created. Thus it is not possible, not even in principle, to distinguish between e.g. spontaneously emitted light reaching the observer directly from the source; similar light that has undergone scattering on its way to the observer; or light predominantly created through stimulated emission, provided these types of light have the same intensity, polarization and coherence as function of wavelength. The deduction of the processes of light emission is therefore made indirectly via theoretical models. Yet, such types of light could have physical differences regarding collective multi-photon properties in the photon gas. Such properties are known for light from laboratory sources, and might ultimately become experimentally measurable also for astronomical ones.

To understand the 'parameter domains' in 'knowledge space' that are accessed by e.g. photometers or spectrometers, we need to understand their working principles on a very fundamen-

tal level, i.e. not superficial specifications such as field-of-view or spectral resolution, but rather their workings concerning the physical observables accessed.

One-photon experiments

We describe light as an electromagnetic wave of one linear polarization component whose electric field E contains terms of the type $\exp(-i\omega t)$ for angular frequencies ω . All classical optical instruments measure properties of light that can be deduced from the first-order correlation function of light, $G^{(1)}$, for two coordinates in space \mathbf{r} and time t (Glauber, 1970). The different classes are collected in Figure 4, where $\langle \rangle$ denotes time average, and $*$ complex conjugate. For example, a bolometer measures $\langle E^*(0,0) E(0,0) \rangle$, yielding the classical field intensity irrespective of the spectrum or geometry of the source (we define the coordinates with the observer initially at the origin). For the case $\mathbf{r}_1 = \mathbf{r}_2$ but $t_1 \neq t_2$, $G^{(1)}$ becomes the autocorrelation function with respect to time, $\langle E^*(0,0) E(0,t) \rangle$, whose Fourier transform yields the power density as function of electromagnetic frequency. That is the spectrum of light which is measured by spectrometers. The function is explicitly sampled by Fourier transform spectrometers while e.g. gratings 'perform' the transform to the spectrum through diffractive interference. For the case $\mathbf{r}_1 \neq \mathbf{r}_2$ but $t_1 = t_2$ we instead have the spatial autocorrelation function $\langle E^*(0,0) E(\mathbf{r},0) \rangle$, which is measured by imaging telescopes and [phase] interferometers, yielding the angular distribution of the source power density. The need for accurate timekeeping at both sites \mathbf{r}_1 and \mathbf{r}_2 originates from the requirement $t_1 = t_2$. In the absence of absolute flux calibrations, $G^{(1)}$ is usually normalized to the first-order coherence $g^{(1)}$.

Two- and multi-photon properties of light

Thus, classical measurements do not distinguish light sources with identical $G^{(1)}$. All such measurements can be ascribed to quantities of type E^*E , corresponding to intensity I , which in the quantum limit means observations of individual photons or of statistical one-photon properties. Possible multi-photon phenomena in the photon stream reaching the observer are not identified.

The description of collective multi-photon phenomena in a photon gas in general requires a quantum-mechanical treatment since photons have integer spin ($S = 1$), and therefore constitute a boson fluid with properties different from a fluid of classical distinguishable particles. The first treatment of the quan-

ONE-PHOTON EXPERIMENTS

1:st order correlation function:

$$G^{(1)}[r_1, t_1; r_2, t_2] = \langle E^*(r_1, t_1) E(r_2, t_2) \rangle$$

Special case: $r_1 = r_2, t_1 = t_2$

$$\langle E^*(0,0) E(0,0) \rangle - \text{BOLOMETER}$$

Special case: $r_1 \neq r_2, t_1 = t_2$

$$\langle E^*(0,0) E(r,0) \rangle - \text{[PHASE] INTERFEROMETER}$$

Special case: $r_1 = r_2, t_1 \neq t_2$

$$\langle E^*(0,0) E(0,t) \rangle - \text{SPECTROMETER}$$

Figure 4: Fundamental quantities measured in one-photon experiments. All such measurements can be ascribed to quantities of type E^*E , corresponding to intensity I , which in the quantum limit means observations of individual photons or of statistical one-photon properties. To this category belong all direct and interferometric imagers, spectrometers, and photometers, i.e. all ordinary instruments used in astronomy. Time average is denoted by $\langle \rangle$ while * marks complex conjugate.

TWO-PHOTON EXPERIMENTS

2:nd order correlation function:

$$G^{(2)}[r_1, t_1; r_2, t_2] = \langle I(r_1, t_1) I(r_2, t_2) \rangle$$

Special case: $r_1 = r_2, t_1 = t_2$

$$\langle I(0,0) I(0,0) \rangle - \text{"QUANTUM SPECTROMETER"}$$

Special case: $r_1 \neq r_2, t_1 = t_2$

$$\langle I(0,0) I(r,0) \rangle - \text{INTENSITY INTERFEROMETER}$$

Special case: $r_1 = r_2, t_1 \neq t_2$

$$\langle I(0,0) I(0,t) \rangle - \text{CORRELATION SPECTROMETER}$$

Figure 5: Fundamental quantities measured in two-photon experiments. All such measurements can be ascribed to quantities of type $I \times I$, i.e. intensity multiplied by itself, which in the quantum limit means observations of pairs of photons or of statistical two-photon properties. The intensity interferometer was the first astronomical instrument in this category.

MULTI-PHOTON PROPERTIES

Chaotic light:

$$\langle I^n \rangle = n! \langle I \rangle^n$$

Stable wave:

$$\langle I^n \rangle = \langle I \rangle^n$$

Chaotic light scattered by Gaussian medium:

$$\langle I^n \rangle = (n!)^2 \langle I \rangle^n$$

Anti-bunched light:

$$\langle I^n \rangle = 0 \quad [n > 1]$$

created or how it has been redistributed (scattered) since its creation. Although such problems are studied in theoretical astrophysics, they are not yet accessible to direct observational tests.

tum theory of coherence in a photon gas was by Glauber (1963a, 1963b), although some properties were inferred earlier from classical treatments, notably the bunching of photons in chaotic (thermal) light, first observed by Hanbury Brown and Twiss. An arbitrary state of light can be specified with a series of coherence functions essentially describing one-, two-, three-, etc. -photon-correlations. A simplified expression for the second-order correlation function is given in Figure 5. It describes the correlation of intensity between two coordinates in space and time. Since a detection of a photon (measurement of I) enters twice, $G^{(2)}$ describes two-photon properties of light.

$G^{(2)}$ is often normalized to the second-order coherence, $g^{(2)}$. Although its strict definition involves quantum-mechanical operators, a simplified expression can be given in terms of intensities: $g^{(2)} = \langle I(r_1, t_1) I(r_2, t_2) \rangle / \langle I(r_1, t_1) \rangle \langle I(r_2, t_2) \rangle$. If the distribution of photons is chaotic, i.e. the photon gas is in a maximum entropy state, the second-order coherence can be deduced as $g^{(2)} = [g^{(1)}]^2 + 1$ (e.g. Loudon 1983). This property can be used to determine $|g^{(1)}|$ from measurements of $g^{(2)}$. In the intensity interferometer this is made for $r_1 \neq r_2$ but $t_1 = t_2$: $\langle I(0,0) I(r,0) \rangle$, thus deducing angular sizes of stars, reminiscent of a classical interferometer. For $r_1 = r_2$ but $t_1 \neq t_2$ we instead have an

intensity-correlation spectrometer, which measures $\langle I(0,0) I(0,t) \rangle$, determining the spectral width of e.g. scattered laser light.

In thermodynamic equilibrium, the [chaotic] distribution of photons corresponds to the value $g^{(2)} = 2$ for first-order coherent ($g^{(1)} = 1$) light. Such photons follow a Bose-Einstein distribution, analogous to a Maxwellian one for classical particles. However, away from equilibrium, photons may deviate from Bose-Einstein distributions (just as classical particles can be non-Maxwellian). For example, light created by stimulated emission in the limiting case of a stable wave without any intensity fluctuations has $g^{(2)} = 1$, corresponding to analogous states in other boson fluids, e.g. superfluidity in liquid helium. Chaotic light scattered against a Gaussian frequency-redistributing medium has $g^{(2)} = 4$.

In the laboratory, one can observe how the physical nature of the photon gas gradually changes from chaotic ($g^{(2)} = 2$) to ordered ($g^{(2)} = 1$) when a laser is 'turned on' and the emission gradually changes from spontaneous to stimulated. Measuring $g^{(2)}$ and knowing the laser parameters involved, it is possible to deduce the atomic energy-level populations, which is an example of an astrophysically important parameter ('non-LTE departure coefficient') which cannot be directly observed with classical measurements of one-photon properties. Just as it is not possible to tell whether one individual helium atom is superfluid or not, it is not possible to determine whether one individual photon is due to spontaneous or stimulated emission: both cases require studies of statis-

tical properties of the respective boson fluid.

For a first-order coherent source with $g^{(2)} \neq 2$, neither an intensity interferometer nor an intensity-correlation spectrometer will yield correct results. E.G. a point source emitting a monochromatic stable wave whose $g^{(2)} = 1$ everywhere, would appear to be spatially resolved by an intensity interferometer at any spatial baseline and spectrally resolved by an intensity-correlation spectrometer at any timelag, and hence give the false impression of an arbitrarily large source emitting white light. This example demonstrates that additional measurements are required to fully extract the information content of light.

Many different quantum states of optical fields exist, not only those mentioned above (which can be given classical analogs) but also e.g. photon antibunching which with $g^{(2)} = 0$ is a purely quantum-mechanical state. This implies that neighbouring photons avoid one another in space and time. While such properties are normal for *fermions* (e.g. electrons), which obey the Pauli exclusion principle, ensembles of *bosons* (e.g. photons) show such properties only in special situations. An antibunching tendency implies that the detection of a photon at a given time is followed by a decreased probability to detect another immediately afterward. Experimentally, this is seen through sub-Poissonian statistics, i.e. narrower distributions of recorded photon counts than would be expected in a 'random' situation. Since the intensity of light is now a function whose average square ($\langle I^2 \rangle$) is smaller than the square of its average ($\langle I \rangle^2$), it cannot be represented through classical mathematics: this requires a quantum description.

For an introduction to the theory of such quantum optical phenomena, see e.g. Loudon (1980; 1983), Meystre & Sargent (1990), or Walls & Milburn (1994). Experimental procedures for studying photon statistics are described by Saleh (1978).

Astronomical Quantum Optics

One can envision applications of nanosecond resolution optical observations to give insight in the physical processes of radiative deexcitation of astrophysical plasmas, fields of study which presently are the almost exclusive realm of theoreticians.

Physics of emission processes

What is the physical nature of light emitted from a plasma with departures from thermodynamic equilibrium of the atomic energy-level populations? Will a

spontaneously emitted photon stimulate others, so that the path where the photon train has passed becomes temporarily deexcited and remains so for perhaps a microsecond until collisions and other effects have restored the balance? Does then light in a spectral line perhaps consist of short photon showers with one spontaneously emitted photon leading a trail of others emitted by stimulated emission? Such [partial] 'laser action' has been predicted in mass-losing high-temperature stars, where the rapidly recombining plasma in the stellar envelope can act as an amplifying medium (Lavrinovich & Letokhov 1974; Varshni & Lam 1976; Varshni & Nasser 1986). Analogous effects could exist in accretion disks (Fang 1981). In the infrared, there are several cases where laser action is predicted for specific atomic lines (Ferland 1993; Greenhouse *et al.* 1993; Peng & Pradhan 1994).

Somewhat analogous situations (corresponding to a laser below threshold) have been studied in the laboratory. The radiation structure from 'free' clouds (i.e. outside any laser resonance cavity) of excited gas with population inversion can be analysed. One natural mode of radiative deexcitation indeed appears to be the emission of 'photon showers' triggered by spontaneously emitted ones which are stimulating others along their flight vectors out from the volume.

In principle, quantum statistics of photons might permit to determine whether e.g. the Doppler broadening of a spectral line has been caused by motions of those atoms that emitted the photons or by those intervening atoms that have scattered the already existing photons. Thus, for such scattered light, its degree of partial redistribution in frequency might be directly measurable.

Although the existence *in principle* of such effects may be clear, their practical observability is not yet known. At first sight, it might even appear that light from a star should be nearly chaotic because of the very large number of independent radiation sources in the stellar atmosphere, which would randomize the photon statistics. However, since the time constants involved in the maintenance of atomic energy level overpopulations (e.g. by collisions) may be longer than those of their depopulation by stimulated emission (speed of light), there may exist, in a given solid angle, only a limited number of radiation modes reaching the observer in a given time interval (each microsecond, say) and the resulting photon statistics might well be non-chaotic. Proposed mechanisms for pulsar emission include stimulated synchrotron and curvature radiation ('free-electron laser') with suggested timescales of nanoseconds, over which the quantum statistics

of light would be non-trivial. In general, photon statistics for the radiation from any kind of non-thermal source could convey something about the processes where the radiation was liberated. For example, the presence of photon 'bubbles' in photohydrodynamic turbulence in very hot stars has been suggested. The bubbles would be filled with light and the photon-gas pressure inside would balance the surrounding gas but due to buoyancy, the bubbles would rise through the stellar surface, giving off photon bursts (Prendergast & Spiegel 1973; Spiegel 1976). Obviously, the list of potential astrophysical targets could be made longer.

Interpreting observed photon statistics

The theoretical problem of light scattering in a [macroscopic] turbulent medium is reasonably well studied. In particular, the equations of transfer for I^2 and higher-order moments of intensity have been formulated and solved (e.g. Uscinski 1977). A result that is familiar to many people implies that stars twinkle more with [moderately] increasing atmospheric turbulence. The value of I , i.e. the total number of photons transmitted may well be constant, but I^2 increases with greater fluctuations in the medium. The quantum problem of scattering of light against atoms is somewhat related, except that the timescales involved are now those of the coherence times of light.

However, theoretical treatments of astrophysical radiative transfer have so far almost exclusively concentrated on the first-order quantities of intensity, spectrum and polarization, and not on the transfer of I^2 and higher-order terms. There are some exceptions, however, like the analytical solution of the higher-order moment equation relevant for radio scintillations in the interstellar medium (Lee & Jokipii 1975; Lerche 1979a; 1979b) and attempts to formulate the quantum mechanical description of the transfer of radiation, including non-Markovian effects (i.e. such referring to more than one photon at a time) in a photon gas (Macháček 1978; 1979), the transfer equation for the density matrix of phase space cell occupation number states (Sapar 1978; Ojaste & Sapar 1979), or the introduction of concepts from non-linear optics (Wu 1993).

Still, there do not yet appear to exist any theoretical predictions for specific astronomical sources of any spectral line profiles of higher-order than one (i.e. ordinary intensity versus wavelength). Until the availability of such theoretical predictions (of e.g. the second-order coherence versus wavelength), this work will continue to have an exploratory character.

Do we understand what we are doing?

When entering new domains of physical measurement, not only the optics and electronics of the experiment, but also the fundamental physics of the quantum-mechanical interaction between the measuring instrument and the photon gas to be studied, must be adequately understood. One example will illustrate the problem. Although in common speech the opposite is often uttered, there actually does *not* appear to exist any known method of *directly* detecting photons. All 'photon-detectors' instead give some electrical signal of photo-electrons as the output to the observer. It is a sobering thought that quantum statistical properties to be measured, e.g. the bunching of several photons in the same quantum state, is a property that can *not even in principle* be possessed by these electrons. Since these have quantum spin = $\frac{1}{2}$, they are fermions and obey the Pauli exclusion principle, which prohibits two or more particles to occupy the same quantum state.

Even the optics inside an instrument may fundamentally affect the signal to be measured. For example, the reader might want to ponder what are the effects of a common beamsplitter, which makes a 50-50% split of the intensity of light. What will become of the statistical distributions of photons after the photon gas has been cleaved by this beamsplitter? (For an introduction to the theory and experiment on such issues, see e.g. Aspect & Grangier 1991.)

Instrumentation for High-Speed Astrophysics

A number of criteria can be defined for optimizing an observing instrument in high-speed astrophysics, and there have been efforts by different groups toward this end.

We have designed one such unit at Lund Observatory, named *QVANTOS* for 'Quantum-Optical Spectrometer'. Its first version was used on La Palma to test instrumentation and observation methods, and to explore what challenges in understanding the terrestrial atmosphere that must be met before astrophysical variability on short timescales can be convincingly demonstrated to exist. The main design criteria for the *QVANTOS* instrument and a description of its performance are in Dravins *et al.* (1994), while examples of data recorded with it appear below. Basically, its key components are rapid photon-counting detectors and very fast digital signal processors for real-time computation of various statistical functions of the photon arrival times. The design issues included:

- Handling huge amounts of data: The highest time resolutions lead to data rates of perhaps megabytes per second. To make the analysis manageable, there is a need for *real-time data reduction* to statistical functions only.

- For faint sources, one wants to study variability also on timescales shorter than typical intervals between successive photons. While not possible with conventional light-curves, it is enabled through a *statistical analysis of photon arrival times*, testing for deviations from randomness.

- The terrestrial atmosphere causes rapid fluctuations of the source intensity, and a segregation of astrophysical fluctuations requires a correspondingly accurate measurement and correction for atmospheric effects.

Previous work by other groups illustrates that meeting all such (and other) requirements is non-trivial. The pioneering *MANIA* experiment at the Northern Caucasus 6-metre telescope (recently used also in Argentina; Shvartsman 1977; Beskin *et al.* 1982; 1994), has limitations in the maximum photon count rates that can be processed. Networks of telescopes used in searches for stellar oscillations, have been limited by atmospheric intensity scintillation. Instruments in space avoid the terrestrial atmosphere: the *High Speed Photometer* on the *Hubble Space Telescope* was a major effort (Bless 1982), but only limited quantities of data could be stored onboard.

The post-CCD era of optical detectors

CCD's and similar silicon-based imaging detectors now dominate optical astronomy, thanks to their high quantum efficiency and ease of use. However, such detectors are not really optimal for measuring rapid variability, due to their relatively long read-out times. Although devices and methods for more rapid CCD-frame readout (milliseconds) are being developed, there seem to be fundamental trade-offs between speed and noise. For timing individual photons on submillisecond scales, one has hitherto been limited to photocathode detectors such as photomultipliers or microchannel plates.

Such photocathode detectors, however, have a limit in their achievable quantum efficiency, and in its extension toward the infrared. As stressed further below, the signal-to-noise ratio in measured statistics of intensity fluctuations increases rapidly not only with telescope size but equally with increased detector efficiency. Since future observational needs will include relatively faint accretion sources in the Galaxy, some of which may be reddened by circumstellar ma-

terial, we are facing the need for a high quantum efficiency extending into the [in-fra]red. Such challenges are now stimulating the gradual emergence of a new post-CCD generation of detectors for optical astronomy: combining imaging at high quantum efficiency, photon counting with nanosecond resolution into the infrared, and even intrinsic spectroscopic resolution.

Photon-counting avalanche diodes

The quantum efficiency for a silicon detector, compared to photocathode ones, can be several times greater, and may extend into the far red to about 1 μm .

During recent years, the development of *silicon avalanche photodiodes* has reached a point, where they can now be used for photon counting (Brown *et al.* 1990; Dauter *et al.* 1993; Nightingale 1991; Sun & Davidson 1992; Szécsényi-Nagy 1993). Absolute quantum efficiencies in single-photon detection up to 76% (at λ 700 nm) have been experimentally demonstrated (Kwiat *et al.* 1994). Some astronomical groups (including ourselves) have now acquired such detectors, at least for the purpose of laboratory evaluation. Besides photon counting at impressive efficiencies, avalanche diodes however also bring a number of new and undesired (and partly unknown) properties. One phenomenon not seen in photocathode detectors is that the electronic avalanche during the photon detection temporarily disturbs the semiconductor and causes light to be *emitted* from the detector surface. The dark count can be *bistable* in the sense of sudden jumps between discrete levels, apparently due to phenomena at impurity sites inside the diode. Awkward problems are caused by their very small physical dimensions. While the light-sensitive area in photomultipliers typically extends over several mm, the usable area of present photon-counting diodes is typically no more than some 1% that of a normal photomultiplier. For use on a large telescope, this circumstance makes the optical and mechanical designs quite challenging.

Developments of larger-area avalanche diodes are being pursued in industry, and prototypes of significantly larger size have been tested (e.g. Woodard *et al.* 1994). Some other problems related to the active quenching of the avalanches (giving shorter dead-times and thus permitting higher count rates) have apparently been solved, but there still remain some non-uniformities in sensitivity across the detector area, and the dark signal increases for larger detectors. Solutions to these and other problems are actively being sought in the industry. Also, photon-counting with *germanium* avalanche diodes has

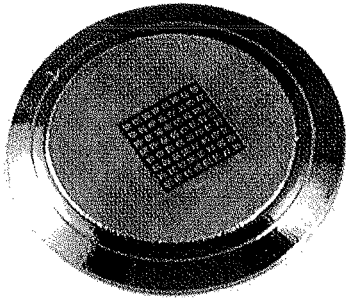


Figure 7: An avalanche photodiode array, example of an optical detector for the post-CCD era. This class of detectors has the potential for quantum efficiency approaching unity (and extending into the infrared), while counting individual photons at nanosecond resolution (Madden 1993).

been demonstrated, extending sensitivities further into the infrared (Lacaita *et al.* 1994; Owens *et al.* 1994).

In another development with silicon devices, *avalanche photodiode arrays* have recently been developed (Fig. 7), stimulated by non-astronomy needs such as detectors for ladar (laser radar), recording laser-pulse illuminated scenes, where the distance to objects imaged in the field is determined by timing photon arrivals within nanoseconds. Although such devices do not yet appear to be available in photon-counting mode, a conceivable future photon-counting 4096×4096 photodiode array with, say, a 1 MHz photon count rate per pixel could generate more than 10^7 Mb (= 10 Terabytes) per second, or 10^{12} Mb (= 1 Exabyte) during a 3-night observing run. The data handling issues will become interesting, but only with such detectors could one begin to really exploit the potential of the VLT for high-speed applications. Even so, they would be far from ultimate, since there is still no intrinsic energy nor polarization resolution, and in order to separate different wavelengths, spectrometers or filters would still have to be used, with all their known inefficiencies in light transmission.

Spectrally resolving detectors

Astrophysical variability may be different in different wavelength regions (where different opacities enable one to see differently deep into accretion flows); inside and outside a spectral line (where the radiative non-equilibrium and deexcitation may be different from that in the continuum); or even in different polar-

izations (where the emission may come from different magnetic regions). Thus, to extract all information, photon arrival times and positions should be recorded with a high spectroscopic and polarimetric resolution. Especially for extended astronomical sources, such studies are hampered by the two-dimensional nature of common photon detectors. Even if spectrometers were efficient, most light would be lost because the instrument must scan in the spatial or spectral domain. Here, energy-resolving detectors are needed, which in addition to spatial and temporal data also measure the photon wavelength. Such detectors are widely used in X-ray astronomy, and developments are in progress to apply related techniques also in the optical and infrared.

One line of development concerns photon counting using superconducting tunnel junctions (Perryman *et al.* 1992; 1993; 1994). The principle is that a photon impinging on the detector generates charge carriers within it, and these are collected by nearby elements in a junction array. The energy required to create a charge carrier within a superconductor is some three orders of magnitude less than in a semiconductor such as silicon. It is of order milli-eV, and thus an optical photon (of a few eV energy) creates a 'cloud' with perhaps 100–1000 of charge carriers. Even if not all are detected, the impact of the optical photon is recorded with an efficiency approaching unity (analogous to X-ray detectors, where an energetic photon liberates many electrons). The timing of the arrival of this 'cloud' to the nearest elements of the junction array permits both positional encoding and time resolution. Pulse counting gives the number of liberated charge carriers, and thus the energy of the absorbed photon, i.e. its wavelength. This concept promises large-area detectors of very high sensitivity, photon-counting at high time resolution, combined with a moderate wavelength resolution ($\lambda/\Delta\lambda \simeq 30$).

Another line of development, permitting extremely high spectral resolution in the detector ($\lambda/\Delta\lambda \geq 500,000$), exploits certain organic molecules, cryogenically cooled. The method involves a persistent spectral hole-burning in a dye-doped polymer film, a technique otherwise being developed for optical data storage; Keller *et al.* (1994a; 1994b).

An organic molecule such as chlorin is used in a film cooled by liquid helium. The natural line width of chlorin at this temperature is about 0.2 pm ($\lambda/\Delta\lambda \simeq 3 \cdot 10^6$). A superposition of such very narrow but overlapping absorption lines forms a broad and smooth absorption band, some 10 nm wide. This wavelength spread of the individual absorp-

tion lines is due to wavelength shifts enabled by local electrical potentials. When a molecule absorbs a photon, it undergoes a photo-reaction which makes the molecule insensitive to light in that particular wavelength band, analogous to the functioning of dyes in a color film. The spectral information is retrieved using a scanning dye laser: tests on the solar spectrum confirm a performance comparable to the highest resolution spectrometers used in astronomy. Time resolution, however, is as yet lacking in this concept.

These examples of detector developments for the post-CCD era in optical astronomy illustrate both the new possibilities that may come, and the many challenges that yet remain. Future detector gains will add to the telescope ones, making a VLT with future detectors enormously more powerful than with its first-generation instruments.

The Role of the VLT

At very high time resolution, data rates are very high, and classical light curves are of little use. Measurements thus have to be of autocorrelations, power spectra, or other statistical properties of the arriving photon stream. All such statistical functions depend on a power of the average intensity that is higher than one. For example, an autocorrelation (which is obtained by multiplying the intensity signal by itself, shifted by a time lag) is proportional to the *square* of the intensity. Due to this dependence, very large telescopes are much more sensitive for the detection of rapid variability than ordinary-sized ones.

A search for e.g. magneto-hydrodynamic instabilities in accretion disks around supposed black holes, using autocorrelation techniques, will benefit a factor $(8.2/3.6)^4 \simeq 27$ if using one 8.2-metre telescope instead of a 3.6-m one, rather than the ratio $(8.2/3.6)^2 \simeq 5$ that is valid for the intensity. For other measures, e.g. those of the fourth-order moments of the photon distribution, the signal will increase as the fourth power of the intensity, making a full Very Large Telescope with four 8-metre units some 185,000 times more sensitive than a 3.6 m one (implying that one night of observing on the full VLT gives the same signal as 500 years of integration with a 3.6-m! (Fig. 8).

These large numbers may appear unusual when compared to the more modest gains expected for classical instruments, and initially perhaps even difficult to believe. Such numbers are, however, well understood among workers in non-linear optics. The measured $\langle I^4 \rangle$ is proportional to the conditional probability that four photons are recorded within a certain time interval. $\langle I^4 \rangle$ itself is,

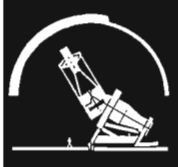
Telescope diameter	Intensity $\langle I \rangle$	Second-order intensity correlation $\langle I^2 \rangle$	Fourth-order photon statistics $\langle I^4 \rangle$
 3.6 m	1	1	1
 8.2 m	5	27	720
 4 * 8.2 m	21	430	185,000

Figure 8: Comparisons between the observed signal of source intensity (I), its square and fourth powers, for telescopes of different size. The signal for classical quantities increases with the intensity I ; the signal in power spectra and similar functions suitable for variability searches, as I^2 ; and that of four-photon correlations as I^4 , as relevant for quantum statistics studies. The advent of very large telescopes greatly increases the potential for high-speed astrophysics.

strictly speaking, not a physical observable: either one detects a photon in a time interval, or one does not. $\langle I^4 \rangle$ therefore has the meaning of a rapid succession of intensity measurements: $\langle I(t) I(t+\Delta t) I(t+2\Delta t) I(t+3\Delta t) \rangle$. In an experiment where one is studying the multi-step ionization of some atomic species, where four successive photons have to be absorbed in rapid succession, one notes how a doubling of the light intensity causes a 16-fold increase in the ionization efficiency. Or indeed, for light of identical intensity, how the efficiency may increase if the illuminating light source is changed to another of the same intensity but with different statistical properties, i.e. a different value of $\langle I^4 \rangle$. But it does not stop here. The prospect of improved detectors will further increase the efficiency in a multiplicative manner. An increased quantum efficiency in the visual of a factor 3, say, or in the near infrared a factor 10, will mean factors of 10 and 100 in second-order quantities, while the signal in fourth-order functions will improve by factors 100 and 10,000, respectively. These factors should thus be multiplied with those already large numbers in Figure 8, to give the likely gains for the VLT equipped with future detectors, as compared to present ones.

Due to analogous steep dependences on intensity, the research field of non-linear optics was opened up for study by the advent of high-power laboratory lasers. In a similar vein, the advent of very large telescopes could well open up the field of high-speed astrophysical variability and bring astronomical quantum optics above a detection threshold.

Signal-to-noise at the quantum limit

In the limit of the highest time resolution, the statistical nature of light has

to be understood, including those properties that may appear non-intuitive, if approached from classical optics. The higher-order optical coherence functions are independent from the first-order ones (which define e.g. the brightness or the spectrum of the source). It then follows that also the signal-to-noise ratios must be independent from the latter. This somewhat non-intuitive situation was encountered already in the intensity interferometer which could not measure cool

(red) stars, not even the brightest ones (Hanbury Brown 1974). The practical observability limit for quantum phenomena is set not by the apparent brightness of the source (measured as photons arriving per unit time), but more by the number of photons per [spatial and temporal] coherence volume.

An ideal telescope may re-create, in its focal volume, the same photon density as in the source (but no more, due to the laws of thermodynamics). Thus a solar telescope may achieve a photon density corresponding to a ≈ 5800 K blackbody: the solar surface temperature, but no hotter. An ideal telescope observing *Sirius*, however, could reach its surface temperature of 10,000 K. *Sirius*' angular size is some 6 milliarcseconds; the diffraction limit for one 8-m telescope is about twice that, i.e. the diffraction-limit volume is $\approx 2^3 = 8$ times that image volume where T_{eff} would be 10,000 K. Compared to the Sun, the *Sirius* surface flux density is $(10,000/5,800)^4 \approx 9$ times greater, and thus one 8-m telescope, if operated at its diffraction limit, will measure about the same photon density in its focal volume if it is pointed at *Sirius* or at the Sun!

Atmospheric Intensity Scintillation

However, before observed intensity fluctuations can be ascribed to any as-

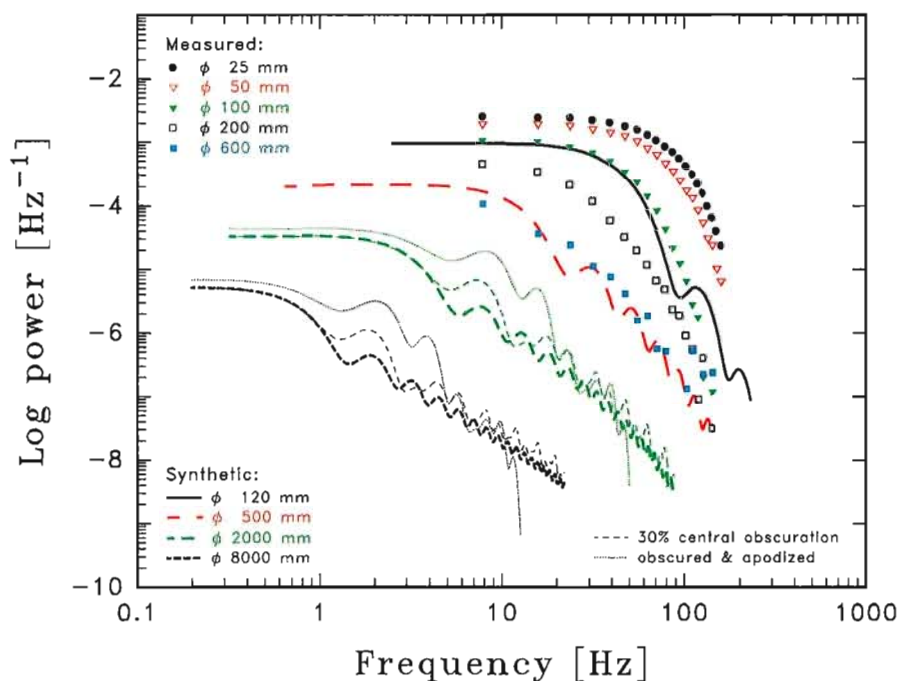


Figure 9: Atmospheric intensity scintillation around $\lambda 500$ nm for telescopes of different aperture sizes. The symbols are values measured on La Palma during good summer conditions for small telescope apertures. This sequence was fitted to synthetic power spectra for up to 8 metre diameter, thus predicting the scintillation in a VLT unit telescope. The bold curves are for fully open apertures. The inclusion of a central obscuration, corresponding to the secondary mirror (here taken as 30% of the primary diameter), increases the scintillation power, while apodization of this aperture (i.e. introducing a smooth intensity fall-off near its edges), decreases it for high temporal frequencies (Dravins et al. 1995).

tronomical source, the intensity scintillations caused by the Earth's turbulent atmosphere must be adequately understood, measured, and calibrated for. An understanding of atmospheric scintillation is needed both for the optimal design of instrumentation and the observing strategies, and in the analysis of the data, segregating astrophysical variability from terrestrial effects.

For this purpose, extensive observations of stellar intensity scintillation on short and very short time scales (100 ms–100 ns) were made during several weeks of observing with the *Mark I* version of our *QVANTOS* instrument, used on the Swedish 60-cm telescope on La Palma (Dravins et al. 1995). Atmospheric scintillation was measured as function of telescope aperture size and shape; degree of apodization; for single and double apertures; for single and binary stars; in different optical colours; using different optical passbands; at different zenith distances; at different times of night; and different seasons of year. Data were recorded as temporal auto- and cross-correlation functions, and intensity probability distributions, sometimes supplemented by simultaneous video recordings of the stellar speckle images, as well as seeing disk measurements in an adjacent telescope.

Several scintillation properties can be understood in terms of the illumination pattern caused by diffraction in inhomogeneities of high atmospheric layers. These structures are carried by winds, resulting in 'flying shadows' on the ground (Codona 1986). The dependence on aperture diameter ϕ was studied, using rapidly changeable mechanical masks in front of the telescope. This aperture dependence disappears for $\phi \leq 5$ cm. On such spatial scales, the structures in the 'flying shadows' on the ground appear resolved (both the autocorrelation half-widths and the amplitudes then become independent of aperture size). On these scales, also differences in scintillation between different colours become apparent.

Measured autocorrelations were transformed to power spectra. The power decreases for larger apertures (especially at high frequencies), reflecting the spatial averaging of small-scale turbulence elements. At frequencies $f \geq 100$ Hz, the power decreases approximately as f^{-5} . The observed statistics of intensity variations can be adequately described by log-normal distributions, varying with time.

Scintillation in the VLT: what will change?

Very large telescopes integrate the 'flying shadow' pattern over a corre-

spondingly larger area, averaging out primarily the smaller-scale (and thus more rapidly varying) components. This is seen in Figure 9, which shows the scintillation power spectrum predicted for the 8-metre VLT unit telescopes. These curves were obtained from theoretical models for apertures of different size (computed by A.T.Young), where the normalization to actual scintillation amplitude and atmospheric windspeed was obtained by fitting the models to representative observations.

What will not change?

By no means will effects of scintillation disappear in very large telescopes. While some quantities (e.g. the power in Fig. 9) will decrease, others are independent of telescope size. An example of the latter is the temporal correlation between scintillation in different colours. Near zenith, the intensity fluctuations are simultaneous, but with increasing zenith angle (and increasing wavelength difference), a time delay may develop (Fig. 10). This is visible as a shift of the cross correlation maximum away from the origin. The 'flying shadows' on the ground become chromatic, a projection onto the

ground of the starlight which has been spectrally dispersed by the atmosphere. The 'blue' part in the 'flying shadows' on the ground is displaced from its 'red' part, but the structure of the 'shadows' is similar. As these race past the telescope, a time difference is visible. In the violet, the dispersion of air changes rapidly with wavelength, which explains the significant differences between the nearby wavelengths of λ 365 and λ 400 nm. These effects, however, appear only if looking along a wind direction, i.e. the direction of motion of the 'flying shadows'. At right angles from this, there is no effect.

An understanding of such phenomena is obviously required when searching for astrophysical phase shifts between variations in different colours, such as between oscillations in different layers inside accretion columns (visible at different wavelengths due to different opacities), or in searching for time delays between fluctuations in different spectral lines, perhaps formed in the same deexcitation cascade with photons of different wavelengths emitted more or less simultaneously.

A deeper understanding of scintillation in the Earth's atmosphere might be ap-

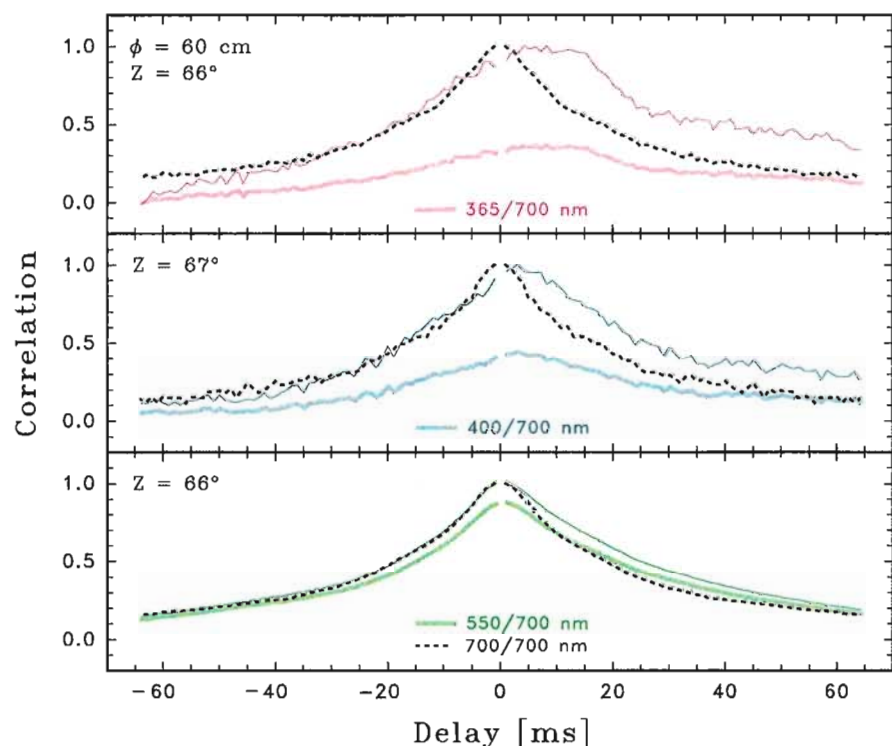


Figure 10: Cross correlation between atmospheric intensity scintillation in different colours. Near zenith such fluctuations are simultaneous, but with increasing zenith angle a time delay develops. In this sequence from La Palma, scintillation at λ 700 nm was auto-correlated, as well as cross-correlated with that simultaneously measured at λ 550, 400, and 365 nm. With increasing wavelength difference, (a) the 'agreement' (i.e. degree of correlation) between scintillation in different colours decreases (thick curves), and (b) a time delay develops, visible as a shift of the correlation maximum (normalized thin curves). This effect is due to atmospheric dispersion, which causes chromatic displacements of the 'flying shadows' on the ground, an effect due to the atmosphere and independent of the size of the telescope (Dravins et al. 1995).

plied also to the study of the fine structure of planetary atmospheres from stellar occultations, another application of high-speed measurements.

Conclusions and Outlook

Various approaches have been outlined for attempts to reach into the new parameter domains of milli-, micro- and nanosecond astrophysical variability. Such studies must of course be made in close contact with those in other wavelength bands (in particular X-rays), and in parallel with theoretical modelling. What makes the prospects especially exciting at the present time, is the new generation of very large optical telescopes. Since the signal of statistical variability increases dramatically with light collecting power, large telescopes become *enormously more sensitive* than ordinary-sized ones; new detector developments further enhance the potential. This quantum jump in sensitivity might well open up the field of high-speed astrophysical variability and bring astronomical quantum optics above a detection threshold.

Acknowledgements

High-speed astrophysics at Lund Observatory is supported by the *Swedish Natural Science Research Council*. L. Lindegren made valuable comments on the manuscript.

References

Abramowicz, M.A., Lanza, A., Spiegel, E.A., Szuszkiewicz, E. 1992, *Nature* **356**, 41.
 Aspect, A., Grangier, P. 1991, in J.W. Goodman, ed. *International Trends in Optics*, Academic, p. 247.
 Bao, G. 1992, *A&A* **257**, 594.
 Beskin, G.M., Neizvestnyi, S.I., Pimonov, A.A., Plakhotnichenko, V.L., Shvartsman, V.F. 1982, in C.M. Humphries, ed. *Instrumentation for Astronomy with Large Optical Telescopes*, IAU coll. **67**, Reidel, p. 181.
 Beskin, G., Neizvestny, S., Plokhotnichenko, V., Popova, M., Zhuravkov, A., Benvenuto, O.G., Feinstein, C., Méndez, M. 1994, *A&A* **289**, 141.
 Bless, R.C. 1982, in D.N.B. Hall, ed. *The Space Telescope Observatory*, NASA **CP-2244**, p. 106.
 Bradt, H.V., Levine, A.M., Morgan, E.H., Remillard, R.A., Swank, J.H., Dingus, B.L., Holt, S.S., Jahoda, K.M., Rothschild, R.E., Gruber, D.E., Hink, P.L., Pelling, R.M. 1990, in Y.Kondo, ed. *Observatories in Earth Orbit and Beyond*, IAU coll. **123**, Kluwer, p. 89.
 Brown, R.G.W., Burnett, J.G., Mansbridge, J., Moir, C.I., Lowans, B.S. 1990, *Appl.Opt.* **29**, 3291.
 Chen, X., Taam, R.E. 1992, *MNRAS* **255**, 51.
 Codona, J.L. 1986, *A&A* **164**, 415.
 Dautet, H., Deschamps, P., Dion, B., MacGregor, A.D., MacSween, D., McIntyre, R.J., Trottier, C., Webb, P.P. 1993, *Appl.Opt.* **32**, 3894.

Dravins, D., Hagerbo, H.O., Lindegren, L., Mezey, E., Nilsson, B. 1994, in D.L. Crawford, E.R. Craine, eds. *Instrumentation in Astronomy VIII*, SPIE proc. **2198**, p. 289.
 Dravins, D., Lindegren, L., Mezey, E., Young, A.T. 1995, *Appl.Opt.*, to be submitted.
 Fang, L.Z. 1981, *MNRAS* **194**, 177.
 Ferland, G.J. 1993, *ApJS* **88**, 49.
 Fukue, J., Yokoyama, T. 1988, *PASJ* **40**, 15.
 Glauber, R.J. 1963a, *Phys.Rev.* **130**, 2529.
 Glauber, R.J. 1963b, *Phys.Rev.* **131**, 2766.
 Glauber, R.J. 1970, in S.M.Kay, A.Maitland, eds. *Quantum Optics*, Academic, p. 53.
 Greenhouse, M.A., Feldman, U., Smith, H.A., Klapisch, M., Bhatia, A.K., Bar-Shalom, A. 1993, *ApJS* **88**, 23.
 Hanbury Brown, R. 1974, *The Intensity Interferometer*, Taylor & Francis.
 Hawley, J.F., Smarr, L.L. 1986, in R.I. Epstein, W.C. Feldman, eds. *Magnetospheric Phenomena in Astrophysics*, AIP conf. proc. **144**, p. 263.
 Heemskerk, M.H.M. 1994, *A&A* **288**, 807.
 Honma, F., Matsumoto, R., Kato, S. 1992, *PASJ* **44**, 529.
 Horne, K., Saar, S.H. 1991, *ApJ* **374**, L55.
 Imamura, J.N., Kristian, J., Middleditch, J., Steiman-Cameron, T.Y. 1990, *ApJ* **365**, 312.
 Iping, R.C., Petterson, J.A. 1990, *A&A* **239**, 221.
 Kaitchuck, R.H., Schlegel, E.M., Honeycutt, R.K., Horne, K., Marsh, T.R., White, J.C., Mansperger, C.S. 1994, *ApJS* **93**, 519.
 Keller, C.U., Graff, W., Rosselet, A., Gschwind, R., Wild, U.P. 1994a, *A&A* **289**, L41.
 Keller, C.U., Gschwind, R., Renn, A., Rosselet, A., Wild, U.P. 1994b, *A&AS*, in press.
 Kwiat, P.G., Steinberg, A.M., Chiao, R.Y., Eberhard, P.H., Petroff, M.D. 1994, *Appl.Opt.* **33**, 1844.
 Lacaíta, A., Francese, P.A., Zappa, F., Cova, S. 1994, *Appl.Opt.* **33**, 6902.
 Lanzafame, G., Belvedere, G., Molteni, D. 1993, *MNRAS* **263**, 839.
 Larsson, S. 1985, *A&A* **145**, L1.
 Lavrinovich, N.N., Letokhov, V.S. 1974, *Zh.Eksp.Theor.Fiz.* **67**, 1609 = *Sov.Phys.-JETP* **40**, 800 (1975).
 Lee, L.C., Jokiipi, J.R. 1975, *ApJ* **202**, 439.
 Lerche, I. 1979a, *ApJ* **234**, 262.
 Lerche, I. 1979b, *ApJ* **234**, 653.
 Livio, M. 1994, in S.N.Shore et al., eds. *Interacting Binaries*, Springer, p. 135.
 Loudon, R. 1980, *Rep.Prog.Phys.* **43**, 913.
 Loudon, R. 1983, *The Quantum Theory of Light*, 2nd ed., Clarendon.
 Macháček, M. 1978, *Bull. Astron. Inst. Czechosl.* **29**, 268.
 Macháček, M. 1979, *Bull. Astron. Inst. Czechosl.* **30**, 23.
 Madden, R.M. 1993, *Photonics Spectra* **27**, No.12, p. 114.
 Marsh, T.R., Robinson, E.L., Wood, J.H. 1994, *MNRAS* **266**, 137.
 Meglicki, Z., Wickramasinghe, D., Bicknell, G.V. 1993, *MNRAS* **264**, 691.
 Meystre, P., Sargent, M. 1990, *Elements of Quantum Optics*, Springer.
 Mineshige, S., Kusunose, M. 1993, in J.C. Wheeler, ed. *Accretion Disks in Compact Stellar Systems*, World Scientific, p. 370.
 Mineshige, S., Wood, J.H. 1990, *MNRAS* **247**, 43.
 Motch, C., Ilovaisky, S.A., Chevalier, C. 1982, *A&A* **109**, L1.
 Nightingale, N.S. 1991, *Exper.Astron.* **1**, 407.
 Nowak, M.A., Wagoner, R.V. 1992, *ApJ* **393**, 697.
 Ojaste, J., Sapar, A. 1979, *Publ.Tartu Astrofiz.Obs.* **47**, 93.
 Owens, P.C.M., Rarity, J.G., Tapster, P.R., Knight, D., Townsend, P.D. 1994, *Appl.Opt.* **33**, 6895.
 Peng, J., Pradhan, A.K. 1994, *ApJ* **432** L123.
 Perryman, M.A.C., Foden, C.L., Peacock, A. 1992, proc. ESA Symp. *Photon Detectors for Space Instrumentation*, ESA **SP-356**, p.21
 Perryman, M.A.C., Foden, C.L., Peacock, A. 1993, *Nucl. Instr. and Meth.* **A325**, 319.
 Perryman, M.A.C., Peacock, A., Rando, N., van Dordrecht, A., Videler, P., Foden, C.L. 1994, in W.Wamsteker et al., eds. *Frontiers of Space and Ground-Based Astronomy*, Kluwer, p. 537.
 Pineault, S., Landry, S. 1994, *MNRAS* **267**, 557.
 Prendergast, K.H., Spiegel, E.A. 1973, *Comm. Aph. Space Phys.* **5**, 43.
 Saleh, B. 1978, *Photoelectron Statistics*, Springer.
 Sapar, A. 1978, *Publ.Tartu Astrofiz.Obs.* **46**, 17.
 Shvartsman, V.F. 1977, *Soobs. Spets. Astrofiz. Obs.* **19**, 5.
 Spiegel, E.A. 1976, in R.Cayrel, M.Steinberg, eds. *Physique des Mouvements dans les Atmosphères Stellaires*, CNRS coll. **250**, p. 19.
 Stone, J.M., Norman, M.L. 1994, *ApJ* **433**, 746.
 Sun, X., Davidson, F.M. 1992, *J. Lightwave Tech.* **10**, 1023.
 Szécsényi-Nagy, G. 1993, in C.J. Butler, I. Elliott, eds. *Stellar Photometry*, IAU coll. **136**, Cambridge, p. 160.
 Torkelsson, U., Brandenburg, A. 1994, *A&A*, in press.
 Uscinski, B.J. 1977, *The Elements of Wave Propagation in Random Media*, McGraw-Hill.
 Varshni, Y.P., Lam, C.S. 1976, *ApSS* **45**, 87.
 Varshni, Y.P., Nasser, R.M. 1986, *ApSS* **125**, 341.
 Wallinder, F.H. 1991, *A&A* **249**, 107.
 Walls, D.F., Milburn, G.J. 1994, *Quantum Optics*, Springer.
 Whitehurst, R. 1994, *MNRAS* **266**, 35.
 Woodard, N.G., Hufstedler, E.G., Lafyatis, G.P. 1994, *Appl.Phys.Lett.* **64**, 1177.
 Wu, Y.C. 1993, *ApSS* **209**, 113.

A Prominent Ionization Cone and Starburst Ring in the Nearby Circinus Galaxy

A. MARCONI¹, A.F.M. MOORWOOD², L. ORIGLIA³ and E. OLIVA⁴

¹Dipartimento di Astronomia e Scienza dello Spazio, Università di Firenze, Italy; ²ESO-Garching;

³Osservatorio Astronomico di Torino, Italy; ⁴Osservatorio Astrofisico di Arcetri, Firenze, Italy

Introduction

The characteristic spectra of Seyfert nuclei have long been generally attributed to photoionization by the hard UV continuum of a central black hole and associated accretion disk. More recently,

within the context of AGN unification schemes, it has been proposed that the primary difference between Seyferts of type 1 and 2, i.e the broad permitted lines seen in the former, could be attributed to the presence of an obscuring torus in which case visibility of the nucleus de-

pends on viewing angle. Supporting evidence has come from the detection of 'hidden' BLR's in reflected polarized, light and of ionization cones which imply some 'collimation' of the nuclear UV continuum (c.f Antonucci 1993 for a review). Also of interest in the context of unification

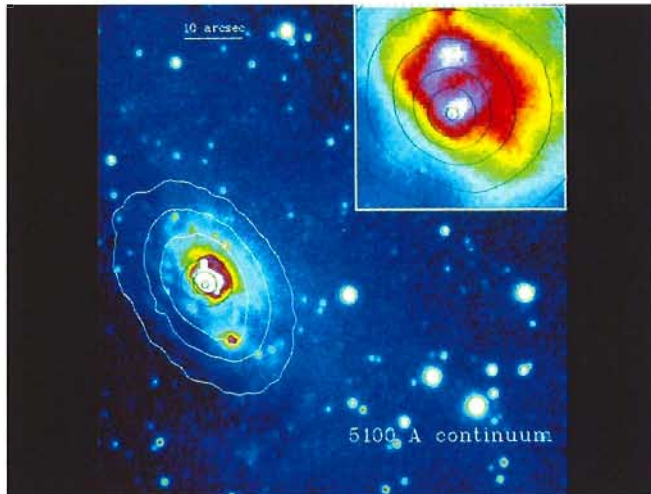


Figure 1: SUSI image of the Circinus galaxy in the 5100 Å continuum. N is at the top and E to the left. The 10'' scale bar applies to the large image and the insert shows the nuclear region enlarged by a factor 5. The contours are from the K'(2.1 μm) image. Note the double nucleus at 5100 Å and the displacement of the K' peak relative to the southern component.

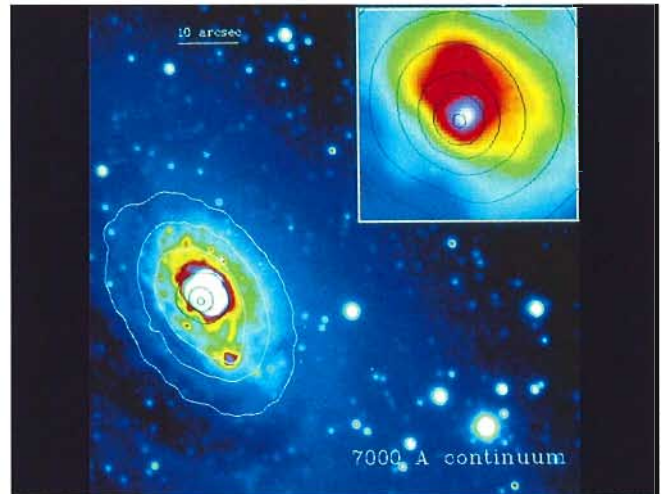


Figure 2: Same as Figure 1 at 7000 Å. Note that only the southern 'nucleus' is visible.

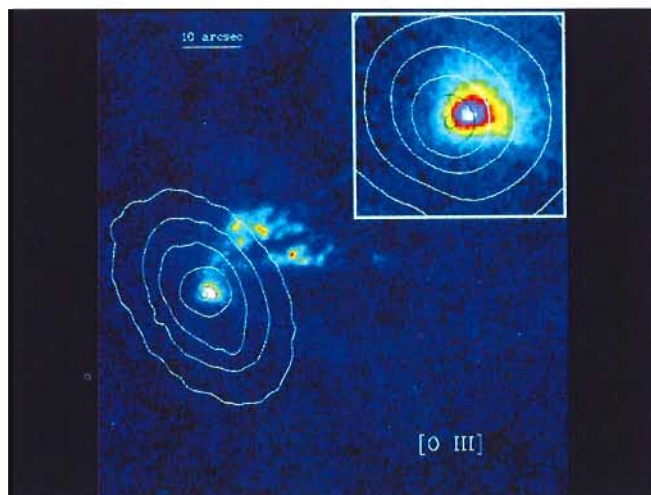


Figure 3: Same as Figure 1 but in the [OIII] line. Note the clear cone-shaped structure and the displacement between the line and K' continuum peaks.

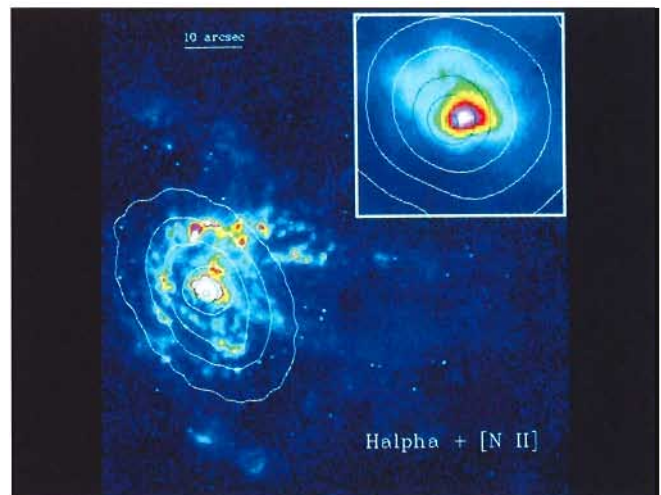


Figure 4: Same as Figure 1 but in the Hα + [NII] which reveals a partial starburst ring.

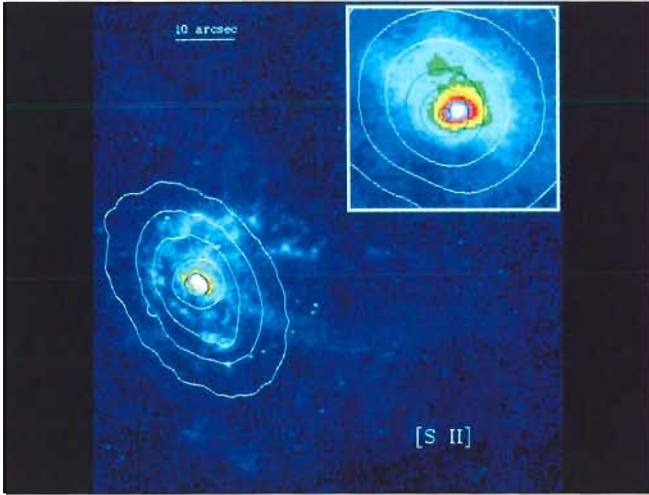


Figure 5: Same as Figure 1 but in the [SII] line. Note the remarkable chain of spots in the SW which are probably supernova remnants.

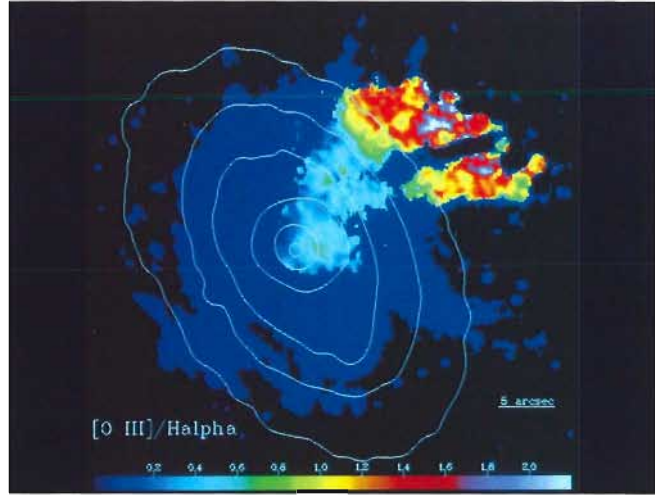


Figure 6: [OIII]/($H\alpha$ + [NII]) showing the ionization structure of the cone. The uniform dark blue region is where $H\alpha$ + [NII] but not [OIII] was detected at more than 10σ .

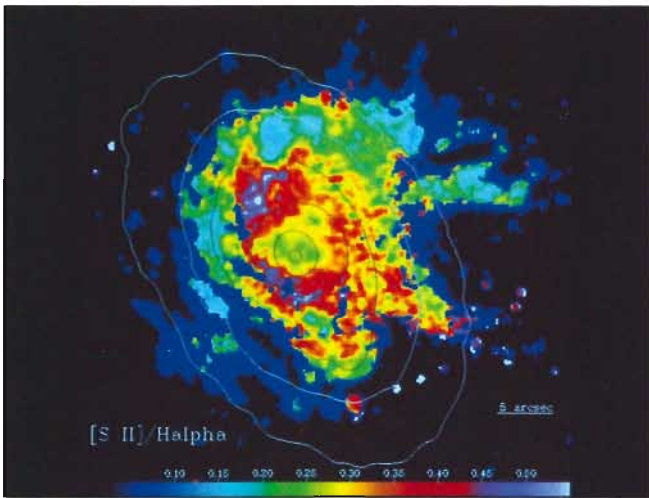


Figure 7: Same as Figure 6 for [SII]/ $H\alpha$. The chain of spots in the SW believed to be supernova remnants are particularly obvious.

the ESO filters (including transmission curves) can be found within MIDAS using the command CREA/GUI FILTER.

In each filter we took several short (15 min) integrations with the object at different positions on the CCD. The images were then flat-fielded, dark-subtracted, realigned and stack together using AVERAGE/IMAGE which also removed cosmic-ray events (using the 'median option'). The resulting frames were then sky subtracted and flux calibrated following standard procedures.

The most difficult part of the reduction was the continuum subtraction. The galaxy lies close to the galactic plane in a field crowded with foreground stars of different colours (Figs. 1, 2) and, within the galaxy itself, there are large colour variations caused by patchy extinction (e.g. a dust lane) and different stellar populations (e.g. a bluer starburst in the central few arcsec). A straight line-continuum (e.g. $H\alpha$ -7000 Å) image subtraction produced negative regions corresponding to red objects (including the compact nucleus of the galaxy) while blue objects left a positive residual. This problem was overcome by creating artificial continuum images at the line wavelengths using a power law interpolation between continuum frames at shorter and longer wavelengths. This gave satisfactory results for all line images except [FeXI] whose underlying continuum (at $\lambda \simeq 8000$ Å) could not be accurately reproduced by extrapolation from 7000 Å (the reddest continuum point) while a suitable longer wavelength filter could not be simultaneously mounted in SUSI for technical reasons. Adding the J (1.25 μm) IR broad band image provided a partial solution but at the cost of decreased image quality (the IR image was taken under poorer seeing conditions).

The IR images were obtained with the IRAC2 camera at the ESO/MPI 2.2-m

is the evidence for circumnuclear starbursts in many Seyferts which may be only circumstantially associated with the AGN activity but could also be consistent with suggestions that the central black hole forms and/or is fuelled by the remnants of a precursor starburst.

In the Circinus galaxy, at a distance of only 4 Mpc, we believe we have discovered the closest example of a Seyfert galaxy showing both a prominent ionization cone and a circumnuclear starburst ring. Circinus is a spiral galaxy of uncertain type which lies close to the galactic plane and whose IRAS infrared luminosity is a moderate $10^{10} L_{\odot}$. Evidence for Seyfert activity is provided by its large [NII]/ $H\alpha$ ratio and, more compellingly, by its extremely prominent visible and infrared coronal lines from ions with ionization energies up to 300 eV (Oliva et al. 1994, hereafter O94) including [SiIX](3.95 μm , 303 eV) and [SiX](1.26 μm , 323 eV) detected for the first time.

In order to further investigate the nature of this galaxy within the above con-

text we have obtained both line ([OIII], $H\alpha$ + [NII], [SII], [FeXI]) and continuum (5100, 7000 Å, J(1.25 μm), H(1.65), K'(2.1)) images using SUSI at the NTT and IRAC2 at the 2.2-m telescope on La Silla. Our purpose here is to describe the observations and show the results which, because of the closeness of this galaxy, provide very striking examples of an ionization cone and circumnuclear starburst. A more detailed analysis, including the modelling referred to below, will be published in a forthcoming paper.

Observations

Optical line and continuum images were obtained in April 1993 with SUSI at the NTT. Seeing which was both good ($\simeq 0.7''$) and stable for several hours contributed to obtaining a satisfactory subtraction of background stars in the final line images. The filters employed were ESO #700 ([SII]), #629 ($H\alpha$ + [NII]), #369 ([OIII]), #430 (5100 Å continuum), #443 (7000 Å continuum) and #415 ([FeXI] λ 7892). More details on

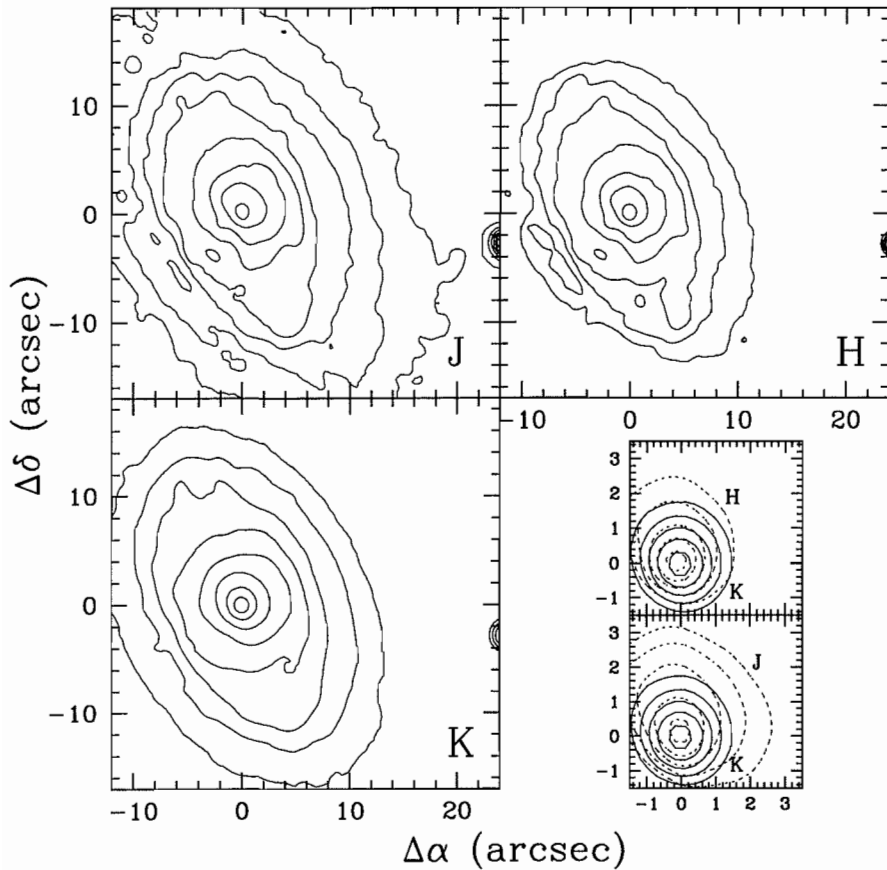
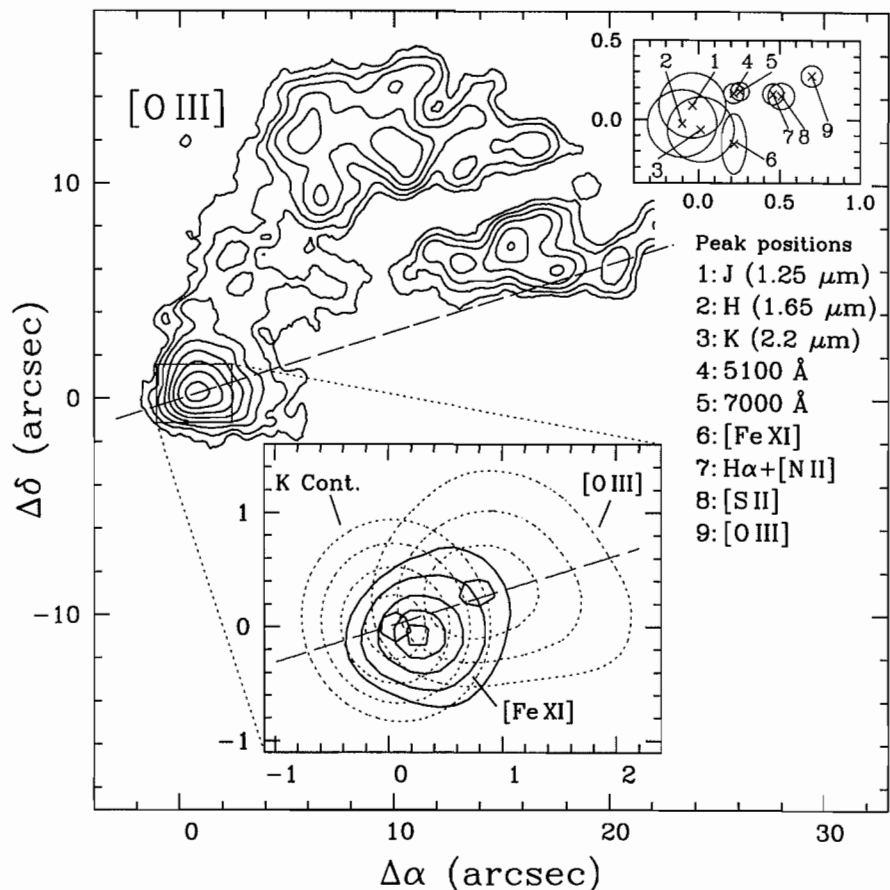


Figure 8: Contour plots from the IRAC2 J, H and K' images. The insert shows an increase in compactness with increasing wavelength but no relative displacements (within the uncertainties) of the single nuclear peak.

telescope. The K'(2.1 μm) image was obtained in July 1993 under photometric conditions but relatively poor seeing conditions ($\text{FWHM} \simeq 1.6''$) while the J and H observations were performed in June 1994 through thin cirrus but with better image quality (seeing $\text{FWHM} = 0.9\text{--}1.0''$). Data consisted of several pairs of object and sky frames plus dome flats with different levels of illumination. The scale in all images was $0.27''/\text{pixel}$ (lens LB of IRAC2) which provided an adequate field of view with proper sampling of the seeing disk.

For the data reduction sky images were first computed from the stack of sky frames (including removal of the back-

Figure 9: Summary plot showing the relative locations of line and continuum features. The contours in the upper part are [O III] and the enlarged view of the nuclear region shows the coronal [Fe XI] line distribution and its location relative to both [O III] and the K' continuum (nucleus). The insert in the upper right hand corner shows the relative displacements of the various line and continuum peaks. Note that all the visible peaks are displaced along the cone relative to the K' peak and that the [S II] (low ionization) line is strongest between the higher excitation [O III] and [Fe XI] line peaks.



ground stars) and subtracted from the object frames. The resulting frames were then flat-fielded and stacked to create the final images which were finally flux calibrated using measurements of standard stars.

One advantage of the large number of foreground stars was that the relative positional alignment of the infrared and visible images could be accurately determined without using features within the galaxy itself.

Results

False-colour representations of the optical continuum and line images are shown in Figures 1–5 together with the overlaid K'(2.1 μm) isophotes and enlargements ($\times 5$) of the nuclear region in the top right corners. Details are given in the captions. Note the small shift between the K' and optical continuum peaks which is about 2.5σ of the residuals in the image alignment.

Line ratio images, produced by smoothing the line frames and including only the pixels where both lines were detected above 10σ , are shown in Figures 6–7; the uniform dark blue zones represent regions with detected H α + [N II] but with no [O III] or [S II] emission within the above limits.

Contour plots of the IR broad band images are displayed in Figure 8 together

with an enlargement of the central region which clearly shows that, although the nucleus is much more peaked in K' than in H and J, its position does not vary significantly with wavelength (the IR images are aligned within $0.2''$).

The relative positions of the central peaks in the various lines and continua are summarized in Figure 9 where we also include the contours of the [FeXI] coronal line image (see also O94). Note that, while the optical line/continua images are aligned within $0.04''$, the relative position of the IR peak is more uncertain ($\pm 0.2''$ 3σ) but sufficient to show a shift between the optical and IR continuum peaks.

A 'true-colour' line image (red = [SII], green = $H\alpha$ + [NII], blue = [OIII]) is shown in Figure 10 where the structure of the cone and of the surrounding galaxy are best visible.

The nucleus

In the continuum at 5100 \AA (Fig. 1) the emission is dominated by late B stars associated with an old starburst and extends over several arcsec with two spatially resolved peaks which are separated by $2''$ N-S but connected by a fainter bridge. The southern peak is coincident with the much more prominent 7000 \AA nucleus (Fig. 2) which is single and unresolved. In the infrared (Fig. 8) the nucleus also shows only a single peak whose position is coincident at J, H and K' but which is more sharply peaked at K'. This infrared peak is also shifted by $0.25''$ relative to the southern visible peak in the direction away from the ionization cone (Fig. 9). We therefore assume that the 'true' nucleus is at or close to the position of the infrared peak and that the shift of the visible peak is an extinction effect. Extinction of the 'true' nucleus by $A_V \simeq 20$ magnitudes would be enough to hide it at 7000 \AA but not at $1.25 \mu\text{m}$ and this value is close to that derived from the $9.7 \mu\text{m}$ silicate feature (Moorwood & Glass, 1984). The northern peak at 5100 \AA shows faint $H\alpha$ and [SII] emission, indicative of HII regions or supernova remnants, but its nature is unclear and we have proposed polarimetric imaging with HST to test if the visible 'nuclear' emission is dominated by scattered light.

The ionization cone

The galaxy shows a spectacular, one-sided [OIII] ionization cone (Fig. 3) whose asymmetry is probably due to extinction by the galaxy disk ($i \simeq 65^\circ$) which also contains a prominent dust lane visible to the SE of the nucleus in the continuum images (Figs. 1, 2).

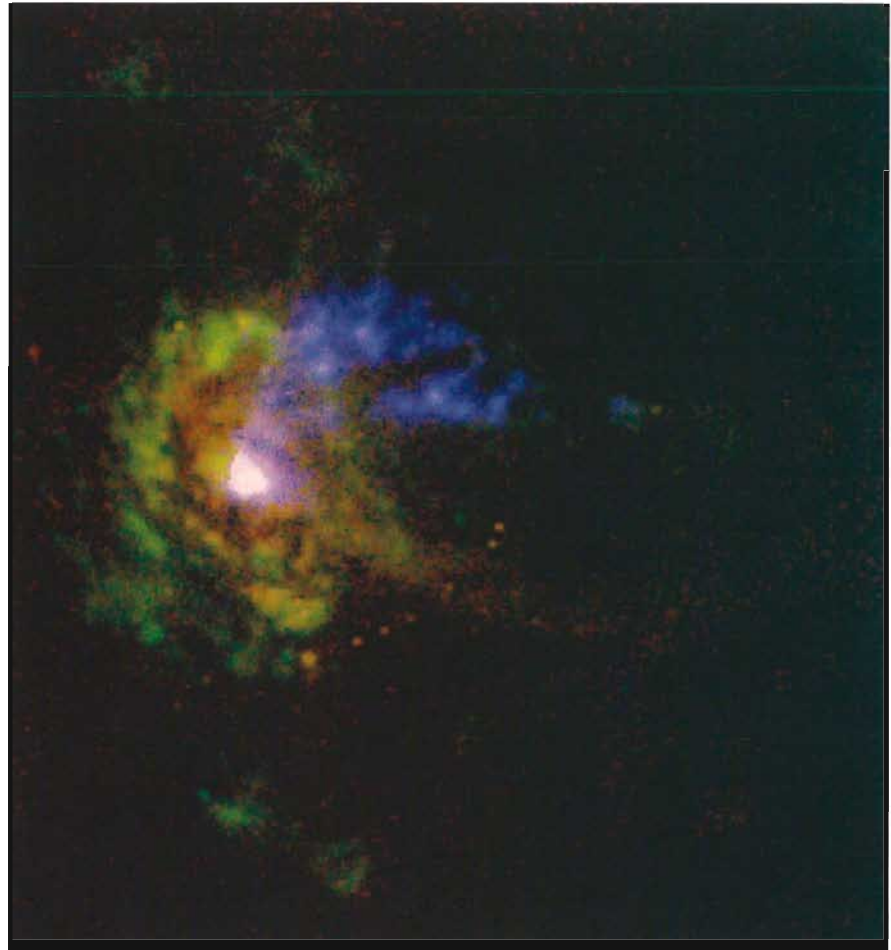


Figure 10: A 'true colour' image of the Circinus galaxy with red = [SII], green = $H\alpha$ + [NII] and blue = [OIII]. This representation clearly shows the ionization cone, the extended circumnuclear starburst and the chain of supernova remnants to the S.

Within the cone there are high-excitation [FeXI] (see O94 for more details of the coronal line emission) and [OIII] clumps with observed $[OIII]/H\alpha + [NII] > 2$ (Fig. 6) or > 4 after correction for reddening. The relative positions of the various line and continuum peaks are shown in Figure 9. Both the intensities and spatial distribution of the high excitation lines can be modelled assuming photoionization by a power law spectrum and a suitably low gas density, i.e. $n_e \sim 40 \text{ cm}^{-3}$, to obtain an ionization parameter $U \approx 0.01$. Pure photoionization models, however, cannot explain the simultaneous appearance of the prominent [SII] emission which peaks between [FeXI] and [OIII] and is coincident within $0.1''$ with the $H\alpha + [NII]$ peak (Figs. 4, 5, 9) and reaches $[SII]/H\alpha + [NII] \geq 0.4$ in some regions (Fig. 7). Our actual model which reproduces the high-excitation species predicts that [SII] should be produced about $0.4''$ beyond the [OIII] peak and pure photoionization models in general are unable to account for this reverse distribution regardless of the adopted nuclear ionizing continuum. A similar problem was found in a

detailed spectroscopic study of the extended NLR of NGC 1068 (Bergeron et al. 1989). One possibility is that the [SII] knot is a photodissociating (or photoevaporating) molecular cloud with a large column density of freshly ionized gas leaving the cloud at sound speed ($\sim 10 \text{ km/s}$) which shields the rest of the material from soft ionizing photons but is transparent to X-rays ($h\nu > 100 \text{ eV}$) which produce a large partially ionized region at the surface of the cloud.

We expect to obtain more detailed information on the relative roles of photoionization and other excitation mechanisms from visible (EMMI) and infrared (IRSPEC) spectroscopy scheduled at the NTT in March 1995.

The line emission outside the cone (P.A. $< 10^\circ$) is typical of low excitation HII regions and is probably associated with the circumnuclear starburst described below.

Circumnuclear starburst activity

The $H\alpha$ image (Fig. 4) clearly reveals the presence of a young starburst ($\leq 10^8$ yr) lying $\simeq 10''$ (200 pc) from the nu-

nucleus and almost encircling it. Our supposition that the brightest extranuclear $H\alpha$ emission is from normal HII regions is also supported by the very low values of $[SII]/H\alpha+[NII]$ (Fig. 7).

Between the nucleus and the outer starburst there are regions with remarkably strong [SII] emission (Fig. 5) which most probably traces shocks from supernova remnants.

A remarkable feature is the series of 'spots' visible in the continuum and low-excitation lines (Figs. 1, 4, 5, 7 and 10) which are aligned along a chain $\simeq 20''$ south of the nucleus. These are the lowest excitation objects (i.e. those with the highest $[SII]/H\alpha+[NII]$ ratio) which, together with their sizes ($\simeq 30$ pc), suggests that they are individual supernova remnants, possibly in small OB associations dominated by B stars. Additional spectroscopy and/or radio observations are needed to clarify their exact nature. As their orientation does not correspond to any obvious morphological feature we can only presume that they trace the location of a gaseous spiral feature in which starburst activity has already ceased.

Within the central $R \leq 2''$ (4 pc) the optical continuum images and the stellar absorption features observed in the opti-

cal and IR spectrum (Oliva et al. 1994, in preparation) are well fitted by a combination of late-B main-sequence stars and late K supergiants, i.e. typical of a starburst which is much older (many $\times 10^8$ yr) than the starburst ring.

The above results are consistent with a simple model in which a starburst propagates out of the nucleus. At the outer edge we see the most massive O stars from the latest generation (those photoionizing the HII regions) while closer inside less massive (early B) stars are still producing supernovae and remnants responsible for the [SII] emission. In the central regions (nucleus excluded) the high density of late B stars is responsible for the unusually blue colours while K supergiants dominate the near IR emission.

Conclusions

Line and continuum images of the Circinus galaxy have revealed a prominent ionization cone with coronal gas ([FeXI]) close to its apex and lower excitation [OIII] emission further out which is consistent with photoionization by a power law central source. Low excitation [SII] emission observed between the [FeXI] and [OIII] peaks, however, can-

not be explained by pure photoionization models. This cone originates in a nucleus whose visible and infrared positions are spatially shifted suggesting that the true nucleus suffers $A_V \simeq 20$ magnitudes of extinction. Our observations are thus consistent with the presence of a torus which both obscures the Seyfert nucleus from direct view and collimates its UV continuum emission. In addition, a starburst ring which may or may not be related to the Seyfert nucleus is also present. Older starburst activity, which is perhaps more relevant to the possible evolutionary connection between starbursts and Seyfert activity, appears to have occurred closer to the nucleus. A puzzling discovery is the chain of compact, low excitation, objects $\simeq 20''$ S of the nucleus which are probably supernova remnants and associated B stars but require further study.

References

- Antonucci, R., 1993, *ARAA*, **31**, 473.
 Bergeron J., Petitjean P., Durret F., 1989, *A&A* **213**, 61.
 Moorwood A.F.M., Glass I.S., 1984, *MNRAS* **135**, 281.
 Oliva E., Salvati M., Moorwood A.F.M., Marconi M., 1994, *A&A* **288**, 457.

Multi-Wavelength Study of ROSAT Clusters of Galaxies

M. PIERRE, CEA/DSM/DAPNIA CE Saclay, France, and Max-Planck-Institut für Extraterrestrische Physik, Garching, Germany

R. HUNSTEAD, A. REID, G. ROBERTSON, University of Sydney, Australia

Y. MELLIER, G. SOUCAIL, Observatoire de Toulouse, France

H. BÖHRINGER, H. EBELING, W. VOGES, Max-Planck-Institut für Extraterrestrische Physik, Garching, Germany

C. CESARSKY, J. OUKBIR, J.-L. SAUVAGEOT, L. VIGROUX, CEA/DSM/DAPNIA CE Saclay, France

1. Clusters of Galaxies as Cosmological Probes

Among the 60,000 X-ray sources detected by the ROSAT All-Sky Survey, about one tenth are expected to be clusters of galaxies. This represents a considerable potential for cosmological studies and has motivated numerous identification campaigns, especially at ESO; we describe here such a programme together with associated observations at other wavelengths.

As the most massive bound enti-

ties known in the universe, clusters of galaxies are key objects for testing the predictions of the various cosmological scenarios. They originated from the highest peaks in the initial density fluctuations, and are expected to have evolved through characteristic processes, namely, "top-down" or "bottom-up" depending on the nature of the dark matter ("hot" or "cold"). Practically, these alternatives correspond to situations in which clusters formed either from the fragmentation of large "pancakes" or from the merging of sub-groups, and

should ideally be reflected in the evolution of the cluster mass function. While the mass of a cluster is not a directly observable quantity, a number of other physical parameters can be measured directly and, therefore, provide a detailed picture of the dynamical cluster environment as a function of redshift.

2. Observational Tests

Relevant observations of clusters encompass the whole electromagnetic spectrum; a short overview includes:

- In the optical, velocity dispersions obtained through extensive spectroscopy of cluster galaxies provide mass estimates, while the presence of sub-groups in the velocity distribution may be the signature of merging events in the past history of the cluster.
 - In X-rays, the cluster temperature function could in principle yield an almost direct determination of the mass function if virialization is assumed. However, temperatures are known for very few clusters, and the sensitivity of the collimators (prior to ASCA) restricts such observations to the closest objects. On the other hand, the cluster luminosity function is much easier to obtain, and evolution was detected in the Einstein Medium Sensitivity Survey sample (e.g. Henry et al. 1992 and references therein). A tight empirical correlation between X-ray luminosity and temperature then enables the shape of the initial fluctuation spectrum in CDM scenarios to be constrained (Henry & Arnaud 1991).
- Because the mean free path of the hot X-ray emitting gas in the cluster potential is considerably shorter than that of the galaxies, the X-ray morphology (and size) of clusters provides insights into subclustering and merging events which are complementary to the optical approach.
- The radio emission from a possible cluster halo or particular cluster galaxies may be also a powerful tool for investigating the physical state and motions of the hot intra-cluster medium. Since the interaction between the hot plasma and galaxy halos strongly affects the shape of the radio emission, the presence of Head-Tailed galaxies at the cluster periphery or Wide Angled-Tailed at the cluster centre (usually cDs) can constrain the properties of the gas and on the gravitational potential.
 - As for the infrared emission of clusters of galaxies as such, only weak IRAS diffuse emission was detected from a small number of poor clusters, but its origin is not yet clear (Bregman 1992). Moreover, clusters are expected to be the sites where galaxy interactions are favoured, leading to enhanced star formation. This is a totally open field, and one expects exciting new results especially from the comparison between infrared and radio properties of clusters.

With the coming of large collecting area instruments, providing high spatial and spectral resolution at wavelengths far beyond the optical regime, a new era will open up, enabling the detailed study of moderately distant clusters.

3. The Cluster Sample Observed at ESO

In 1990 we started an observing programme at ESO, aiming at identifying all clusters detected by ROSAT in a single contiguous area covering about 1700 deg² around Hydra (a similar programme is being pursued at the AAT around the SGP). The main goals of the project are to derive the *cluster X-ray luminosity function* and study the *large-scale structures* by the spatial cluster distribution. The cluster candidates are selected by cross-correlating the X-ray source lists, issued from the ROSAT survey standard analysis, with the ROE/NRL cluster catalogue, the latter resulting from an automated analysis of the COSMOS object database derived from the scans of the UK/AAO Schmidt plates. With this method about 150 cluster candidates have been selected down to an X-ray flux limit of $\sim 5 \times 10^{-13}$ erg s⁻¹ cm⁻² in our area.

During the 1990–92 period the programme was allocated a total of 13 nights with EFOSC on the 3.6-m telescope. The strategy has been to observe the target objects in order of decreasing X-ray flux, so that at any stage the current data set is flux limited. For most clusters the multi-slit mode is used (otherwise, long slit) so that 5–12 redshifts per cluster are available, providing in some cases an estimate of the velocity dispersion. For this first identification step, the EFOSC+MOS mode – giving on average 7 redshifts per cluster – presents the ideal observing set-up, for it allows us to assess directly the membership of our cluster candidates. Unfortunately, we should mention several practical problems encountered in all runs during the fabrication of the masks, which turned out to be very time consuming: bad transmission between the computer holding the slit positions and the punching machine, punching pin breaking down several times, and overall uneven slit quality leading to unrecoverable artefacts in the sky subtraction during the subsequent data analysis. But we acknowledge here the valuable assistance of the local technical team which enabled us every night to have our masks ready in time. At present, the redshifts of some 60 clusters have been measured and a detailed optical/X-ray analysis of the 42 brightest ones is presented in Pierre et al. (1994). The most distant cluster in the sample found so far has a redshift of ~ 0.31 , and the X-ray sensitivity of the area leads us to expect objects up to $z \sim 0.4$. The programme will be continued in the coming years in order to complete the identification of the sample and thus achieve our scientific goals. *For the first time, we shall have at our disposal a complete X-*

ray flux limited sample of clusters over a large area which will constitute a unique tool for studying luminosity and clustering evolution.

4. Combined Observations

The analysis of the optical/X-ray properties of the clusters discovered in the Hydra region revealed some very interesting objects which motivated a more detailed multi-wavelength follow-up starting in 1992. We selected a subsample of intrinsically X-ray-bright clusters, which are therefore expected to be massive and with redshifts preferentially above 0.15. The following observing programmes are now underway:

(1) In the optical, the northernmost objects of the sample have been subsequently studied at the 3.6-m Canada-France-Hawaii telescope in 1993 and 1994. Deep B, R photometry and extensive spectrometry (~ 80 spectra per cluster) – with the MOS/SIS device using a 10' \times 10' CCD (2048² pixels) – have been obtained in collaboration with the Toulouse group.

(2) ROSAT PSPC pointings, for a few selected cases, in order to investigate the outer cluster regions, where on-going merging events are expected to be most readily detected, and to obtain a first estimate of the temperature.

(3) ROSAT HRI deep pointings, to study in detail the gas morphology and the cluster potential at the centre: substructures and correlation with the cD position (in progress).

(4) Radio observations started in 1993 in collaboration with the University of Sydney. The selected clusters are first imaged at 843 MHz with the Molonglo Observatory Synthesis Telescope (MOST; 43'' resolution); subsequently, higher resolution maps of the cluster radio sources are obtained with the Australia Telescope (AT; 1.4–5 GHz, 2–7'' resolution).

(5) A subsample of 14 objects will be observed by the ISO satellite (1995) in the Central Programme at 7, 14 and 90 μ m (29 hours are allocated to this project: Cesarsky et al.).

5. Multi-Wavelength Maps

In order to exploit fully the 2-D information provided by the images obtained at different wavelengths, the ideal is to overlay them accurately so that a comprehensive picture of the cluster environment is readily available. Of special interest is any correlation amongst the optical galaxy positions, particularly the cD, the X-ray centroid of the hot ICM (and possibly other field X-ray sources), and the radio sources. This provides important clues:

(i) Radio sources can be identified and localized within the cluster;

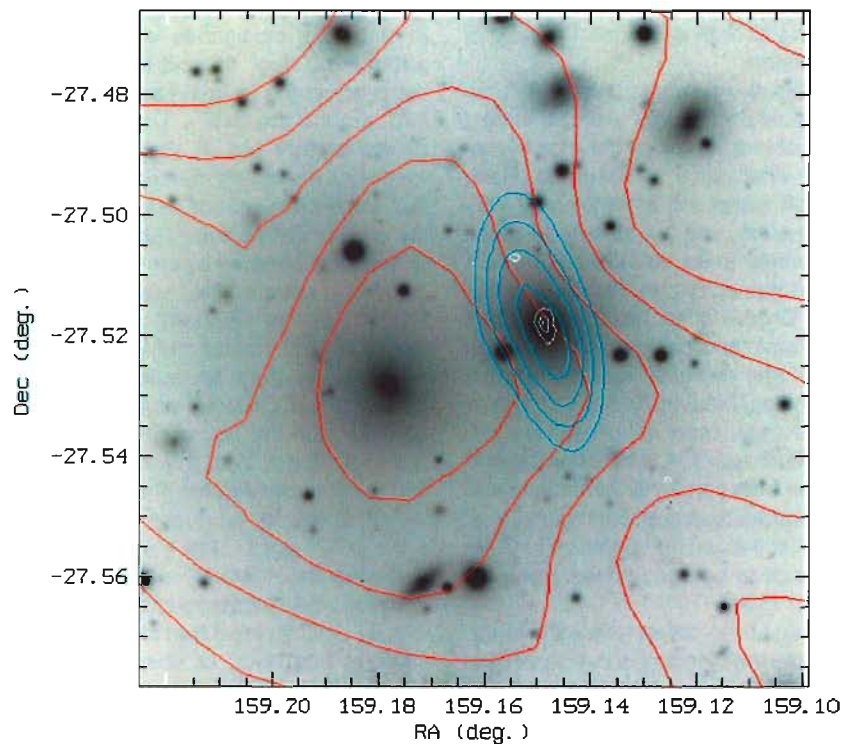
(ii) It enables a detailed morphological study, such as a comparison of the overall shape of the cluster emission in X-rays (elongation, clumps) with the galaxy distribution in the optical (alignments, sub-groups). This point is especially relevant for the investigation of the formation processes of clusters: the presence of structures in the X-ray emission associated with (velocity) sub-groups of galaxies is undoubtedly a strong argument in favour of the merging hypothesis (see Section 1). Moreover, if both X-ray and radio spatial resolutions are high enough ($\sim 5''$), then for the nearest objects, an even more detailed study of the motions within the ICM is possible with the combined morphological analysis of interactions between the hot X-ray emitting plasma and the energetic particles producing the radio lobes (Böhringer et al. 1993);

(iii) Another interesting point to investigate is the location of the cD galaxy with respect to the X-ray centroid. In the optical, there are evidences for the existence of substructures when the cluster dominant galaxy velocity shows a significant offset with respect to the cluster's mean (Beers et al. 1991). A non-coincidence between the optical and X-ray centres (the latter is supposed to indicate the centre of the cluster potential) may be the signature of merging events in the cluster's history.

(iv) Finally, it allows flagging X-ray emitting point-like objects (stars or AGNs), which may contaminate the diffuse cluster emission (a crucial problem in the further determination of the X-ray cluster luminosity function). Such an overlay is presented in the Figure, and the procedures followed to produce this image are described on page 46 in this issue of *The Messenger*.

ROSAT [0.4-2.4 keV]

MOLONGLO [843 MHz]



1st contour: (cnt/sec/sq.arcmin) (Jy/Beam)
 step: 1.72800E-03 5.39926E-04
 1.15200E-03 1.50000E-03

ROSAT X-ray (red) and Molonglo radio (blue) contours overlaid on the corresponding CCD optical image. The absolute instrumental positional accuracy is $\sim 1-2''$ in the optical and radio, and $\sim 20''$ in the X-ray band (1σ); the plotting accuracy is discussed on page 46 in this issue of *The Messenger*. First and step contours are indicated on the figures.

(Left) Abell 1060 ($z = 0.0124$) is a nearby cluster with low radio power ($\log P(\text{WHz}^{-1}) = 22.3$, $H_0 = 50 \text{ km s}^{-1} \text{ Mpc}^{-1}$) and X-ray luminosity ($\sim 5 \times 10^{43} \text{ erg s}^{-1}$). In this case the number of X-ray survey photons is greater than 1000; in order to improve the angular resolution, we selected only photons falling into the inner part of the detector so that the resulting PSF has a FWHM of $\sim 1'$ instead of $\sim 2'$ (but the number of photons is decreased by a factor of ~ 5.5). Two large elliptical galaxies occupy the centre of the cluster. The radio emission clearly coincides with the brighter galaxy (NGC 3309), whereas the X-ray centroid appears to favour the other

6. Preliminary Results

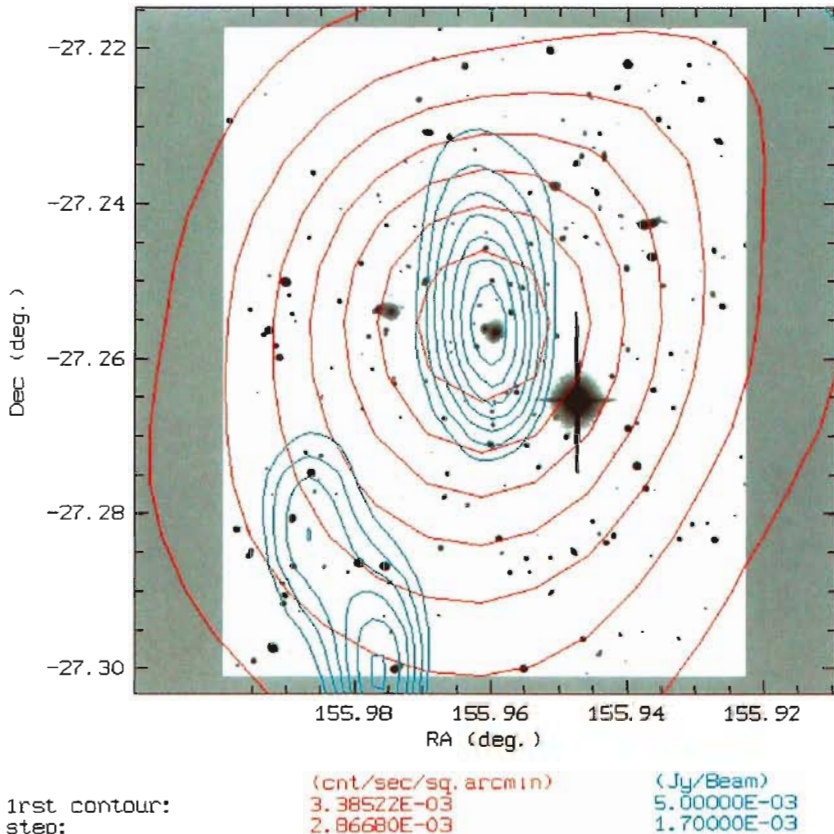
Reduction of the CFH data and ROSAT pointings is in progress, as well as the processing of the AT observations. MOST and AT images have been obtained for 25 clusters so far (from $z \sim 0.01-0.3$). A preliminary comparison between X-ray, optical and radio survey images reveals that for a high fraction of clusters there is coincidence between the X-ray centroid (or an X-ray peak) and the presence of a radio galaxy (see Pierre, Hunstead & Unewisse 1994 for more details). This is in agreement with the findings of Burns et al. (1994) who attribute this to a combination of clumped hot gas and AGN emission. We will be investigating this more closely with the high-resolution X-ray and radio images. More-

over, our sample, which possesses a significant fraction of objects at $z \geq 0.1$, suggests that the coincidence between X-ray and radio maxima is even stronger for high redshift clusters. One explanation for this effect could arise from the fact that the original sample is close to being X-ray flux limited, which means that the distant clusters are 10-100 times brighter intrinsically than the nearby ones. Consequently, we might have been selecting objects in which the X-ray flux is contaminated significantly by emission from an active galactic nucleus. Indeed, in our sample we found the second brightest BL Lac object in the sky. Detailed optical spectroscopy as well as high resolution radio observations of the galaxies

concerned is now underway, in order to characterize their properties.

At the present stage it is too early to draw definitive conclusions from the X-ray/radio correlations, but if these preliminary results are confirmed with better statistics, this may have serious consequences for the practical determination of the cluster X-ray luminosity function. On the other hand, this is only one aspect of the entire programme which, once completed, should provide a unique set of data for the dynamical study of clusters up to $z \sim 0.3$. In this way, we hope to be in a position to understand better their formation process, and thus to constrain the nature and amount of dark matter present in the universe.

ROSAT [0.4-2.4 keV] MOLONGLO [843 MHz]



(NGC 3311). The white contours are from a recent high-resolution image obtained at 13 cm with the Australia Telescope; the radio source appears, however, not to be resolved. The CCD image is a 250 s exposure obtained in B band at the AAT.

(Right) Abell 3444 ($z = 0.254$) is one of the most distant clusters in the present sample. At the survey resolution, the X-ray image is point-like. The radio emission is probably slightly extended to the north (which should not be confused with the natural N-S elongation of the beam). Both X-ray and radio intensities are high: $\sim 3 \times 10^{45} \text{ erg s}^{-1}$ and $\log P(\text{MHz}^{-1}) = 24.4$ respectively, and clearly centred on the cluster dominant galaxy. The exact coincidence observed here appears to occur in many of the cluster fields, especially for the high redshift clusters in the sample. The CCD image is a 3-minute EFOSC exposure in R band.

Acknowledgements

M.P. is grateful to the Max-Planck-Institut für Extraterrestrische Physik for long-term financial support. We also acknowledge a grant by the EC Human Capital Programme, contract CHRX-CT92-003.

References

- Beers T.C., Forman W., Huchra J.P., Jones C., Gebhardt K., 1991 *AJ*, **102**, 1581.
 Böhringer H., Voges W., Fabian A.C., Edge A.C., Neumann D.M., 1993 *MNRAS* **264**, L25-28.
 Burns, J. O., Rhee G., Owen F., Pinkey, J. 1994 *ApJ*, **423**, 94.
 Bregman J. N., 1992 in *Clusters and Superclusters of Galaxies*, p. 119, Cambridge, July 1991, Ed. A. Fabian, Kluwer.
 Henry J.P., & Arnaud K.A., 1991, *ApJ*, **372**, 410.
 Henry J.P., Gioia I.M., Maccacaro T., Morris S.L., Stocke J.T., Wolter A., 1992, *ApJ*, **386**, 408.
 Pierre M., Böhringer H., Ebeling H., Voges W., Schuecker P., Cruddace R., MacGillivray H., 1994, *Astronom. Astrophys.* **290**, 725.
 Pierre M., Hunstead R., Unewisse A., 1994, Combined X-ray/optical/radio observations of ROSAT clusters of galaxies, in *Cosmological Aspects of X-Ray Clusters of Galaxies*, p. 73-77, Munster, June 1993, ed. Seitter, Kluwer.

The VLT Site at Paranal: September 1994

The centrefold of "The Messenger" shows an aerial view of Cerro Paranal, the site of ESO's Very Large Telescope. This photo was obtained in mid-September 1994 and shows the rapid developments at the time of the construction of the concrete base for the four telescope enclosures. Also visible is the complex infrastructure for the various associated laboratories. This work is being done by the Skanska/Belfi consortium. The installations for the technical equipment can be seen to the left.

The blasting work is now finished and excavations for the various connecting tunnels are clearly visible; they will be covered again when the concrete work is ready. To the right, the work on the base for Unit Telescope no. 1 is already well under way and in September reached the "floor level" on which the enclosure will be placed. The basement concrete floor on which the coudé focus for Telescope no. 2 will be installed is in place, and the concrete work will soon start in the holes for Telescopes 3 and 4.

To the extreme right and a little lower than the rest of the platform are the excavations for the control building. The platform altitude is about 2640 metres above sea level and it measures about 150 metres across. The width of the access road is no less than 12 metres, i.e. nearly equal to that of a three-lane highway; this is necessary to ensure the safe transport of all telescope parts to the top, especially the four 8.2-m fragile mirrors.

In October 1994, the first shipment of steel parts of this enclosure (manufactured by the SEBIS consortium) with a total weight of more than 100 tons left Europe for the sea journey to Chile. While the smaller parts were packed in large containers, special packing was necessary for the very large structures. The ship left the port of Marghera, Italy, and is expected to dock in Antofagasta towards the end of December 1994, after which the parts will be transported by truck to the top of Paranal.

This first shipment will be soon followed by others. It is expected that consignments of about 100 tons each will be sent to Chile over the next eight months. The enclosure erection will start in January 1995 and will be completed in about 8 weeks.

M. Tarenghi





The Cluster Environment of BL Lac Objects

R. FALOMO, *Osservatorio Astronomico di Padova, Italy, and*
J.E. PESCE, *STScI, Baltimore, U.S.A.*

Introduction

BL Lac objects (hereafter BL Lacs) are an unusual kind of active galactic nuclei (AGN) which exhibit extreme properties of flux variability (large amplitude and short time scales) and polarization together with a strong non-thermal emission over a wide frequency range (e.g. Angel & Stockman 1980; Bregman 1990; Kollgaard 1994).

At variance with most of the other AGN, the optical spectra of BL Lac objects lack the strong emission lines that characterize quasars and Seyfert galaxies. This peculiar characteristic prevents an easy determination of the redshift and the discovery of BL Lacs in optical surveys. Imaging studies have shown, however, that many BL Lacs reside in the nuclei of giant elliptical galaxies, whose contribution is sometimes detectable in the optical spectra, allowing the measurement of the redshift of the sources. In contrast to the thousands of quasars that have been discovered in the last decades, the number of known BL Lacs is less than a few hundred. Only recently with X-ray surveys and/or with a combination of radio, optical and X-ray surveys has it been possible to construct sizeable and complete samples of BL Lacs (Giommi et al. 1991; Stocke et al. 1991; Stickel et al. 1991; Schachter et al. 1993).

The peculiar properties of this class of AGN are currently interpreted, in the framework of unified models, as radio galaxies with a relativistic jet which is closely aligned to the observer's line of sight. The power-law continuum and its polarization and variability together with the superluminal motion shown by many objects are all suggestive of the presence of anisotropic relativistic emission. It is also remarkable that BL Lacs (and blazars in general) are luminous γ -ray emitters (Hartman et al. 1993) providing model-independent support for the presence of relativistic motion in jets (Maraschi, Ghisellini, & Celotti 1992).

This hypothesis, originally proposed by Blandford and Rees (1978), implies the existence of a large number of objects intrinsically identical to the BL Lacs but with the jet pointing away from the observer. It is currently proposed that the low-luminosity (F-R I) radio galaxies (or a fraction of them) may represent the parent population of BL Lacs (e.g. Browne 1989; Urry, Padovani, & Stickel 1991; Kollgaard et al. 1992). As a test of this model one can compare unbeamed

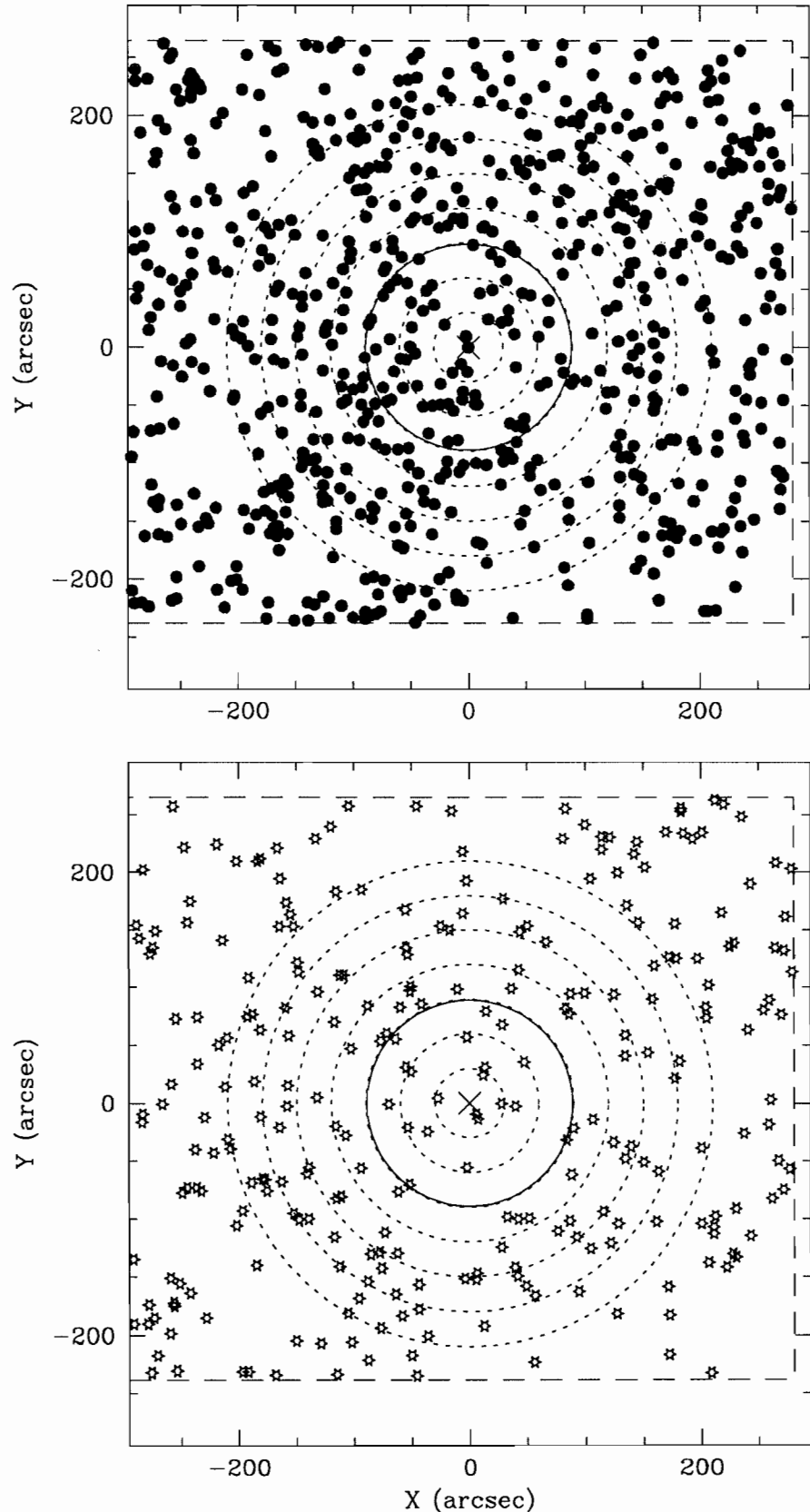


Figure 1: *Distribution of galaxies (top) and stars (bottom) in an EMMI frame (R filter 20 min) as derived from the classification obtained by FOCAS.*

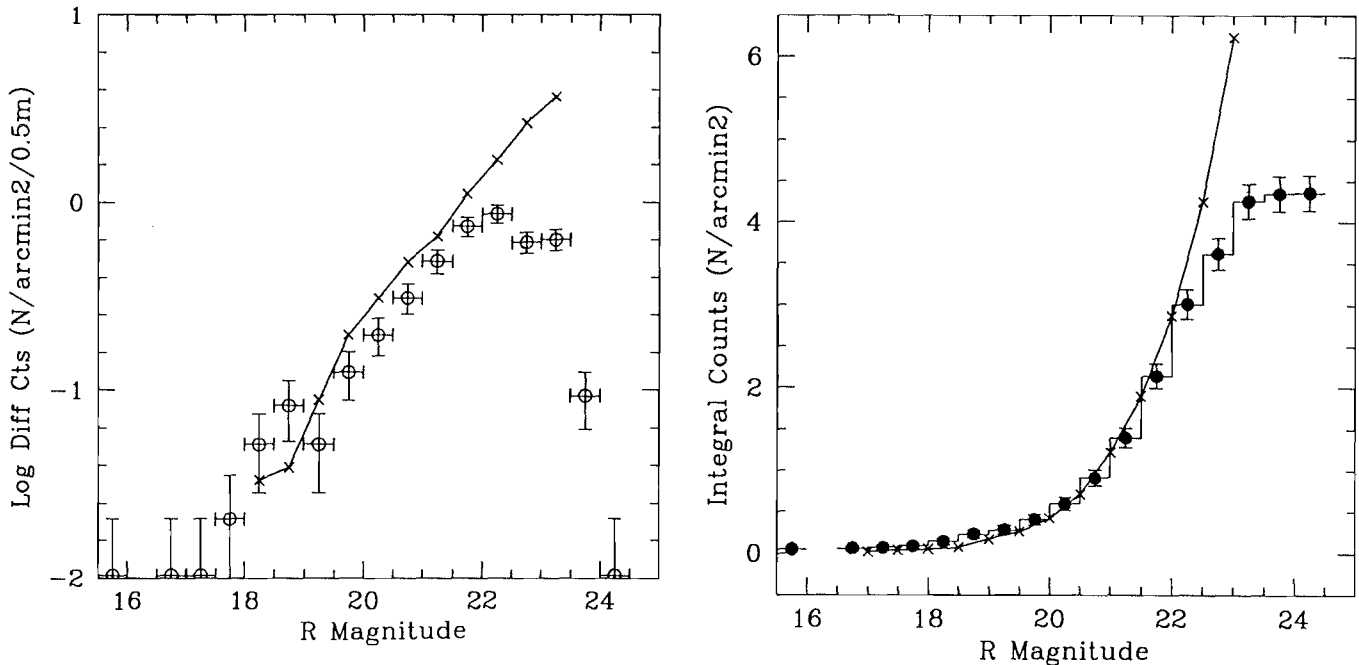


Figure 2: The differential (left) and integral (right) galaxy counts derived from a single CCD EMMI frame (20-min exposure) compared, respectively, with counts by Metcalfe *et al.* (1991) and Hintzen *et al.* (1991) background counts.

properties (such as extended radio emission, host galaxies and environments) of BL Lacs and parent objects or study the relative luminosity functions.

The Environment of BL Lacs

The study of the environment of BL Lac objects may be a useful tool for understanding the BL Lac phenomena. It gives clues to the role played by the environment for triggering and fuelling the activity in elliptical galaxies and in particular may help to enlighten the relationship between BL Lacs and their parent population.

Contrary to the case of quasars, the study of the environs of BL Lacs is complicated by the faintness of their spectral lines with respect to the continuum, hindering the derivation of redshifts and, thus, the proof of physical association with nearby galaxies.

Until recently only a few studies have been conducted on the cluster environment of BL Lacs (Disney 1974; Craine, Tapia, & Tarengi 1975; Butcher *et al.* 1976; Fosbury & Disney 1976; Ulrich 1978). These investigations generally failed to provide clear evidence of a physical association and it was suggested that BL Lacs may avoid cluster environments (Weistrop *et al.* 1981).

The use of modern instrumentation on large optical telescopes enabled the study of BL Lac environments in a much more effective way. For more than half of the known BL Lacs the redshift has been determined either from weak absorption lines of the host galaxy or from interven-

ing absorption lines that give a lower limit to it. On the imaging front the capability to detect and classify galaxies over a large field of view is now easily achievable.

Here we present a summary of the results obtained from a programme undertaken at La Silla to investigate the environments of BL Lacs and outline the analysis procedure adopted. To date we have observed ~ 20 targets that are a mixture of radio- and X-ray selected objects.

The capability of NTT to change the instrument configuration during the same observing night also enabled us to obtain high-resolution images with SUSI in order to study the close environment and host galaxy properties for a number of BL Lacs. Here, however, we concentrate on the large-scale environment.

Observations and Data Analysis

We used the ESO NTT operated both at La Silla and via remote control from Garching to obtain images and spectra of the fields around BL Lacs. Conditions were photometric and seeing (FWHM), as measured on the CCD frames, ranged from 0.7 to 1.5 arcsec for most of the data obtained. We obtained pairs of images of the fields around BL Lacs using EMMI in the R filter with typical exposure times of 2 and 20 minutes. The EMMI images cover a useful field of 7.5×7.5 arcmin² at a scale of 0.44 arcsec pixel⁻¹ (TH 1024 \times 1024 pixels; pixel size 19 μ m) or 9.7×8.5 arcmin² at a scale of 0.35 arcsec pixel⁻¹ (1660 \times 1450 pixels) depending on the CCD used. This corresponds to

0.5–4 Mpc² for objects at $z = 0.07$ –0.6 (we assume $H_0 = 50$ km s⁻¹ Mpc⁻¹ and $q_0 = 0.5$ throughout).

After reduction of images using procedures available in the Image Reduction and Analysis Facility (IRAF; bias subtraction, trimming, flat fielding), cosmetic defects such as saturated rows and columns were cleaned. In certain cases, some saturated stars were removed as these were found to cause problems in a later phase of the analysis. We also removed all detectable cosmic-rays using the IRAF task COSMICRAYS.

In addition to direct images, we obtained spectra of some of the galaxies in the field of BL Lacs for a selected number of objects. A long slit (2'' wide) was oriented in such a way as to secure at least two objects at a time. For all spectra, we employed a grism of 300 gr mm⁻¹ giving a dispersion of 246 Å mm⁻¹ in the range 4000 to 8000 Å. Spectra were wavelength calibrated using an HeAr lamp, and relative flux calibration was derived from observations of standard stars (Stone 1977).

Classification of Objects

Because we want to study the distribution of the galaxies around our programme objects, the most important part of the analysis involves the detection and classification of objects in each image. To detect and classify objects (as stars, galaxies, or noise) we adopted the Faint Object Classification and Analysis Software (FOCAS), developed by Jarvis & Tyson (1981), revised and expanded by

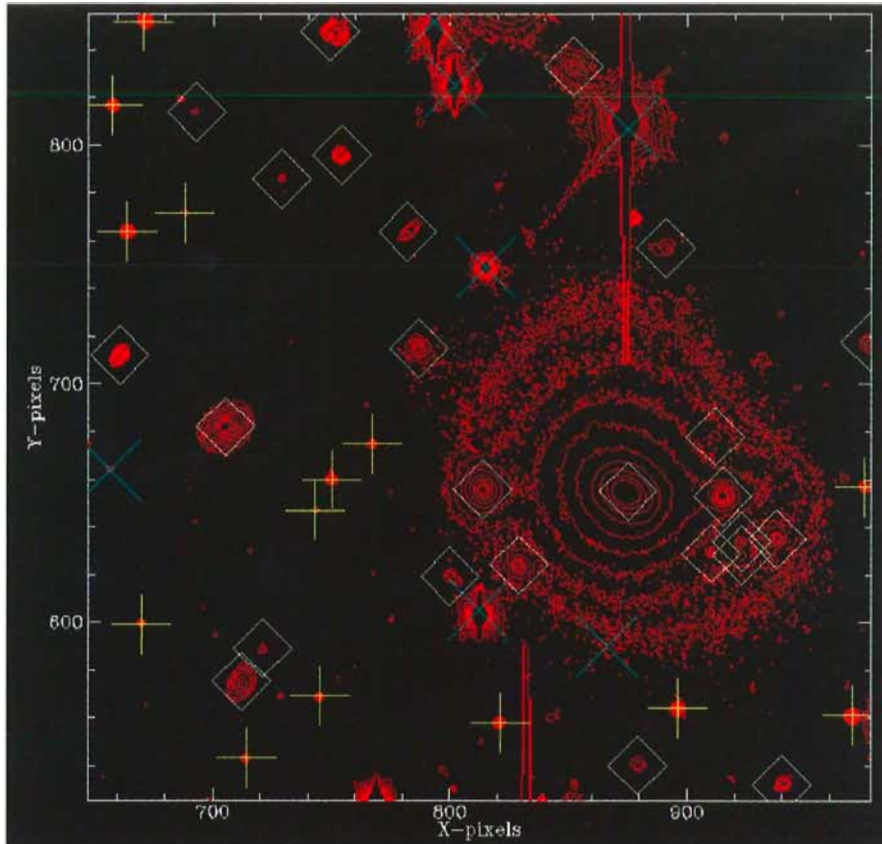


Figure 3: Contour plot of a portion of an EMMI CCD frame with superposed the classified objects (\circ galaxies, $+$ stars, \times defects or saturated stars).

Francisco Valdes of the National Optical Astronomy Observatories.

Classification of the objects is based on a comparison of their shape with the point spread function (PSF) determined from many (usually more than 20) stars in the field. Standard classification templates were used following Hintzen *et al.* (1991). For images taken under good conditions, the total number of objects classified can be more than 600 for a typical 20-minute exposure (see example in Fig. 1).

Objects were detected and classified up to the magnitude limit (usually $R = 22-23$ for a good-quality, 20-minute exposure) for each image. These limits were determined from the peaks of the differential number-count distribution of galaxies (see Fig. 2). Above this limit it becomes difficult to distinguish galaxies from stars with the automatic detection algorithm of FOCAS. Catalogues of objects detected were created for each image. The automatic classification can be checked by manual inspection of random objects all over the image. This however requires a considerable amount of time.

In order to speed up the process of checking the identified objects, we combined more catalogues (e.g., derived with different exposure times or conditions) of the same field. To allow an immediate vi-

sualization of results, we implemented a set of procedures using the SuperMongo command language. These include contour plots of the field with all classified objects identified (see Fig. 3) and a number of interactive tools to look at the distribution of galaxies (and stars) in the catalogue (see Fig. 1) and its behaviour as a function of the magnitude (see Fig. 4).

This was extremely useful in providing rapid feedback with the output catalogues derived from the FOCAS analysis. After adjusting the critical parameters (e.g., minimum image size for detection, sigma above and below the sky for detection) the FOCAS classifications appear accurate for about 90% of the objects. As a general remark we found that 20-50% of the objects can be misclassified if they are at the faintest flux levels (near the magnitude limit) or if images obtained under poor seeing conditions ($\gtrsim 1.7''$).

Results

Our investigation of BL Lac environments has provided clear evidence that, contrary to previous suggestions, BL Lacs are often located in regions of higher than average galaxy density. This is estimated by studying the density distribution of galaxies as a function of the distance from the BL Lac object and

computing the angular and spatial cross-correlation functions. For about 10 objects of known redshift we obtained spectra of 1 to 5 galaxies in the field and found that these galaxies are physically associated with the BL Lac objects.

The richness of the cluster may be estimated using the number, $N_{0.5}$, of excess galaxies with $m \leq m_3 + 2$ (where m_3 is the third-ranked cluster galaxy, projected within a 0.5 Mpc radius of the cluster centre. This parameter is related to N_R , the number of galaxies within the standard Abell radius (3 Mpc; Abell 1958) of the cluster centre by the empirical relation: $N_R = 3.3N_{0.5}$ (Bahcall 1981).

As an example we report the case of the bright ($m_V \approx 12.5$) BL Lac object PKS 2155-304 at $z = 0.116$. This is an extensively studied object at every frequency (e.g., Treves *et al.* 1989 and references therein). Our imaging and spectroscopic study shows that the BL Lac is hosted by a giant elliptical galaxy of $M_V \sim -22.5$ which is the dominant member of a poor cluster of galaxies (see Fig. 5). The host galaxy has two faint companion galaxies (G1 and G2) at projected distances less than 50 kpc at the same redshift as PKS 2155-304. Moreover, a more conspicuous ($M_V = -21.4$) galaxy (G4), still at the same redshift, is located $\sim 113''$ south of the BL Lac object, corresponding to a projected distance of ~ 300 kpc. This galaxy is itself surrounded by faint companions. The richness of the cluster derived from galaxy counts yields an Abell richness class of about 0 (see Falomo, Pesce, & Treves 1993 for more details).

From our study we found that, on average, BL Lacs are associated with poor

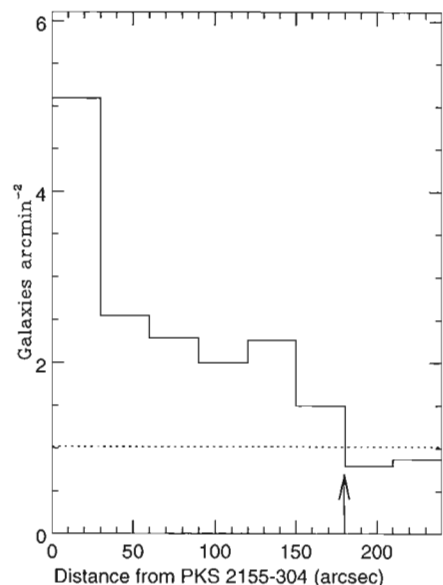


Figure 4: Density distribution of galaxies as a function of the distance from the BL Lac object PKS 2155-304. The arrow marks the distance corresponding to 0.5 Mpc radius.

Figure 5: (Top) The central part ($2.5' \times 2.5'$) of the field of the bright PKS 2155–304 (EMMI R filter 20 min). The BL Lac object (at the centre) is here clearly saturated. North is up and east to the left. The inset shows the immediate environments as imaged with SUSI (R filter 5 min) under sub-arcsec seeing conditions. This image has been deconvolved using the Richardson-Lucy algorithm. (Bottom) Contour plot of the field with main objects labelled.



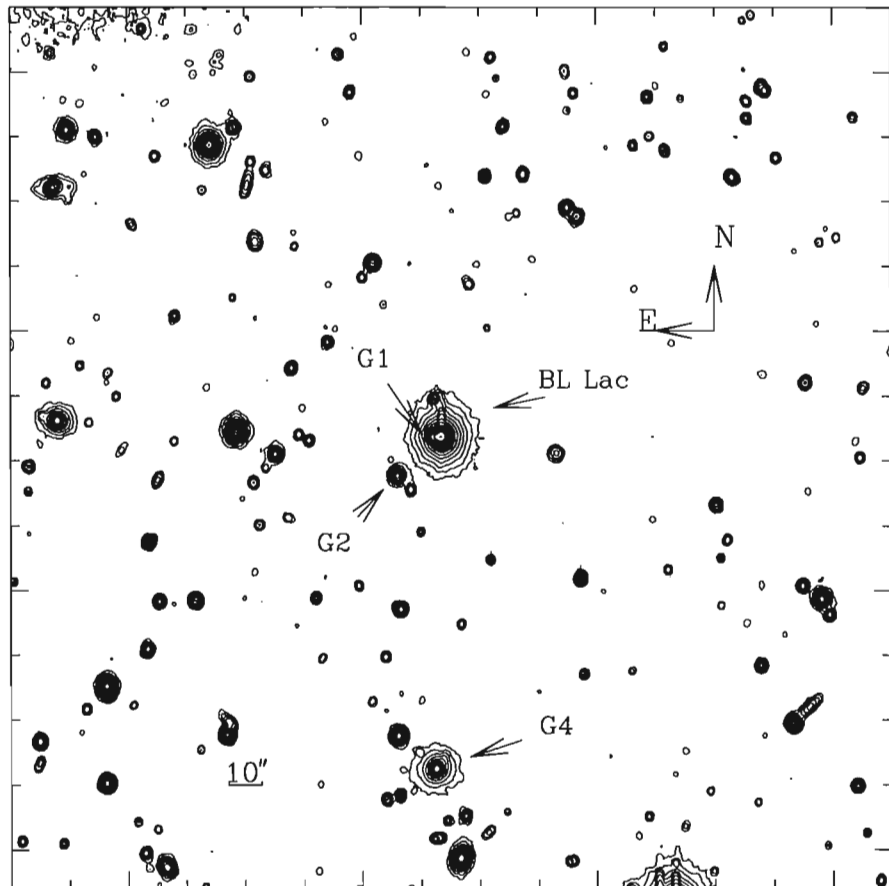
clusters of galaxies (Abell richness class ~ 0). However, some cases of association with medium rich clusters exist.

Objects in Rich Environments

One interesting BL Lac object in a rich environment is PKS 0548–322. This is a bright ($m_V = 15.5$) and nearby BL Lac object for which the association with a cluster of galaxies at $z \sim 0.04$ was suggested (Disney 1974). The hypothesis was, however, soon ruled out by the measurement of the redshift ($z = 0.069$) of PKS 0548–322 (Fosbury & Disney 1976).

Our images (see Fig. 6) clearly show an enhancement of galaxies around the source within 0.5 Mpc of projected distance from PKS 0548–322. Spectroscopy of five of the galaxies in this field (G1, G2, G4, G5, G6) confirm they form a cluster of galaxies physically associated with the BL Lac object. The host galaxy of PKS 0548–322 is a giant elliptical of $M_V = -23.4$ and is likely the dominant member of the cluster. Moreover, it has a pair of companion galaxies at projected distance < 40 Kpc, with a clear signature of tidal interactions. Our estimate of the richness of the cluster yields $N_{0.5} = 29$ corresponding to Abell richness class 2 (see Falomo, Pesce, & Treves 1994 for more details).

Another interesting case is represented by the X-ray selected BL Lac H 0414+009. This is a relatively more distant object ($z = 0.287$) that is also embedded in a luminous ($M_V \sim -23.5$) elliptical galaxy (Falomo & Tanzi 1991). H 0414+009 (see Fig. 7) is surrounded by many faint galaxies exhibiting a peculiar disposition (Falomo, Tanzi, & Treves 1991). The clustering of the galaxies around the object suggests they form a loose group, with some of the galaxies forming pairs. The excess of galaxies within 0.5 Mpc with respect to the average galaxy density is quite clear. We found 29 galaxies down to the magnitude limit of $m_R = 21.5$ while a total of 14.4 ± 3.8 is expected from average counts. Spectroscopy of three of the galaxies confirm their physical association while one appears to be a foreground object. Moreover, the redshifts of galaxies A1



and A2 are identical within the errors, confirming that they form a physical pair. The richness parameter estimated from $N_{0.5}$ yields an Abell richness of class 0. (See McHardy *et al.* 1992 and Falomo, Pesce, & Treves 1993 for more details).

Conclusions

Our ongoing study of BL Lac environmental properties has shown that BL Lacs are indeed found in regions of enhanced galaxy density. They seem to

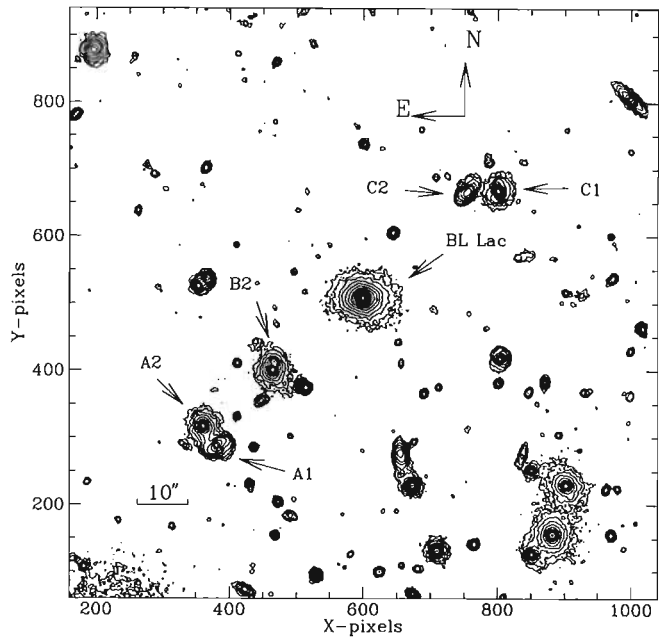
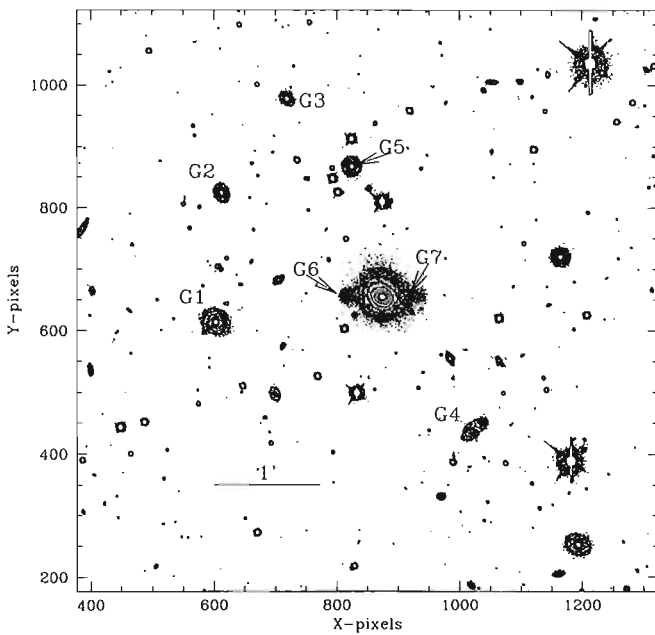
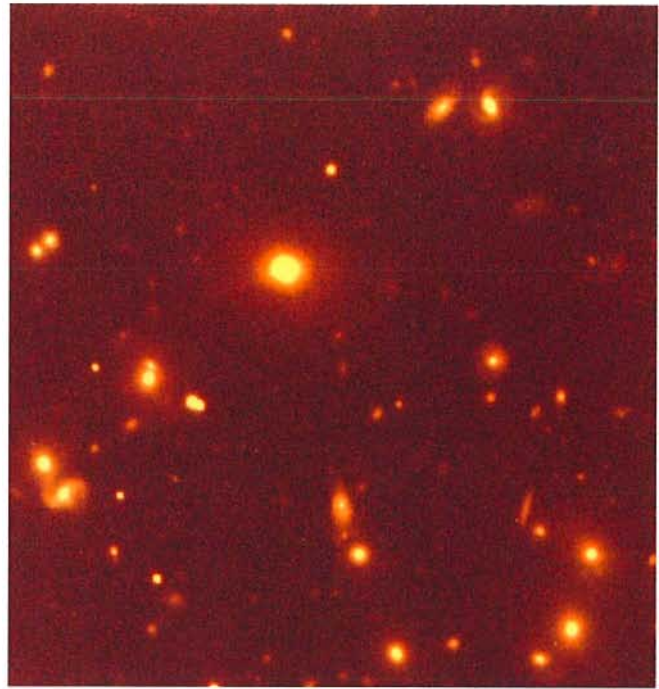
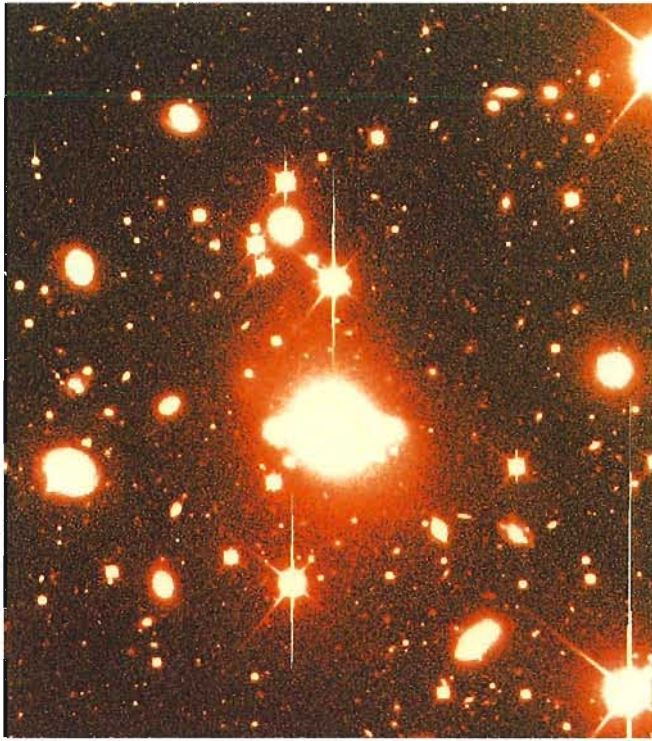


Figure 6: (Top) The central part ($4' \times 4.5'$) of the field of PKS 0548-32 (EMMI R filter 20 min). North is up and east to the left. The BL Lac (main object at centre) is surrounded by a group of galaxies at the same redshift as the giant elliptical hosting 0548-322. (Bottom) Contour plot of the field with main objects labelled.

Figure 7: (Top) The field ($1.4' \times 1.5'$) around the X-ray BL Lac ($z = 0.287$) H0414+004 (SUSI R filter 20 min). North is up and east to the left. The BL Lac (brightest object near the centre) is clearly in a cluster of galaxies with some of them forming pairs. (Bottom) Contour plot of the field with main objects labelled.

prefer groups or poor (Abell richness class 0) clusters. We found that on average $N_{0.5} = 6 \pm 4$. While some individual BL Lacs are found in rich clusters, these seem to be a small minority.

From the 18 objects so far investigated (about 50% of our whole sample) we derived an average amplitude of the angular correlation function (BL Lac - galaxies) A_{bg} normalized to the

general galaxy-galaxy amplitude A_{gg} of $\langle A_{bg}/A_{gg} \rangle = 7 \pm 4$. This value is very similar to what is found in the case of radio loud quasars (see e.g. Hartwick and Schade 1990 and references therein).

Because the properties of the BL Lac environments are not dependent on orientation effects, they may be a useful tool to test the beaming model, by comparison with the environmental properties

of the proposed BL Lac parent population. Although the properties of the environments of F-R I class radio galaxies may be somewhat different depending on the sample considered (e.g., Prestage & Peacock 1988, 1989; Yates, Miller, & Peacock 1989; Hill & Lilly 1991), they appear consistent with that derived for BL Lac objects based on the present data. The average value of $N_{0.5}$ for F-R

I radio galaxies derived combining available samples (see Pesce 1993) yields $\langle N_{0.5} \rangle_{FRI} = 7.1 \pm 8$. The large scatter being due in part to differences of samples and redshift distribution.

We note also that F-R I radio galaxies represent an heterogeneous class and it is possible that the parent objects of BL Lacs form a subset of F-R I galaxies.

Objects in our sample are a mixture of radio selected and X-ray selected targets (corresponding to radio-strong and radio-weak emitters). Although a number of different emission properties are found to characterize these subclasses (see e.g. Giommi *et al.* 1994), we do not find systematic differences of environment between the two.

Our results are consistent with what is being found by other similar studies. Wurtz *et al.* (1993) and Smith *et al.* (1995) have concentrated on X-ray selected BL Lac objects while Stickel *et al.* (1993) and Fried *et al.* (1993) have studied some of the radio selected BL Lacs. In most cases, the clusters found are relatively poor (Abell richness class 0-1) with a few objects in richer environments.

If BL Lacs are aligned versions of low-luminosity (F-R I) radio galaxies, it might be expected that Flat Spectrum Radio Quasars (FSRQs), which share many of the properties of BL Lacs but have strong and broad emission lines, are aligned examples of high-luminosity (F-R II) radio galaxies. We point out that a detailed comparison of environmental and host properties of BL Lacs and F-R I galaxies with FSRQs and F-R II radio galaxies

would help to constrain the proposed unified schemes of AGN.

Acknowledgement

We thank A. Treves for useful suggestions to this manuscript. J.E.P. and work on BL Lac environments at STScI are supported by NASA grants NAG5-1034 and NAG5-2154.

References

- Abell, G. O., 1958, *ApJS*, **3**, 211.
 Angel, J. R. P., & Stockman, H. S., 1980, *ARAA*, **18**, 321.
 Bahcall, N. A. 1981, *ApJ*, **247**, 787.
 Blandford, R. D., & Rees, M. J. 1978, in Pitts. Conference on BL Lac Objects, ed. A. N. Wolfe (Univ. of Pitts. Press), 328.
 Bregman, J. P., 1990, *A&AR*, **2**, 125.
 Browne, I. W. A. 1983, *MNRAS*, **204**, 23.
 Butcher, H. R., *et al.* 1976, *ApJ*, **209**, L11.
 Craine, E. R., Tapia, S., & Tarengi, M., 1975, *Nature*, **258**, 56.
 Disney, M. J., 1974, *ApJL*, **193**, L103.
 Falomo, R., Pesce, J. E., & Treves, A., 1993, *AJ*, **105**, 2031.
 Falomo, R., Pesce, J. E., & Treves, A. 1994, *ApJ Letters*, in press.
 Falomo, R., & Tanzi, E. G., 1991, *AJ*, **102**, 1294.
 Falomo, R., Tanzi, E. G., & Treves, A., 1991, *A&A*, **249**, 341.
 Fosbury, R. A. E., & Disney, M. J., 1976, *ApJL*, **207**, L75.
 Fried, J. W., Stickel, M., & Kühr, H., 1993, *A&A*, **268**, 53.
 Giommi, P., *et al.* 1991, *ApJ*, **378**, 77.

- Giommi, P., Ansari, S. and Micol, A. 1994, *A&ASS*, in press.
 Hartwick, F.D.A. and Schade, D. 1990, *Ann. Rev. Astr. Astrophys.* **28**, 437.
 Hartman, R., *et al.* 1993, in Proc. of the 2nd Compton Symposium, College Park, MD, Sept. 1993, in press.
 Hill, G. J., & Lilly, S. J., 1991, *ApJ*, **367**, 1.
 Hintzen, P., Romanishin, W., & Valdes, F., 1991, *ApJ*, **366**, 7.
 Jarvis, J. F., & Tyson, J. A., 1981, *AJ*, **86**, 476.
 Kollgaard, R. I., *et al.* 1992, *AJ*, **104**, 1687.
 Kollgaard, R. I. 1994, *Vistas in Astronomy*, **38**, 29.
 Maraschi, L., Ghisellini, G., & Celotti, A., 1992, *ApJ*, **397**, L5.
 McHardy, I. M., Luppino, G. A., George, I. M., Abraham, R. G., & Cooke, B. A., 1992, *MNRAS*, **256**, 655.
 Metcalfe, N., Shanks, T., Fong, R., & Jones, L. R., 1991, *MNRAS*, **249**, 498.
 Pesce, J. E. 1993, PhD Thesis.
 Prestage, R. M., & Peacock, J. A., 1988, *MNRAS*, **230**, 131.
 Prestage, R. M., & Peacock, J. A., 1989, *MNRAS*, **236**, 959.
 Schachter, J. F., *et al.* 1993 *ApJ*, **412**, 541.
 Smith, E. P., O'Dea, C. P., & Baum, S. A., 1995, *ApJ*, in press.
 Stickel, M., *et al.* 1991, *ApJ*, **374**, 431.
 Stickel, M., Fried, J. W., & Kühr, H. 1993, *A&AS*, **98**, 393.
 Stocke, J. T., *et al.* 1991, *ApJS*, **76**, 813.
 Stone, R. P. S., 1977, *ApJ*, **218**, 767.
 Treves, A., *et al.* 1989, *ApJ*, **341**, 733.
 Ulrich, M.-H. 1978, *ApJ*, **222**, L3.
 Urry, C. M., Padovani, P., & Stickel, M. 1991, *ApJ*, **382**, 501.
 Weistrop, D., *et al.* 1981, *ApJ*, **249**, 3.
 Wurtz, R., Ellingson, E., Stocke, J. T., & Yee, H. K. C., 1993, *AJ*, **106**, 869.
 Yates, M. G., Miller, L., & Peacock, J. A., 1989, *MNRAS*, **240**, 129.

COME-ON+ Adaptive Optics Images of the Pre-Main Sequence Binary NX Pup

E. TESSIER¹, J. BOUVIER², J.-L. BEUZIT^{3,5} and W. BRANDNER^{4,5}

¹Royal Greenwich Observatory, Cambridge, England; ²Observatoire de Grenoble, Université Joseph Fourier, France;

³Observatoire de Paris, Section de Meudon, France; ⁴Astronomisches Institut der Universität Würzburg, Germany;

⁵ESO-La Silla

Introduction

Using adaptive optics (AO) at the ESO 3.6-m telescope, we obtained diffraction limited JHK images of the region around the Herbig AeBe star NX Pup. NX Pup is resolved as a close binary with a separation of 0.128'' (the binary nature of NX Pup was originally discovered by HST) that we refer to as NX Pup AB; a third component NX Pup C is found at a distance of 7.0'' and is classified as a classical T Tauri star. We first describe the

procedure that we followed in order to extract the maximum information from the AO images. We then discuss the evolutionary status of the NX Pup system on the basis of its IR properties derived from the AO images, as well as from the visual photometry and spectroscopy subsequently obtained at ESO.

AO Observations

We used the ESO adaptive optics system ComeOn+ (CO+), which was devel-

oped in collaboration by the Observatoire de Paris, ONERA, ESO, Laserdot and LEP, in combination with the SHARP II (System for High Angular Resolution Pictures) camera from the Max-Planck Institute for Extraterrestrial Physics (MPE). See Beuzit *et al.* 1994, *The Messenger* **75**, 33 and references therein for a description of the CO+ system. The SHARP II camera is equipped with a Rockwell NICMOS-3 array. The image scale was 0.050''/pixel giving a field size of 13'' × 13''. We observed NX Pup on

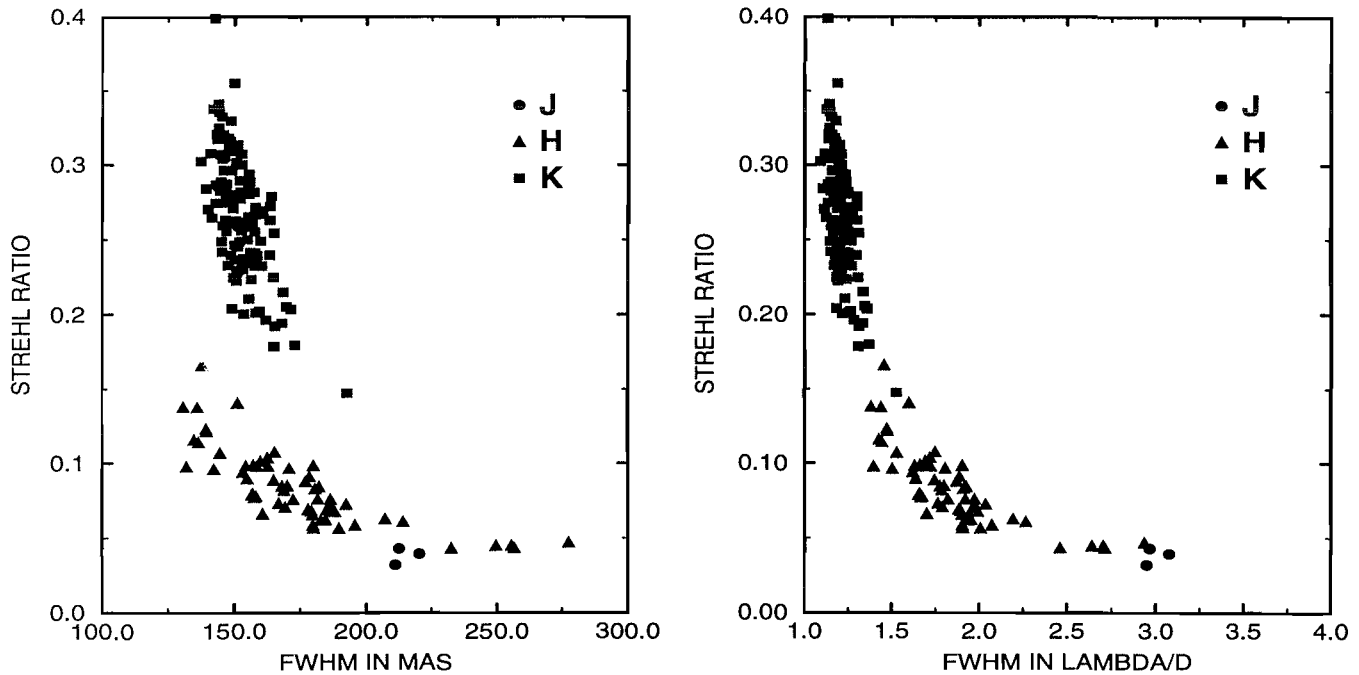


Figure 1: Plot of FWHM versus Strehl ratio (SR) for individual images obtained with the Adaptive Optics system Come-On+. The exposure time was 1s in HK and 20s in J. In K, the FWHM is well stabilized, and always better than $0.18''$. The scatter in the HK points shows that short individual images are influenced by the continuous change of the turbulence conditions due to the short coherence time of the turbulence during that night. For longer exposure times, these effects average out as shown by the small scatter of the three 20s images in J. Note that the narrower diffraction core in H allows better FWHM than in K for some images in spite of a lower SR. The same plot is rescaled by λ/D on the right (which is the diffraction limit) to show the relation between FWHM and SR which characterizes AO images. This curve is valid for the Come-On+ experiment.

January 1, 1994 in the J, H, and K bands. The total exposure time in each filter was 5 minutes. Immediately after NX Pup, we observed a reference point source $10'$ away (star no. 985 in the HST Guide Star Catalogue) later used to measure the instrumental point spread function (PSF) which is necessary to deconvolve images; we will refer to it as the calibration PSF source. The guide source used by the AO system was in both cases the observed source itself. Since NX Pup is a rather bright source (around 6th mag in K) and the calibration source is selected to match the same flux, we obtained series of short exposures in the H and K band (respectively 0.5s and 2s for NX Pup) in order to fall in the linear response region of the detector. Because NX Pup is fainter in J and because of the lower sensitivity of the detector in this wavelength region, the exposure time in J was 1 minute in each frame for NX Pup. We therefore have a large number of individual exposures in the H and K bands and we will show below how we can take advantage of it.

Characterization of AO Images

Since an AO system partially or fully compensates the wavefront distortions, we now have access to imaging with a point spread function much sharper than the seeing disk. The shape of the

PSF could be described as a diffraction-limited core superimposed on a residual halo with a size corresponding approximately to the seeing disk. This halo comes from the high-order Zernike modes not corrected by the Adaptive Optics system. The diffraction-limited core may be wider (we can represent this by a Gaussian convolution) when errors of correction for the low-order Zernike modes are important. The performance of an AO system at any wavelength is usually defined by the Strehl ratio (SR). The Strehl ratio is the ratio of the observed PSF maximum to the theoretical diffraction-limited PSF maximum; the latter is the Airy pattern for a clear circular aperture telescope of diameter D . When the SR increases, the halo size will reduce and its power will move to the diffraction limited core (see Rigaut *et al.* 1991).

Consequently the image obtained is that of the source convolved with the instrumental PSF and image deconvolution may therefore be needed (particularly to clearly access structures superimposed on the PSF patterns such as the first Airy ring or the residual seeing halo). The PSF may be calibrated on a point source in similar seeing conditions. We will talk about a deconvolution procedure in a next section.

Figure 1 shows the distribution of the full width half maximum (FWHM) versus

Strehl ratio (SR) for each individual exposures of the calibration PSF in JHK. The exposure time was 1s in HK bands, 20s in J. We can see that the image in the K band is very well stabilized, FWHM being always less than $0.18''$. In H, the SR drops below 10%, a key value below which the correction is much more sensitive to turbulence effects as shown by the large variations of the FWHM between $0.13''$ and $0.25''$. The distribution of the points in the HK-bands illustrates how the PSF varies as the turbulence conditions continuously change during the observations. The scatter of the points depends upon the coherence time of the turbulence: had the coherence time been longer that night, the PSF would have been much less sensitive to varying turbulence conditions. As a rule, the worst the turbulence, the less efficient the correction. The PSF variation in response to the changing turbulence is reduced with longer exposure times and/or by coadding individual images. This is why the scatter of the 3 images in J is much reduced due to the exposure time of 20s compared with 1s for the HK bands (see Fig.1).

When the plot abscissa is rescaled by a factor λ/D (which corresponds to the diffraction limit at the wavelength λ for a telescope of diameter D), points clearly gather along a single curve. As shown by this curve, the Strehl ratio describes

very well the PSF with a SR above 10% but poorly for lower values. In the latter case, the FWHM will provide additional information on the PSF.

This curve is valid for the ComeOn+ experiment and characterizes the PSF response. Other AO systems may give different responses. Anyway, these plots could be used to define the best strategy in AO observing. As a rule, the turbulence effects get worse as one goes to shorter wavelengths; consequently, the correction and the SR are poorer. However, in some cases, by going to shorter wavelengths one can get higher resolution in spite of a lower SR; this is because the FWHM becomes sharper thanks to the narrower diffraction core (following a λ/D law). For example, in the observation of NX Pup, in terms of FWHM, the best individual images are in the H-band rather than in the K-band (see Fig. 1).

Sharpening Methods for Short-Exposure AO Images

The number of individual exposures on NX Pup was 5 in J, 150 in H, and 600 in K for a total exposure time of 300 seconds in each filter.

A simple coaddition of these individual frames yields the final image. However, when a large amount of images is available, it is worth selecting them according to a Strehl ratio criterium. Also, when a short exposure time is used, the residual tilt is further reduced by applying a shift-and-add algorithm (SAA).

While SAA mostly improves the resulting FWHM, applying image selection increases the final Strehl ratio. However, the rejection rate of images with poor SR must be limited in order to preserve a large enough signal-to-noise ratio in the final image. Table 1 quantitatively shows the improvement on the calibration PSF obtained with image selection (IS) and SAA in comparison to the simple coaddition of individual frames. The number of individual exposures on the calibration PSF source was 3 in J, 60 in H, and 120 in K for a total exposure time of 60 s in JH and 120 s in K. All these opera-

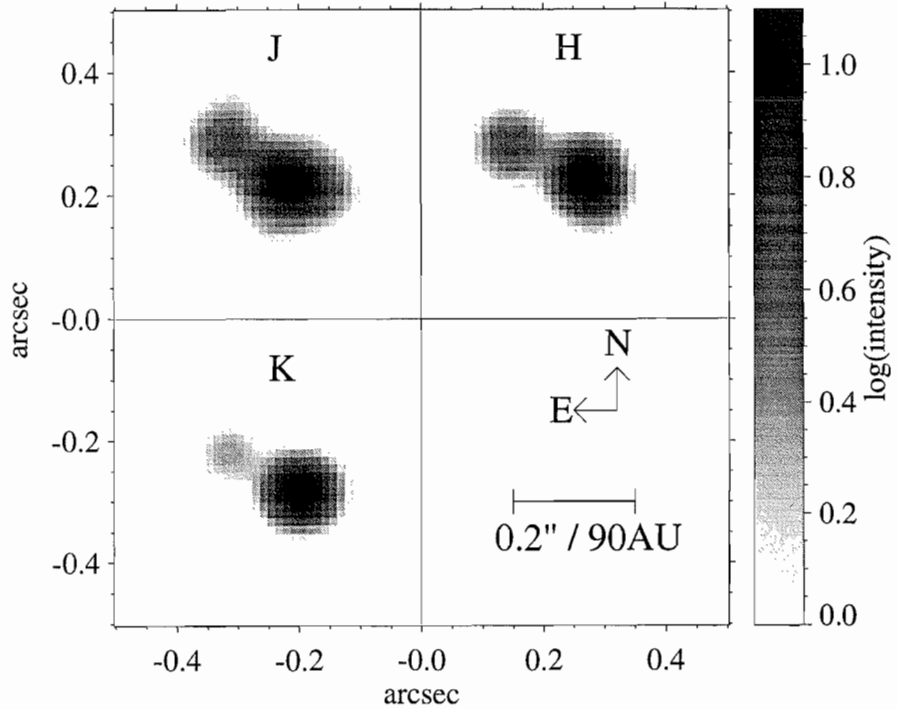


Figure 2: Cleaned images of NX Pup AB obtained in JHK with the Adaptive Optics system CO+ at the ESO 3.6-m telescope on January 1, 1994. The images were rebinned by a factor of 4, the FWHM of the Gaussian beam is 80 mas (see text for details). The components A and B (sep. $0.128''$, PA 63.1°) are clearly resolved. At a distance of 450 pc, $0.128''$ correspond to a projected separation of 58 AU. The faint feature in the J image north-west of NX Pup A is an artefact from the image deconvolution. A logarithmic gray scale was used. Component C is outside these frames. North is up and east is to the left.

tions were performed with the local IRAF package c128 developed by E. Tessier at the Observatory of Grenoble (available through anonymous FTP at the site [hplyot.obspm.fr](http://lyot.obspm.fr) in the directory /iraf_hra).

NX Pup AB: CLEANed AO Images

A simple coaddition of the individual images allows already to resolve the NX Pup AB system with a separation of $0.128''$; and this shows how efficient AO imaging is. Nevertheless, even sharper angular resolution can be reached by applying CLEAN deconvolution to the data. We briefly describe here the CLEAN algorithm we used (see also Tessier *et al.* 1993). Using the terms common among

radio astronomers, the (SAA+IS) image of the source provides the “dirty map”, while that of the calibration PSF is used as the “dirty beam”. Both maps are apodized to reject non-physical spatial frequencies beyond the effective cut-off. Then they are resampled by a factor 4 and convolved with a Gaussian beam before running the CLEAN algorithm with a loop gain of 3%. Because we first try to detect close stellar sources and not low-level extended structures, it is important to control the formation of ghost sources and consequently it is better to stop the CLEAN process as soon as the level of the negatives in the Cleaned map reach the level of the residues in the residual map. Usually, for 256×256 maps, convergence is reached in less than 500 iterations. The Cleaned map is then convolved with the same Gaussian beam as used previously and the residuals map is added to get the final Cleaned image.

As a rule, low-level extended structures require that we run the CLEAN algorithm until the noise level is reached. By the way, Maximum Entropy Methods (MEM) are known to be more efficient when dealing with extended structures. Another way to study the presence of extended structures is via analysis in the Fourier space (see Malbet *et al.* 1993). From this analysis, NX Pup AB does not show any significant deviation from the

TABLE 1. Sharpening result from short exposure AO images through shift and add (SAA) and image selection (IS).

	J	H	K
FWHM	0.214''	0.172''	0.156''
FWHM (SAA)	0.209''	0.157''	0.147''
FWHM(SAA+IS)	–	0.138''	0.143''
SR	3.8%	8.0%	25.1%
SR (SAA)	3.8%	8.6%	27.1%
SR (SAA + IS)	–	12.4%	31.0%
Selection rate (IS)	–	20%	40%

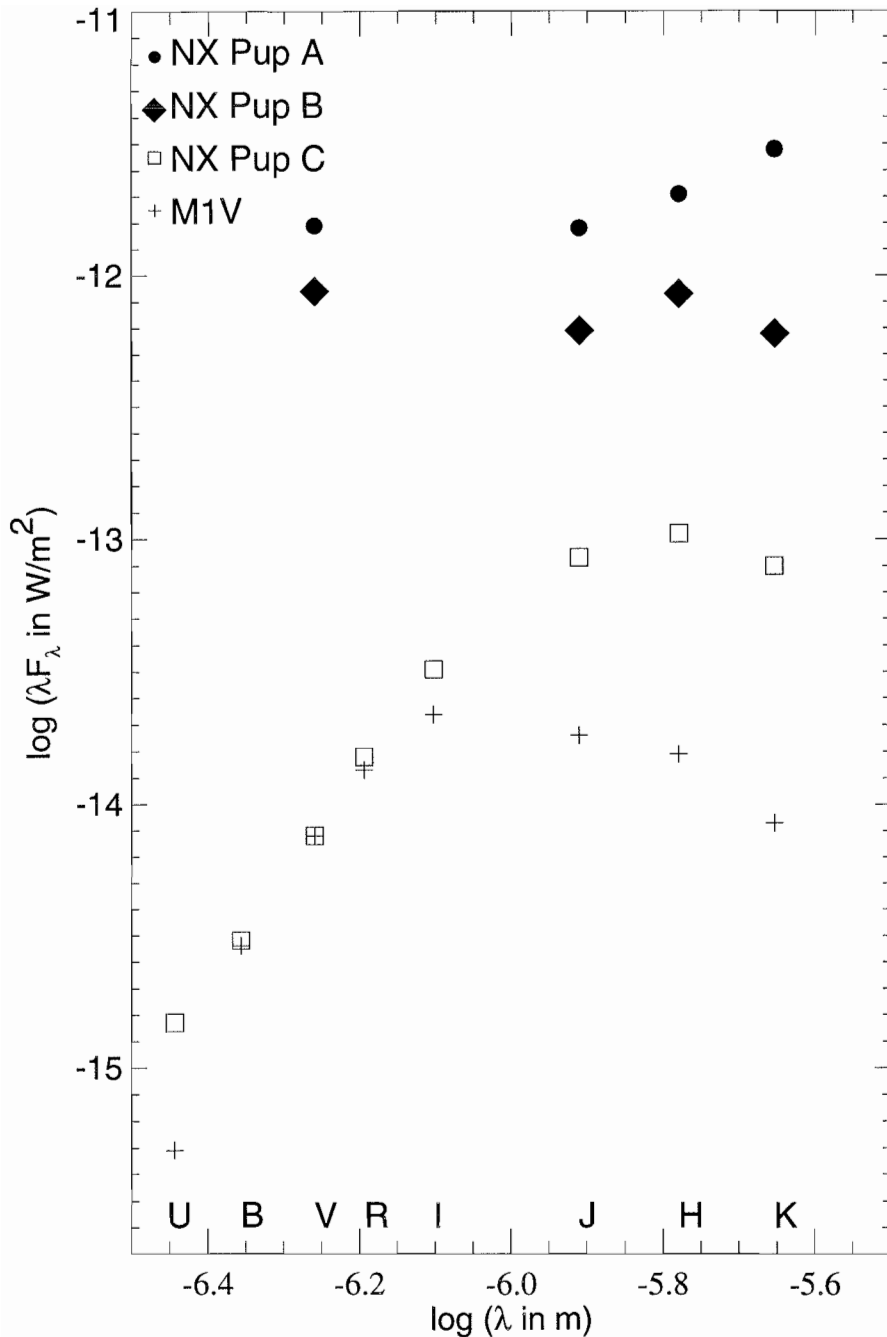


Figure 3: Spectral energy distribution λF_λ of NX Pup A and B (VJHK) and C(UBVRIJHK). For comparison we also show the spectral energy distribution of an M1-type star of the same apparent V magnitude as NX Pup C. Note that the SED is rising towards longer wavelengths for NX Pup A while the SEDs of NX Pup B and C peak near $1.5 \mu\text{m}$. All 3 stars exhibit a strong IR excess compared to normal photospheres and NX Pup C also shows an UV excess. The errors in flux are 5% or less.

binary model in the HK bands (the quality of J data is inadequate to confirm this), consequently no other features are detected.

Astrometry of the system was performed on Cleaned images which are shown in Figure 2. The FWHM of the Gaussian beam was 80 mas. Residues in % of the peak value were 8%, 4%, and 1% in JHK, respectively. The separation of $0.128'' \pm 0.008''$ and the position angle of $63.1^\circ \pm 3.5^\circ$ are in good

agreement with the values determined by Bernacca *et al.* (1993) from HST observations: $0.126'' \pm 0.007''$, $63.4^\circ \pm 1.0^\circ$.

The total flux is conserved by the CLEAN algorithm. However, though the Cleaned PSF has a sharper peak, it is surrounded by a residual pattern made of positive and negative values due to the noise and to uncertainties in the calibration PSF (incidentally, some features in the Cleaned images of NX Pup located on the first Airy ring are probably arte-

facts connected with some intensity variations of the PSF in this region – see Figure 2). For that reason, we prefer not to rely on peak values in the Cleaned images to derive photometry. Instead, the photometry was performed on the shift-and-add images using IRAF/DAOPHOT routines. These routines can be compared with a basic blind deconvolution-like process using the calibration PSF only in the first iteration and assuming the source is a binary, which provides a very strong constraint. By doing this, we avoid the calibration PSF problem.

NX Pup C: Off-Axis Sources and Anisoplanatism

NX Pup C is located $7''$ away from NX Pup AB. Since the wavefront correction used NX Pup AB as a guide source, NX Pup C is off-axis and image correction might therefore suffer from anisoplanatic effects. Anisoplanatism refers to the case where the distorted wavefront of the observed source (the astronomical target) is different from that of the guide source used by the AO system. As a result, the adaptive correction on the target is degraded. Various types of anisoplanatism affect current AO systems; some ideas, such as using multiple laser beacons, would overcome this limitation (Beckers *et al.* 1993). At the moment, CO+ uses a natural guide star which can be the target itself or a nearby star. We briefly describe below two kinds of anisoplanatism that might result from this observing mode: angular anisoplanatism and temporal anisoplanatism.

If we observe an off-axis source, the telescope is viewing to a direction making an angle θ with the direction of the guide source used by the AO instrument. The light path across the turbulence layers and, therefore, the induced phase perturbations are different for the on- and off-axis sources. The adaptive-optics correction is consequently less efficient for the off-axis source. This direction-dependent anisoplanatism is usually called angular anisoplanatism.

Because the bandwidth B of any AO instrument transfer function is finite, the correction applied at the time t is based on a perturbed wavefront recorded at a time $t - \delta t$. According to the approximation of frozen turbulence, the degradation of the correction is then related to the ratio \bar{V}/B , where the wind speed V of the turbulent layers is mainly responsible for the continuous change of the perturbed wavefront. This anisoplanatism is usually called temporal anisoplanatism.

Observations have recently been carried out at the ESO 3.6-m telescope to study the anisoplanatism, and more observations are scheduled in January 1995 (M. Faucherre, private communi-

TABLE 2. JHK photometry (1.1.1994, ESO 3.6-m/CO+).

Filter	NX Pup A	NX Pup B	NX Pup C
J	8.58 ^m	9.56 ^m	11.71 ^m
H	7.43 ^m	8.37 ^m	10.66 ^m
K	6.15 ^m	7.90 ^m	10.10 ^m

cation). As long as the final results of these observations are not available, it is therefore difficult to estimate whether angular anisoplanatism is important under good seeing conditions in the case of NX Pup C, 7'' away from the guide source NX Pup AB. Because we might expect some angular anisoplanatism effects (Wilson and Jenkins 1994), we did not try to deconvolve NX Pup C. Another reason is that we got a lower signal-to-noise ratio for NX Pup C.

The first effect of angular anisoplanatism is that the Strehl ratio falls off and the PSF gets wider as the angular distance to the guide star increases: consequently an off-axis PSF will be less sharp. As expected from angular aniso-

planatism, the FWHM of NX Pup C is systematically wider than for the calibration source in each JHK filter. Moreover, on the shift-and-add K image, NX PUP C appears elongated in the east-west direction (FWHM 0.18'' × 0.27'' in the N-S and E-W directions, respectively, compared to 0.16'' × 0.16'' for the on-axis calibration PSF source). This elongation is also observed in the H image but is less significant, and is not seen in the J image.

Such an image elongation can, in principle, result from either angular or temporal anisoplanatism (or both). Angular anisoplanatism would lead to an elongation of the off-axis PSF in the direction of the guide source. This effect has been

observed and described by McClure *et al.* (1991). In the case of NX Pup, the expected direction of elongation for NX Pup C would be at a PA of ~ 45°, i.e. from north-east to south west but not in the east-west direction as observed. Elongation in another direction can be explained by temporal anisoplanatism due to the wind in the dominant turbulent layer (see Roddier *et al.* 1993 and Wilson and Jenkins 1994). The prevalent wind direction at La Silla near the ground is north-south, but we do not know the wind direction in the dominant turbulent layer at the time of our observations. While an off-axis PSF should suffer both effects, the on-axis PSF should show pure temporal anisoplanatism. Yet, the on-axis PSF of the calibration source does not show any significant deviation from circular symmetry. The PSFs of NX Pup A and B computed from the basic blind deconvolution (see above) are quite similar to that of the calibration source. Summing up, neither angular nor temporal anisoplanatism are very likely explanations for the observed elongation of NX Pup C, which may therefore be real. NX Pup C will

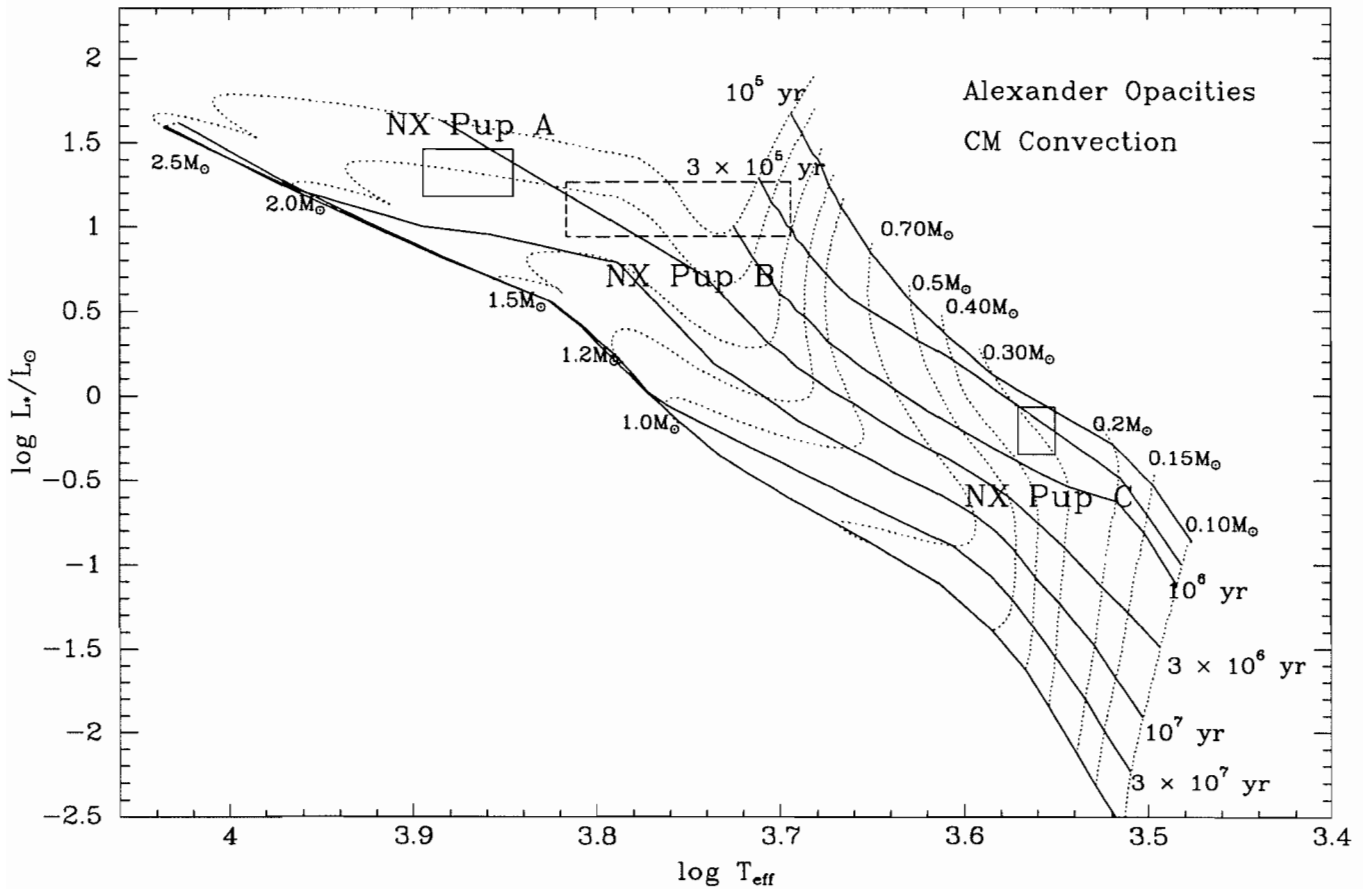


Figure 4: Position of NX Pup A, B, and C in the HR-Diagram. The pre-main sequence evolutionary tracks are from D'Antona and Mazzitelli (1994). The solid lines represent isochrones and the zero-age main sequence, the dotted lines are the evolutionary tracks for stars in the mass range from 0.1 to 2.5 M_\odot . The positions of NX Pup A, B, and C in this diagram are marked by boxes. For NX Pup A we assume a spectral type A7-F2, $V = 10.1^m - 10.5^m$, and $A_V = 0.^m - 0.7^m$ (Blondel and Tjin A Djie 1994). For NX Pup B we assume the same extinction, a spectral type F5-G8 and $V = 10.7^m - 11.1^m$. The evolutionary status of NX Pup C is better defined, yielding an age around 5×10^5 yr and a mass of 0.3 M_\odot . (From Brandner *et al.* 1994.)

TABLE 3. Equivalent width (in nm) of emission (<0) and absorption (>0) lines in the spectra of NX Pup AB and C (28.1.1994, ESO 1.5-m/B&C; 20.3.1994, NTT/EMMI).

NX Pup	AB	C
H α	double peaked	-2.85
O I 630.0	-0.068	-0.11
H β	0.25	-0.58
H γ	0.53	-0.17
Li I 670.8	-	0.054

TABLE 4. Evolutionary status of NX Pup A, B, and C.

NX Pup	A	B	C
Sep.	-	0.128'' \pm 0.008''	6.98'' \pm 0.04''
PA	-	63.1° \pm 3.5°	45.3° \pm 0.2°
SpT	A7-F2 ¹	F5-G8	M0.5-M1.5
L/L \odot	15-29	9-18	0.45-0.85
Age	5 \times 10 ⁶ yrs	0.3-5 \times 10 ⁶ yrs	5 \times 10 ⁵ yrs

¹ Brand *et al.* 1983, Reipurth 1983, Blondel & Tjin A Djie 1994.

need to be re-observed and at the same time, anisoplanatism should be quantitatively studied.

The Evolutionary Status of the NX Pup System

NX Pup is located at the edge of CG1, a Cometary Globule in the Gum Nebula (see e.g. Henkel 1989, *The Messenger* 57, 8), which is suspected to have been a region of star formation for more than 10⁶ years (e.g. Reipurth and Pettersson 1993).

NX Pup, a Herbig AeBe star (Irvine 1975) was also resolved as a close binary with a separation of 0.126'' by Bernacca *et al.* (1993) using data from the Fine Guidance Sensor system aboard the Hubble Space Telescope. Thus all previous evolutionary interpretations should be reevaluated as the total observed luminosity in fact comes from at least two stars.

CO+ observations in JHK have easily resolved the NX Pup system, thus allowing us to estimate the flux contribution of each of the components of the system in the infrared. In addition, we used on January 8, 1994 the optical CCD camera at the Danish 1.5-m telescope at La Silla and complemented the IR observations by getting UBV, Gunn I and H α photometry for NX Pup AB (unresolved) as well as for NX Pup C that we identify as a low-mass classical T Tauri star. Additional photometric measurements of NX Pup were obtained in the course of the LPTV programme at the Danish 50-cm Strømgren Automatic Telescope (P.S. Thé, private communication, Sterken *et al.* 1995, in preparation).

NX Pup AB and NX Pup C both show a strong excess of H α emission compared to normal stars included in the same optical images. From the location of these stars in colour-colour J-H vs H-K and V-K vs H-K diagrams we can conclude that NX Pup A belongs to the group of Herbig AeBe stars. All three stars show an intrinsic IR excess. The IR excess is clearly apparent in the spectral energy distributions of the 3 stars plotted in Figure 3.

Spectra of NX Pup C and NX Pup AB were obtained on March 20, 1994 with the ESO Multi-Mode Instrument (EMMI) attached to the NTT. Table 3 lists the main features present in the spectra. The presence of the strong H α emission (EW = 2.85 nm) and the Li I 670.8 nm absorption make NX Pup C a *bona fide* classical T Tauri stars.

Finally, we inferred from these results the luminosity and effective temperature of each star. Figure 4 locates NX Pup A, B, and C in the HR diagram within observational uncertainties. PMS evolutionary tracks from D'Antona and Mazzitelli (1994) are overplotted. Table 4 summarizes the evolutionary status of the NX Pup system. Since the projected distance between NX Pup C and NX Pup AB is 3150 AU, it is likely that NX Pup C is not physically bound to NX Pup AB. On the other hand, we have clear evidence that NX Pup C is a pre-main sequence star. Furthermore it is the only other PMS within a 2.5' \times 2.5' field around NX Pup. Therefore, the three stars could quite well form a hierarchical triple system. The identification of NX Pup C as a classical T Tauri star provides the first evidence for low-mass star formation in CG 1.

Acknowledgements

Discussions with C. Jenkins and R. Wilson are gratefully acknowledged. We thank P.S. Thé and C. Sterken for providing us with LPTV measurements prior to publication and A. Tokovinine for providing us some IRAF scripts using DAOPHOT. W. Brandner was supported by a student fellowship of the European Southern Observatory.

References

- Brandner W., Bouvier J., Grebel E.K., Tessier E., de Winter D. and Beuzit J.-L., 1994, *A&A* submitted.
 Beckers J. M., 1993, *ARAA*, Vol. 31.
 Bernacca P.L., Lattanzi M.G., Bucciarelli B., Bastian U., Barbaro G., Pannunzio R., Badiali M., Cardini D., Emanuele A., 1993, *A&A*, **278**, L47.
 Blondel P.F.C., Tjin A Djie, H.R.E. 1994, ASP Conf. Ser. 62, 211.

- Beuzit J.-L. *et al.*, *The Messenger*, **75**, p. 33.
 Brand P.W.J.L., Hawarden T.G., Longmore A.J., Williams P.M., Caldwell J.A.R., 1983, *MNRAS*, **203**, p. 215.
 Henkel 1989, *The Messenger*, **57**, p. 8.
 Irvine N.J., 1975, *PASP*, **87**, p. 87.
 Malbet F., Léna P., Bertout C., 1993, *A&A*, **271**, L9.
 Mc Lure R.D., Arnaud J., Murray Fletcher J., Nieto J. and Racine R., 1991, *PASP*, **103**, p. 570-575.
 Reipurth B., 1983, *A&A*, **117**, p. 183.
 Reipurth B., Pettersson B., 1993, *A&A*, **267**, p. 439.
 Rigaut F., Rousset G., Kern P., Fontanella J.-C., Gaffard J.P., Merkle F., Léna P., 1991, *A&A*, **250**, p. 280.
 Roddier F., Northcott M.J., Graves J.E., McKenna D.L., Roddier D., 1993, *J. Opt. Soc. Am. A*, Vol. 10, p. 957-965.
 Sterken *et al.* 1995, in preparation.
 Tessier E., 1993, Thesis, University of Paris 6.
 Tessier E., Bouvier J., Lacombe F., 1994, *A&A*, **283**, p. 827.
 Wilson R. and Jenkins C., 1994, *MNRAS* in preparation.

Observations of the Sunyaev-Zeldovich Effect Towards ROSAT Clusters with SEST and the Italian Double-Channel Photometer

P. ANDREANI¹, H. BÖHRINGER², R. BOOTH³, G. DALL'OGGIO⁴, L.-A. NYMAN⁵, L. PIZZO⁶, P. SHAVER⁷, N. WHYBORN³

¹ Dipartimento di Astronomia, Università di Padova, Italy; ² Max-Planck-Institut für Astrophysik, Garching, Germany;

³ ONSALA Space Observatory, Onsala, Sweden; ⁴ Dipartimento di Fisica, III Università di Roma, Italy;

⁵ ESO-La Silla, Chile; ⁶ Istituto TESRE, Bologna, Italy; ⁷ ESO-Garching, Germany

Scientific Aims

A double-channel (1.2 and 2 mm) photometer has been installed at the focus of the SEST antenna to perform measurements of the Sunyaev-Zeldovich effect towards X-ray ROSAT clusters. Here we report the performance of the instrument and the first results obtained during the August-September 1994 observing run.

The Sunyaev-Zeldovich effect (Sunyaev and Zeldovich, 1972) is a shift of the Cosmic Microwave Background spectrum by the inverse Compton scattering of microwave photons by the hot electron gas present in rich clusters of galaxies. The resulting cluster signal shows a decrement at wavelengths longer than 1.4 mm and an enhancement at shorter ones relative to its planckian value. After many attempts to detect this effect (see e.g. the review paper Birkinshaw, 1990) radio observations seem finally to show the expected decrement at centimetre wavelengths towards A2218, A665, 0016+16 and A773 (Birkinshaw, 1991; Klein et al., 1991; Jones et al., 1993; Grainge et al., 1993) and more recently even at 2.2 mm towards

A2163 (Wilbanks et al., 1994). However, a more definitive detection of the S-Z effect requires the measurement of both the decrement and the enhancement. In order to minimize systematic errors and to eliminate spurious signals, simultaneous detections of the decrement and enhancement are mandatory.

The Italian group of the III University of Rome have therefore built a photometer with two channels centred at 1.2 and 2 mm to feed the O.A.S.I. (Osservatorio Antartico Submillimetrico Infrarosso) telescope installed at the Italian base in Antarctica (Dall'Oglio et al., 1992). This photometer has been adapted to be placed at the focus of the SEST antenna in Chile.

The Instrument

The photometer uses two Si-bolometers cooled at 300 mK by means of a single stage ³He refrigerator. They are located inside the cryostat orthogonal to each other. With this configuration the radiation coming from the telescope is split by a dichroic mirror (beam-splitter) onto two interference filters centred at 1.2

and 2 millimetres with bandwidth 350 and 560 μ m respectively. The central wavelengths have been chosen to match the atmospheric transmission windows and to maximize the ratio between the expected signal from the S-Z effect and that from the atmosphere, I_{SZ}/I_{atm} . Note that the 2 mm band includes the peak brightness of the decrement in the S-Z effect: $\Delta I \sim -56.3 y$ Jy (or in temperature: $\Delta T \sim -2.53 y$ K), while in the 1.2 mm band we expect a positive signal of $\sim +32.3 y$ Jy (or $\Delta T \sim +1.33 y$ K), where y is the Comptonization parameter depending on the electron gas temperature and density. It ranges between 2 and $6 \cdot 10^{-4}$ for the chosen clusters. More details on the characteristics of the photometer and the refrigerator system can be found in Pizzo et al. (1994a, 1994b).

Before installing the photometer in the receiver cabin, we measured the r.m.s. values of the responsivities (the detector output signals in Volts per degree Kelvin or per Watts falling onto the detectors): we find $5.9 \mu V/K$ (or $2 \cdot 10^7$ V/W) at 1.2 mm and $2.8 \mu V/K$ (or $3.8 \cdot 10^7$ V/W) at 2 mm. The noise equivalent temperatures (N.E.T., i.e. the brightness temper-

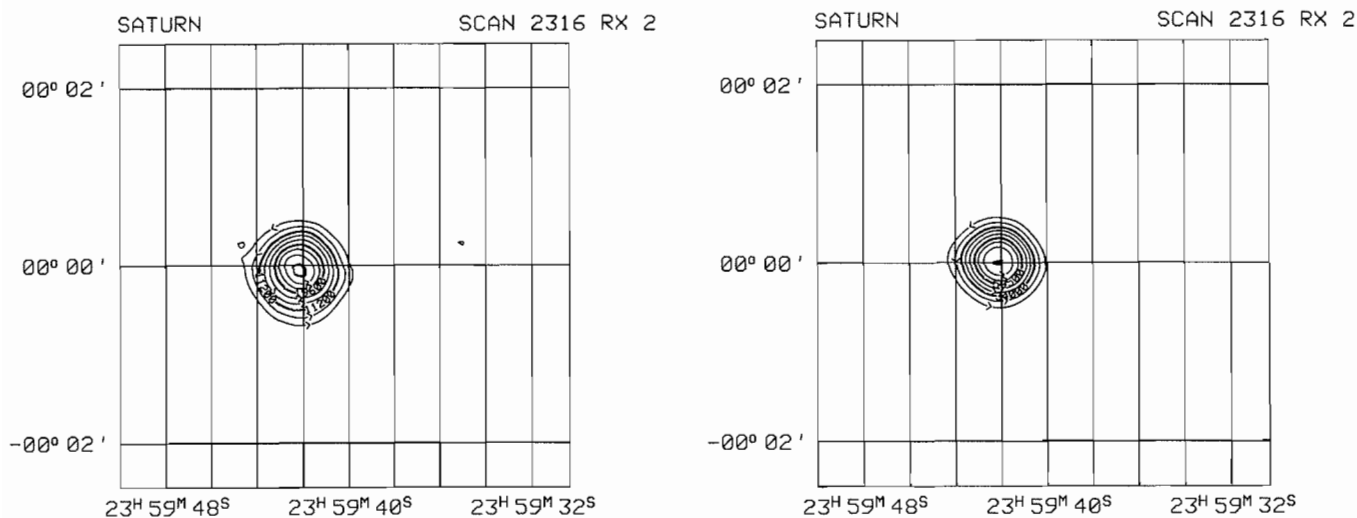


Figure 1: The raster map on Saturn of the (left) 1.2 mm channel and (right) 2 mm channel. From the map the HPBW of the beam turns out to be $44''$ and $46''$ at 1.2 and 2 mm respectively. Beams are aligned within $3''$.

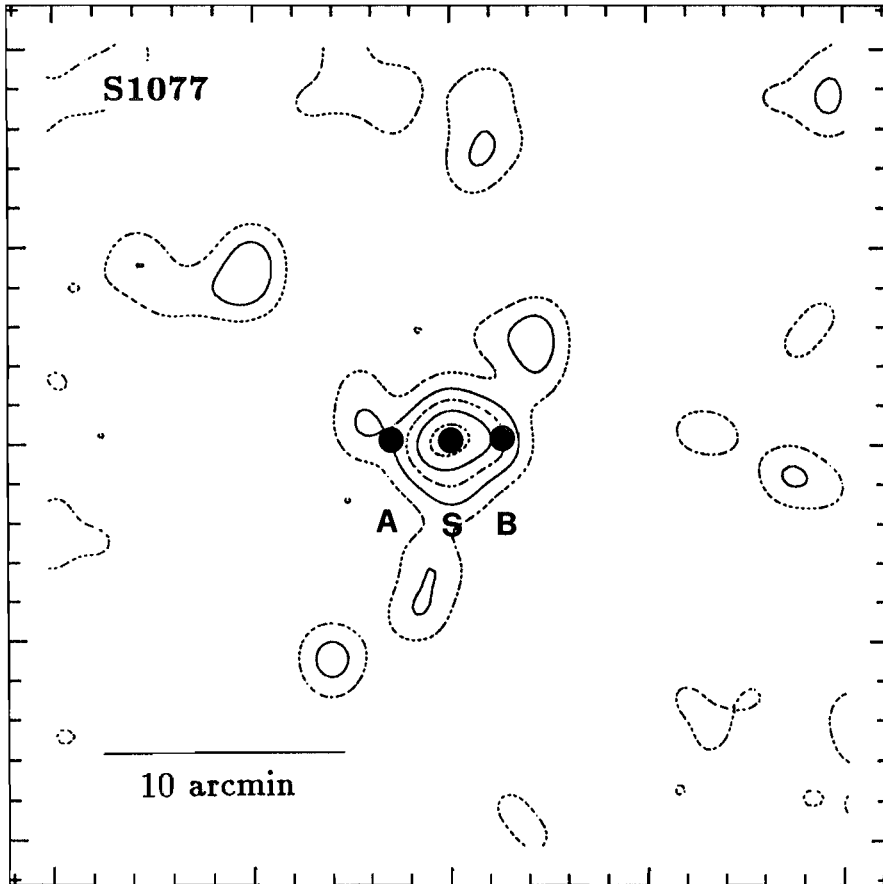


Figure 2: The ROSAT all-sky survey image of S1077. The central beam (S) and the reference beams (A and B) are shown as filled circles superposed on the X-ray isophotes.

ature producing a signal with a signal-to-noise ratio of 1) are: 4.2 and 9 $\text{mK}/\sqrt{\text{Hz}}$ at 1.2 and 2 mm respectively. Since we expect a cluster signal of the order of 1 mK (see above), this means that in principle to get a 1σ value of 1 mK we have to integrate for 5 and 20 seconds at 1.2 and 2 mm respectively.

The coupling between the optics of the telescope and that of the photometer is provided by a PTFE lens converting the $F/d = 5.1$ beam from SEST to the $F/d = 4.3$ configuration of the photometer. The lens focal length of 570 mm gives the optimum coupling at both 2 mm and 1.2 mm and it is fixed on the cryostat window. The lens was designed and built at Onsala.

The electronic chain consists of a preamplifier and a variable gain amplifier for each detector. The signal from each channel is fed to two separate acquisition systems: (a) by means of a two-channel Voltage-to-frequency converter, the outputs from the variable gain amplifiers are integrated with counters and stored on the HP computer controlling the antenna. The acquisition software has been modified by Roland Lemke of the SEST team in La Silla in order to store the two outputs of our photometer. (b) The secondary outputs from the variable gain amplifiers are fed to Stanford Research Lock-In

amplifiers. The analogue outputs from the lock-in amplifiers are measured in a DI-200 data-acquisition system which is controlled by a 80386 PC through a parallel port. The programme uses the serial port COM1 to read the data from the antenna HP control computer. The data-acquisition programme was implemented by Angel Otárola of the SEST team at La Silla.

Measured Performance

We used the dual-beam mapping programme adapted by Roland Lemke for the two-channel photometer to perform raster scans on planets. These scans provide a measurement of the beam shapes and dimensions and the beam separation in the sky. Figure 1 shows the two-dimensional appearance of the beams of the two channels. As it is clear from the figure, the beams are symmetric around the optical axis. Planet scans at the two wavelengths overlap well (within $3''$), indicating the good alignment of the two beams. The Half Power Beam Width turns out to be 44 and $46''$ at 1.2 and 2 mm respectively as we expect from the dimensions of the Winston cone entrance. Note that we are not working in a diffraction limited configuration and

therefore the beams at the two different frequencies are comparable. We have set the chop throw in order to have a beam separation in the sky of $135''$.

The detector noise in the receiver cabin turned out to be twice as large as that measured in the laboratory. In particular, because of its mounting inside the cryostat, the 2 mm channel suffered microphonics very likely caused by vibrations of the mechanical devices cooling the heterodyne receivers. In order to measure the N.E.T.s, sky noise and responsivities must be evaluated: the former is obtained during each night by looking at blank sky, the latter with calibration on planets. The average values of the N.E.T. measured at the focus were 28 and 70 $\text{mK}/\sqrt{\text{Hz}}$, i.e. 14 and 35 mK in one second integration time. To compare these values with those expected from the effect we have estimated, the magnitude of the latter by convolving $\Delta T = T y (x \coth(x/2) - 4) K$ (T is the CMB temperature, $x = h\nu/kT$ and $y = \int kT_e/mc^2 n_e \sigma_T dl$ is the comptonization parameter, n_e , T_e being the electron density and temperature) with the spectral filter response, the atmospheric transmission and the cluster core radius. We find: $\Delta T \sim 1.3 y K$, $\Delta T \sim -2.7 y K$ at 1.2 and 2 mm respectively. For a typical cluster in our list we estimate a comptonization parameter of $y \sim 4 \cdot 10^{-4}$, therefore we get $\Delta T \sim 0.5 \text{ mK}$ and $\Delta T \sim -1.1 \text{ mK}$ at 1.2 and 2 mm respectively. This means that 3σ values can be reached in 2-3 hours with the present instrumentation.

Observations of X-Ray Clusters A2744, S1077 and S295

Candidate sources were selected from the ROSAT southern clusters according to the following prescriptions: (a) high X-ray luminosity and (b) redshift larger than 0.25. This choice matches the two fundamental requirements: a small apparent angular dimension of the cluster core and a large Comptonization parameter. The cluster angular dimensions should not largely exceed the instrument beam width and they must be smaller than the maximum chop throw otherwise the amplitude of the signal cannot be correctly estimated. A large y parameter enhances the amplitude of the effect and therefore its detectability. Figure 2 shows superposed to the X-ray map of S1077 the location of the main beam (at the centre) with the reference beams (position A and B). Beam switching + nodding provides the real-time comparison between the emission from the cluster centre and that from the reference beams A and B.

The effect we are looking for is very weak. We have therefore to check carefully all the systematics which could affect the measurements. Spill-over from the

ground, difference in temperature from one side to the other of the main mirror and other effects could certainly plague the observations. Since it is hard to identify and quantify each effect, we have measured them according to the following observing strategy: each source was integrated over time chunks of 600 s, this time interval plus the needed overheads gives a total tracking time on the source of 15 minutes. The same time was spent on a blank sky located with equatorial coordinates 15 minutes larger in right ascension. This means that the antenna tracks twice the same sky position in horizontal coordinates: once ON the source and the second time on the reference blank sky position. This enables us to compare the two different measurements and eliminate the spurious signals.

Because of the time spent for installation and tests and that lost due to bad weather, the number of useful observations in our August-September run was small. Some observations were

obtained towards the clusters A2744, S1077 and S295. Careful data analysis is in progress: the real signal will be compared with a template one obtained by simulating the observational setup on the X-ray map of the source. A rough analysis gives some preliminary positive results: we find a 3σ value for the decrement towards S1077 of -2.5 ± 0.8 mK. This result makes us confident that with some improvements and the acquired knowledge of the system a next observing run will be successful in detecting the effect. We foresee changing the bolometer mounting by building a more robust cryostat and a different adapter. Both improvements will damp vibrations in the receiver cabin thus largely reducing microphonics and enhancing the detector sensitivity.

Acknowledgements

We would like to warmly thank the SEST team and in particular Glenn Pers-

son, Roland Lemke and Angel Otàrola for their fundamental help and assistance during the observations. We are very grateful to the ESO Workshop team at La Silla, which was of great help during the photometer setup.

References

- Birkinshaw M., 1991, in *Physical Cosmology*, ed. A. Blanchard et al. (Gif-sur-Yvette: Editions Frontières), 177.
- Dall'Oglio G. et al., 1992, *Exp. Astron.*, **2**, 256.
- Jones M. et al., 1993, *Nature* **365**, 322.
- Pizzo L. and Dall'Oglio G., 1994a, preprint.
- Pizzo L., Andreani P., Dall'Oglio G., Lemke R., Otàrola A. and Whyborn N., 1994b, *Exp. Astr.*, submitted.
- Sunyaev R.A. and Zeldovich YaB., 1972, *Comm. Astroph. Space Phys.*, **4**, 173.
- Wilbanks T.M., Ade P.A.R., Fischer M.L., Holzappel W.L. and Lange A.E., 1994, *ApJ* **427**, L75.

The AstroWeb Database of Internet Resources

H.-M. ADORF¹, D. EGRET², A. HECK³, R. JACKSON⁴, A. KOEKEMOER⁵, F. MURTAGH¹ and D. WELLS⁶

¹ST-ECF, Garching, Germany; ²CDS, Strasbourg, France; ³Strasbourg Astronomical Observatory, France;

⁴CSC/STScI, Baltimore, U.S.A.; ⁵MSSSO, Canberra, A.C.T., Australia; ⁶NRAO, Charlottesville, U.S.A.

Introduction

The Internet has succeeded – and with it the World Wide Web. This model of hypertext information with embedded pictures and hyperlinks to other local or remote information pages – as well as to other Internet services – greatly facilitates public near-realtime participation of astronomical events, such as the observations of the Shoemaker-Levy-9 comet crash on Jupiter (Murtagh & Fendt 1994, West 1994, Whitehouse 1994). The World Wide Web, or WWW for short, is also increasingly used for scientific communication and information dissemination in all natural sciences, and astronomy is one of the most active communities in this respect.

With the success of the Internet, a mechanism better than individual “hot-lists” for organizing useful collections of astronomical Internet resources is clearly needed. This is where the “AstroWeb” database (Adorf *et al.* 1994, Jackson *et al.* 1994, 1995a, b) enters. It aims at being the most complete and useful on-line collection of Uniform Resource Locators (URLs) for astronomical Internet resources, pointing to entities as diverse as societies, observatories, databases, preprint servers, telescopes, telescope schedules, weather information or individual astronomers. As such the AstroWeb database complements the recent annotated compilation of astronomical Internet resources (Andernach, Hanisch & Murtagh 1994).

Organization

The AstroWeb database, which is maintained by the “AstroWeb Consortium”, currently comprises more than 1100 records of FTP, Gopher, Telnet, News, WAIS and WWW resources. Each record minimally consists of a headline and an associated URL. Many records are augmented by a paragraph of descriptive text. If known, the e-mail address of the resource’s maintainer is stored along with the record. As added value, the AstroWeb consortium has classified each record according to one

or more of about 25 categories, such as observatory, radio, optical, infrared, telescope, database or software.

The AstroWeb database is actually a distributed system of databases maintained at five different sites (CDS, MSSSO, NRAO, ST-ECF, and STScI) on three continents. The master copy is currently kept at the Space Telescope Science Institute, Baltimore. There the aliveness of all URLs (except of Telnet records) is verified three times a day, and “unreliable” or “dead” URLs are

flagged. Once a day each site automatically fetches a copy from the master, and formats a local rendition of the AstroWeb database.

Each site offers the AstroWeb database in a different style of presentation. The ST-ECF rendition, for instance, is terse and suitable for quick reference, whereas the STScI or NRAO renditions are more verbose and particularly suitable for browsing. Some sites even offer more than one rendition for the convenience of the users.

The screenshot shows a web browser window with a menu bar containing 'File', 'Options', 'Navigate', 'Annotate', and 'Help'. Below the menu bar, there are two input fields: 'Document Title' with the text 'AstroWeb: Astronomy/Astrophysics on the Inter...' and 'Document URL' with the text 'http://ecf.hq.eso.org/astroweb/yp_astro_resou...'. The main content area has a small image of a galaxy on the left and the title 'AstroWeb: Astronomy/Astrophysics on the Internet' on the right. Below the title is a paragraph of text: 'This collection of pointers to astronomically relevant information available on the Internet is maintained by the AstroWeb Consortium, which will be pleased to accept contributions of new resources, as well as reports of corrections to existing records. In addition to classified lists of resource records, the Consortium also provides a utility to search the AstroWeb database:'. Below this text is a search box containing the text 'villafraanca'. Further down, there is a paragraph: 'Three times a day, most of the URL's are validated to verify aliveness (see "AstroWeb Dead URLs" and "AstroWeb Unreliable URLs"). These ST-ECF AstroWeb pages are updated at about 10:30 UT each day, if the master database has changed.' Below this is another paragraph: 'Neither ST-ECF nor the AstroWeb Consortium has any control over the contents or the availability of the information located at other Internet sites.' At the bottom of the main content area, there is a section titled 'Publication-related Resources' with a list of items: 'Preprint Lists (54 records)', 'Abstracts (35 records)', and 'Bibliographical Services (25 records)'. At the very bottom of the browser window is a navigation bar with buttons for 'Back', 'Forward', 'Home', 'Reload', 'Open...', 'Save As...', 'Clone', 'New Window', and 'Close Window'.

Figure 1: View of the top-level page of the AstroWeb database at the ST-ECF. Hyperlinks to forms for entering new records, and for error corrections are provided.

Figure 2: The list of "telescope schedules" accessible from the AstroWeb information pages.

Accessing the AstroWeb Database

The natural place for offering the AstroWeb database is the WWW. The ST-ECF rendition can be accessed either through hyperlinks originating from the ESO web (<http://www.hq.eso.org/eso-homepage.html>), or from the ST-ECF web (<http://ecf.hq.eso.org/>), or directly via the "yellow pages" URL

http://ecf.hq.eso.org/astroweb/yp_astro_resources.html (Fig. 1), from where links to the other AstroWeb renderings are provided. The AstroWeb database is an excellent starting point for browsing topics on the astronomical Internet (Figs. 2 and 3), as well as for finding other resources of potential interest to astronomers.

At a size of well over 1000 records, it is mandatory that the database is also *searchable*. To this end one may use the simple text matching facility built into most, if not all, WWW clients. A more powerful search mechanism, however, is offered by the AstroWeb WAIS index, which can be queried using natural (English) language from all AstroWeb sites. Since complete records are indexed, queries may include categories and URLs, which are usually hidden in HTML-comments. The results are returned as WWW-pages with ready-to-use hyperlinks to interesting resources found.

Submission of New Records

The AstroWeb Consortium, consisting of the authors above, *welcomes* submissions of new records from the astronomical community; WWW forms have been put in place to facilitate this process. Submissions are reviewed by Consortium members and entered manually into the database to ensure a minimum quality. Those recent submissions not yet entered into the main database may be viewed (and used).

The Consortium also encourages corrections to existing records (e.g. via e-mail to astroweb@noao.edu). AstroWeb Consortium members can globally edit the database, in order to better respond to change requests.

Figure 3: Portion of the "abstracts" resource listing in the AstroWeb database.

Schedules

- [Anglo-Australian Telescope - Schedules \(AAT \)](#)
- [Australia Telescope Compact Array - Schedules \(ATNF \)](#)
- [Bologna 152cm Telescope - Schedules](#)
- [Canada France Hawaii Telescope - Archive & Schedules \(at DAO\) \(CFHT \)](#)
- [Canada France Hawaii Telescope - Schedules \(at Hawaii\) \(CFHT \)](#)
- [Cerro Tololo Interamerican Observatory - Schedules \(CTIO \)](#)
- [Five College Radio Astronomy Observatory - Schedules \(FCRAO \)](#)
- [Infra-Red Telescope Facility - Schedules \(IRTF \)](#)
- [Infrared Space Observatory - Schedules \(ISO \)](#)
- [James Clark Maxwell Telescope - Schedules \(JCMT \)](#)
- [Kitt Peak National Observatory - Schedules \(KPNO \)](#)
- [La Palma - Isaac Newton Group - Schedules \(ING \)](#)
- [La Palma - Nordic Optical Telescope - Schedules \(NOT \)](#)
- [La Silla - All Telescopes - Schedules](#)
- [La Silla - ESO Schedules](#)
- [Mount Stromlo and Siding Spring Observatories - Schedules \(MSSSO \)](#)
- [Padova Ekar 182cm Telescope - Schedules](#)
- [UCO/Lick: Keck Telescope - Schedules \(UCO \)](#)
- [UCO/Lick: Mt. Hamilton 3m - Schedules \(UCO \)](#)
- [University of Hawaii IfA: 2.2m Telescope - Schedule](#)
- [Very Large Array - Schedules \(VLA \)](#)
- [Very Long Baseline Array / Global Network - Schedules \(VLBA \)](#)
- [Whipple Observatory / Multiple Mirror Telescope - Schedules \(Whipple / MMT \)](#)

Abstracts

- [Abstract searches - Cambridge, UK](#)
- [ADASS-94 abstracts](#)
- [Astrophysics Data System Abstract Service \(ADS Abstracts \)](#)
- [Astrophysics Data System \(ADS \)](#)
- [CDS Abstract Service](#)
- [CEA abstracts and publications](#)
- [ESO Preprints Database \(Bibliographic catalogue \)](#)
- [ESO Publications](#)
- [NASA ApJ abstracts](#)
- [NASA RECON abstracts](#)
- [NASA SCAN](#)
- [NASA Stellar DataBase Request Form](#)
- [NASA Technical Report Server \(NTRS \)](#)
- [NASA/STI/RECON STELAR abstracts database \(GSFC \)](#)
- [PASP Abstract Service at CDS](#)
- [PASP abstracts archive, STScI](#)
- [Peter Tribble's Papers](#)
- [Princeton University - Astrophysics Library](#)
- [Space Telescope Science Institute \(STScI \)](#)
- [Stanford Public Information Retrieval System \(SLAC-SPIRES \)](#)
- [STELAR Abstracts - Astronomical Journal](#)
- [STELAR Abstracts - Astronomy and Astrophysics Review \(A&AR \)](#)
- [STELAR Abstracts - Astronomy and Astrophysics Suppl.](#)
- [STELAR Abstracts - Astronomy and Astrophysics](#)
- [STELAR Abstracts - Astrophysical Journal Suppl.](#)
- [STELAR Abstracts - Astrophysical Journal](#)

Possible Future Steps

After a rapid growth, the AstroWeb is currently being consolidated. It is hoped that, with the help of the astronomical community, the degree of completeness and quality of the AstroWeb database can be further improved. Certainly, database internal cross-referencing within the descriptive paragraphs is far from complete. Here the situation can presumably be remedied with an appropriate software tool.

In the future the AstroWeb database might be used as a starting base for indexing all astronomical WWW pages out on the Internet. This would involve a "robot" repeatedly fetching all relevant HTML pages, similarly to how Archie indexes all files in all registered any-

nous FTP servers. Such a project is by no means out of question. In fact, general indices spanning the whole WWW already exist, but none thus far is specific to astronomy.

References

- Adorf, H.-M., Egret, D., Heck, A., Jackson, R., Koekemoer, A., Murtagh, F., Wells, D.: 1994, "AstroWeb – Internet resources for astronomers", *ST-ECF Newsl.* **22**, (in press).
- Andernach, H., Hanisch, R.J., Murtagh, F.D.: 1994, "Network resources for astronomers", *Publ. Astron. Soc. Pacific*, (in press).
- Jackson, R., Wells, D., Adorf, H.-M., Egret, D., Heck, A., Koekemoer, A., Murtagh, F.: 1994, "The AstroWeb Database", *Bull. CDS* **45**, 21–25.

Jackson, R., Wells, D., Adorf, H.-M., Egret, D., Heck, A., Koekemoer, A., Murtagh, F.: 1995a, "AstroWeb – A database of links to astronomy resources – Announcement of a database", *Astron. Astrophys. Suppl.* **108**, 235–236.

Jackson, R.E., Adorf, H.-M., Egret, D., Heck, A., Koekemoer, A., Murtagh, F., Wells, D.: 1995b, "AstroWeb – Internet resources for astronomers", in: *Proc. Astronomical Data Analysis Software and Systems (ADASS) 1994*, Baltimore, MD, D. Shaw, H. Payne, and J. Hayes (eds.), Astronomical Society of the Pacific, (in press).

Murtagh, F., Fendt, M.: 1994, "The SL-9/ESO Web Encounter", *ESO Messenger* **77**, 47.

West, R.: 1994, "Comet Shoemaker-Levy 9 Collides with Jupiter", *ESO Messenger* **77**, 28–31.

Whitehouse, K.: 1994, "Comet Explodes on Jupiter – and the Web", *IEEE Computer Graphics and Applications*, **Nov. 94**, 12–13.

Producing Multi-Wavelength Overlays with MIDAS

M. PIERRE, CEA/DSM/DAPNIA CE Saclay, France, and
Max-Planck-Institut für Extraterrestrische Physik, Garching, Germany

Astronomy is no longer solely a science where data obtained in different wavelength ranges are analysed separately. Astronomers are becoming more and more involved in combined multi-wavelength programmes (optical, radio, IUE, ROSAT and soon ISO . . .) for which basic coordinates transformation facilities constitute the starting point for any further data analysis. This contribution describes the method used for making the optical/X-ray/radio overlays, presented in the preceding article "Multi-wavelength study of ROSAT clusters of galaxies".

For each cluster, we have at our disposal ESO 3.6-m EFOSC R images ($\sim 4' \times 6'$; scale: $0.6''/\text{pixel}$), ROSAT survey images (~ 1 sq. degree, resolution: $\sim 2'$), MOST images ($70' \times 70'$ cosec(δ), resolution: $43'' \times 43''$ cosec(δ); we thus adopted a final layout where the X-ray and radio contours are superimposed onto the optical pixel image. The latter determines the final overlay size.

Because of the very different processes by which these images are obtained, the production of the overlays is a long and tedious procedure, all the more so since no regridding programmes are available in MIDAS, nor are there commands for converting pixel coordinates into celestial. To summarize the starting situation:

– X-ray ROSAT survey images are routinely obtained by the EXSAS package (MPE) in a J2000 system, using $25''$ pixels; the sky projection can be as-

sumed to be tangential within the overlay field.

– The radio images were initially reduced with the AIPS package, using $\sim 15''$ (not square) pixels, in a SIN projection (B1950). In order to match the X-ray data, the radio images are in turn regridded into J2000 and tangential projection using AIPS.

– The accurate sky projection of the optical images is undefined. We stress here that, for our purpose, CCD images are essential (rather than Schmidt plate scans) to provide a detailed description of the galaxy distribution of our distant clusters.

– The MIDAS (EXSAS) and AIPS image header information regarding absolute coordinates, centre of projection, etc., are incompatible.

We therefore wrote a series of MIDAS procedures to cope with the lack of coherence between the systems, knowing that without proper regridding programmes it is not possible to have exact coincidence between the three wavelengths. The method is based on the fact that after the processing, overlays (which cover a small area) will have as "world coordinates" true coordinates, i.e. RA and Dec in decimal degrees aligned with the X and Y axes respectively (owing to the radio and X-ray resolutions, a minimal $2''$ accuracy for the three wavelengths is required over a $5' \times 5'$ field). This not only a tractable way to treat the unknown distortions of the optical image, but also enables us to get object positions directly

using the command `GET/CURSOR` after the final overlay has been displayed on the screen. We now describe briefly how each image was processed to reach this stage.

– For the purpose of aligning optical images, telescope coordinates are not accurate enough, and thus reference stars are needed. As the GSC does not provide enough objects on such a small field at high galactic latitude, and most objects are too bright and saturated on the CCD image, we make use of the general COSMOS object catalogue. The figure presents a finding chart produced by the NRL/ROE package available at MPE. The brightest stars are referenced with numbers, their coordinates are listed on the right-hand side of the figure, and a corresponding ASCII list is simultaneously produced by the programme; this file is then transformed into a MIDAS table (*TA*). In a second step, the CCD image is displayed on the screen and pixel coordinates of reference stars (at least 5), well distributed over the whole field, are interactively determined using the command `CENTER/GAUSS` with a table as output option (*TB*); selected stars are given the same identifier as in the COSMOS list. Then the two tables, *TA* (celestial coordinates) and *TB* (pixel coordinates), are compared with the command `ALIGN/IMAGE` letting all parameters free (i.e. rotation angle, X and Y scale factors, X and Y translations). In this way, the image is stretched in all directions so that the residuals for the

ROSAT Identification

Survey UKST IIIaJ

Field No. 381

Plate Epoch: 1976.4100

ROSAT Position: 12 36 41.9 -33 54 46

ROSAT / MPE / RSDC 27-OCT-94 09:20:28

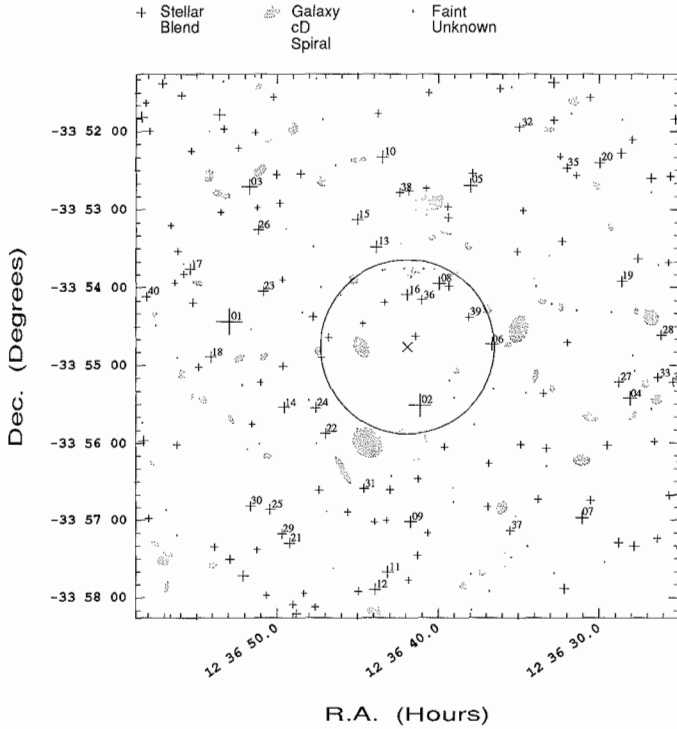
ROE/NRL Finding Chart

in : PRG7.MOS;1

out: prg7.ps

ROSAT Source Name: 000001RX J1236.7-335

Error radii: 1 sig = 40.8, 1.645 sig = 67.2, 2 sig = 81.7, 3 sig = 122.5 arcsec



#	CLASS	B	R.A.	Dec.	DIST.
01	Stellar	10.84	12 36 52.9	-33 54 26	138.8
02	Stellar	11.59	12 36 41.1	-33 55 31	46.4
03	Stellar	13.91	12 36 51.7	-33 52 43	173.6
04	Stellar	14.82	12 36 28.1	-33 55 26	176.7
05	Stellar	14.86	12 36 38.0	-33 52 41	133.6
06	Stellar	15.26	12 36 36.7	-33 54 44	65.4
07	Stellar	15.36	12 36 31.1	-33 56 58	189.2
08	Stellar	15.53	12 36 39.9	-33 53 57	54.7
09	Stellar	15.99	12 36 41.7	-33 57 02	135.7
10	Stellar	16.03	12 36 43.4	-33 52 20	147.3
11	Stellar	16.09	12 36 43.1	-33 57 41	175.2
12	Stellar	16.16	12 36 43.9	-33 57 54	189.7
13	Stellar	16.34	12 36 43.8	-33 53 29	80.5
14	Stellar	16.47	12 36 49.6	-33 55 33	106.2
15	Stellar	16.53	12 36 45.0	-33 53 08	105.5
16	Stellar	16.59	12 36 41.9	-33 54 06	40.5
17	Stellar	16.68	12 36 55.4	-33 53 46	178.3
18	Stellar	16.68	12 36 54.1	-33 54 54	151.7
19	Stellar	16.91	12 36 28.6	-33 53 55	173.5
20	Stellar	17.24	12 36 29.9	-33 52 24	205.7
21	Stellar	17.26	12 36 49.2	-33 57 18	177.2
22	Stellar	17.45	12 36 47.0	-33 55 53	92.2
23	Stellar	17.47	12 36 50.9	-33 54 03	119.4
24	Stellar	17.61	12 36 47.6	-33 55 33	85.1
25	Stellar	17.65	12 36 50.4	-33 56 52	164.6
26	Stellar	17.82	12 36 51.2	-33 53 16	146.4
27	Stellar	17.97	12 36 28.7	-33 55 13	166.3
28	Stellar	18.01	12 36 26.1	-33 54 37	196.5
29	Stellar	18.05	12 36 49.7	-33 57 11	174.4
30	Stellar	18.18	12 36 51.7	-33 56 49	172.9
31	Stellar	18.26	12 36 44.6	-33 56 36	114.7
32	Stellar	18.34	12 36 34.9	-33 51 57	190.2
33	Stellar	18.38	12 36 26.3	-33 55 10	195.5
34	Stellar	18.38	12 36 25.4	-33 55 13	207.6
35	Stellar	18.43	12 36 32.0	-33 52 28	185.2
36	Stellar	18.61	12 36 41.0	-33 54 10	38.1
37	Stellar	18.65	12 36 35.5	-33 57 08	163.1
38	Stellar	18.86	12 36 42.4	-33 52 47	118.7
39	Stellar	18.93	12 36 38.1	-33 54 23	53.1
40	Stellar	19.01	12 36 58.1	-33 54 07	205.8

Selection criterion: bright stellar objects

Example of a ROE/NRL/MPE finding chart (Abell 700) used in the alignment of the optical CCD images. Galaxies are plotted as grey ellipses and stars with crosses. The ROSAT centroid (X) and the 90% error circle are also indicated.

reference stars are minimized. The obtained transformation parameters finally enable us to rebin the image into RA, Dec via the command `REBIN/ROTATE`. A last check, using COSMOS reference stars not involved in the determination of the transformation, shows that a 1'' accuracy is reached – which is actually the nominal precision of the COSMOS positions. We must stress that we have encountered a difficulty due to the output format of the command `CENTER/GAUSS`: only 6 digits are available. This means that for the final check, as image coordinates are now equatorial, it is not possible to reach arcsec accuracy (e.g. we get in output: RA = 156.342). We overcame this difficulty (which is just an output problem, the computed START and STEP descriptor values being in double precision) by temporarily subtracting the integer part of the START value in the descriptor (e.g. this time `CENTER/GAUSS` will give 0.3423). We recommend that, in future, this command (as well as `GET/CURSOR`) works in double precision, which seems to be logical, considering that the START and STEP descriptors of the image header are double precision numbers.

– The X-ray image has world coordinates in unit of 0.5'' (coordinates 0,0 at the field centre) but possesses in its descriptor the coordinates of centre of the projection (`POINT_LONG`, `POINT_LAT`). This is used by the EXSAS command `TRANSFORM/COORDINATES` to convert pixel coordinates into celestial coordinates; the X and Y axes are aligned along the RA and Dec directions. With the aim of introducing celestial coordinates as world coordinates to match the optical image, we determine the equatorial coordinates of two reference pixels (usually the centre C and a 2nd point A about 2' off the centre). This provides unique pixel transformation equations, $(i, j) \rightarrow (RA, Dec)$, assuming that all over the field: (1) projection effects are negligible and (2) $STEP(x) = STEP(y) \cdot \cos(Dec(C))$. Descriptor START and STEP values are consequently modified to yield world coordinates in decimal degrees. In this new coordinate system, RA and Dec are exact for point C and all points located on the circle (C,A). At a distance of 10' from the centre we have computed a 2'' discrepancy with the new coordinates, and the true ones are provided by the command `TRANSFORM/COORDINATES`,

which is fully within the above accuracy requirements.

– The AIPS descriptors of the radio image provide in principle accurate information as to the celestial coordinates of any pixel; however, there is no way to handle them easily with the current MIDAS commands. Therefore, we adopted the following steps. The RA, Dec of the projection centre (C) of the image can be determined by simple linear equations: $RA = START(x) + NPIX(x)/2 \cdot STEP(x)$, $Dec = START(y) + NPIX(y)/2 \cdot STEP(y)$, but this is not true for any other pixel. Thus, to have a scale compatible with the optical image and assuming again that projection effects are negligible, we set: $STEP(x) = STEP(x)_{old} \cdot \cos(Dec(C))$ and $STEP(y) = STEP(y)_{old}$. This finally enables us to reset the START values adequately. Checking with AIPS point source positions over a large field gives satisfactory accuracy (comparable to that reached in the X-ray band).

The procedure described above provides the desired positional accuracy for the proposed scientific goals. However, one can easily imagine cases for which comparable accuracy will be required on much larger fields, or, alterna-

tively, with significantly higher accuracy, on smaller fields (e.g. VLA, VLBI positions, etc.). This procedure, unless it is further adapted, is unlikely to provide the expected precision. Therefore, we would recommend that the MIDAS environment

provide the opportunity of processing images obtained with different projections, mapped in different equinoxes as well as related header information fully compatible with those obtained with other standard packages.

Acknowledgements

It's a pleasure to thank R. Hunstead, A. Reid and A. Unewisse for detailed information about the radio data structure.

The 94NOV Release of ESO-MIDAS

SCIENCE DATA ANALYSIS GROUP

Introduction

The new 94NOV release of ESO-MIDAS will contain several improvements and new features in the core system as well as in the application areas. In this article you will find a summary of the most interesting new ones. More detailed descriptions can be found in the recent *ESO-MIDAS Courier* (October 1994).

The new release has been tested on a variety of platforms: SUN/SunOS 4.1.n and SUN/Solaris 2.3, HP/HP-UX, SG/IRIX, IBM/AIX, VAX/VMS, DEC/OSF1, DEC/Ultrix, VAX/Open-VMS and VAX/VMS, and PC/Linux. At the time this *Messenger* is distributed, the official 94NOV version will be released and all registered sites informed about its availability in the "midas" ftp account.

In order to optimize the distribution of this new release we request that MIDAS sites with Internet connectivity retrieve it from the "midas" ftp account. Sites with no connectivity can obtain the new release on magnetic media after having sent a completed ESO-MIDAS Request Form to the MIDAS Group (midas@eso.org).

System

New Line Editor for the 94NOV Release

One of the most prominent changes that (Unix) users will immediately experience is the implementation of a new line editor. In previous releases of ESO-MIDAS the monitor used the "TermWindows" library for its line-editing capabilities. "TermWindows" was implemented on VMS and UNIX systems and contained line-editing features inspired by those working on VAX/VMS. The 94NOV release of MIDAS includes and uses a new line-editor for the monitor based on the GNU "readline" library (also used in the GNU "bash" shell). This library, widely supported on UNIX platforms, enhances the line-editor capabilities of MIDAS with features like a history stack of commands, emacs or vi editing func-

tions, command and filename completion functions and a communication channel to the MIDAS GUI "help" for on-line help. This line-editor will be the default one for UNIX systems. For VMS systems the 94NOV release of MIDAS still provides the same line-editor as before.

FITS data decompression on the fly

The 94NOV release will contain an automatic "decompression on-the-fly" procedure from which commands like `INTAPE/FITS` can benefit. The biggest improvement is that previous processing sequences like e.g. separate decompression of files, removal of the compressed files to save disk space, and finally reading the decompressed files by `INTAPE/FITS` are now greatly simplified: `INTAPE/FITS` now takes care of the decompression without the need for extra disk space for the decompressed data.

Applications

Upgrade of the CCD package

In order to monitor the quality of the CCDs used on La Silla, ESO has started a programme of standard CCD tests. To support this programme from the software side, a number of new commands are incorporated in the CCD context. These commands operate on catalogues of images like bias, dark and low-count flat frames and will for example give the hot and cold pixel locations, the linearity and transfer curves, the shutter pattern, and the charge transfer efficiency.

A new astrometry context

A new context `ASTROMET` contains the astrometry package previously known as the programme `POS1` originally written by Richard West and implemented in MIDAS by Olivier Hainaut. For the MIDAS implementation the algorithm was not changed as it proved to be extremely accurate. While the original `POS1` was doing everything in one pro-

gramme, the MIDAS version has been split into 3 steps.

Firstly, read the measurements and standard stars, and compute the transformation parameters (this step is performed by command `ASTROMETRY/TRANSFORM`). Secondly, edit the standard star table to remove/restore some stars. This step is performed by the command `ASTROMETRY/EDIT`. Finally, compute the converted coordinates by the command `ASTROMETRY/COMPUTE`.

Graphical user interfaces

Two new graphical user interfaces (GUIs) will be included in the 94NOV release: a GUI for the Data Organizer (DO) and one for the infrared spectroscopy package `IRSPEC`.

Because the DO is particularly intended to be used in an on-line environment, it is essential that observers can interact efficiently with the tools offered to them. Therefore, a versatile graphical user interface has been fitted to the DO. The main interface window contains the Observation Summary Table on which all subsequent operations can be performed. With a number of special widgets the user can e.g. edit the classification rules, classify the biases, etc. A customized on-line version of the DO is now running at the NTT.

A second new GUI was created for the `IRSPEC` context by Cristian Levin at La Silla. Its main purpose is to provide an easy way to reduce infrared data on-line at the NTT, but it can also be very useful for off-line data reduction. The main features are:

- It has interfaces to all the commands of the existing context to reduce infrared data.
- A file management feature that allows to keep sets of input frame names in ASCII files.
- Some commands were grouped in the interface, and default values are provided for most of the parameters, so the user can reduce the data very quickly.

From the main menu of the `IRSPEC` graphical interface the user can create

sub-windows to start up the different steps of the reduction process.

User Support

ESO-MIDAS on the WWW

A description of the ESO-MIDAS project is now available via the ESO World Wide Web server (WWW). The information contains an overview of the MIDAS hard- and software requirements, distribution policy (including the ESO-MIDAS Request Form), documentation and support, and User Guides. Registered ESO-MIDAS sites can also start the MIDAS Xhelp Graphical User Interface directly from the XMosaic ESO-MIDAS home page. Besides consulting the on-line MIDAS help documentation, this facility also enables the users to send problem reports and questions to the MIDAS account at ESO headquarters in a pre-specified format that facilitates automatic processing. The ESO-MIDAS WWW pages can

be accessed via the ESO home page (<http://http.hq.eso.org/eso-homepage.html>) or directly reached using the ESO-MIDAS page <http://http.hq.eso.org/midas-info.html>. We hope to extend this service with e.g. information about the 94NOV release and further ongoing developments.

Handling of problem reports

Until the beginning of this year the handling of incoming problem reports was almost completely manual and rather time consuming, and an increase in efficiency would certainly free our hands for other priorities. For that reason we looked into products that administer problem reports (semi-)automatically. After evaluation of a few of these software products we have chosen to use the GNU Problem Report Management System, GNATS.

In GNATS, each problem report arriving at ESO is stored as a separate file within a main GNATS repository (direc-

tory). All these repositories make the entire Problem Report database that can be accessed by regulated editing to maintain consistency. However, anyone with access to electronic mail may submit Problem Reports. Provided a submitted Problem Report contains a minimal set of field descriptors, GNATS is able to forward the PR automatically to the responsible person, and keep track of its status.

One of the most important requirements of a new system is the user friendliness, in particular for new and inexperienced users who even more than experienced ones are in need of a good reporting system. This requirement is fulfilled via two possibilities of forwarding problem reports to ESO. The first one is by simply composing a text file containing the obligatory fields and forwarding it to the MIDAS e-mail address (midas@eso.org). The second way, however, is simpler and also saves time of the Problem Report manager at ESO: the XHelp Graphical User Interface.

ANNOUNCEMENT

European SL-9/Jupiter Workshop

Date: February 13–15, 1995

Venue: ESO Headquarters, Garching bei München, Germany

This ESO Workshop will serve to bring together European astronomers who have obtained observational data before, during and after the collision of comet Shoemaker-Levy 9 with Jupiter. Only by combining these data will it be possible to arrive at a good understanding of the complex phenomena and the meeting will thus contribute to the ongoing interpretative efforts. It will further the preparation of joint papers to be delivered at the major IAU Colloquium 158 on the same subject three months later (May 9–12, 1995; Baltimore, Maryland, U.S.A.) and also provide a useful forum for those European observers who are unable to come to Baltimore. The participation of Central and East European astronomers in the ESO Workshop will be supported by the ESO C&EE Programme. Some key people from outside Europe will provide additional input from other sides.

The meeting will be held in the ESO Auditorium and in view of its limited capacity (approx. 125), participation in this Workshop may have to be restricted.

The deadline for submission of abstracts to contributed talks and posters is January 15, 1995.

Please note that there will be a conference fee of 80 DM; this includes a copy of the Proceedings, to be available on May 1, 1995.

TOPICS

- I. The comet before impact
- II. The impacts
- III. Long-term effects
- IV. Summary

PRELIMINARY LIST OF SPEAKERS

H. Barwig, D. Bockelee-Morvan, R.W. Carlson, J. Crovisier, G. Chernova, K. Churyumov, F. Colas, P. Drossart, C. Emeric, T. Encrenaz, A. Fitzsimmons, E. Gerard, O. Hainaut, D. Hamilton, T. Herbst, K. Horne, W.-H. Ip, D.C. Jewitt, K. Jockers, H. Käufel, P. Lagage, J. Lecacheux, E. Lellouch, T. Livengood, D. Lupishko, J.-P. Maillard, A. Marten, K.-H. Mantel, S. Miller, F. Moreno, B. Mosser, G. Neukum, J. Ortiz Moreno, G. Paubert, R. Prange, P. Schleicher, R. Schulz, Z. Sekanina, J.A. Stuewe, N. Thomas, N. Walton, J. Watanabe, R.M. West.

ORGANIZING COMMITTEE

Heinz Barwig	(University Observatory, Munich, Germany)
Hermann Bönhardt	(University Observatory, Munich, Germany)
Jacques Crovisier	(Observatoire de Paris-Meudon, France)
Therese Encrenaz	(Observatoire de Paris-Meudon, France)
Benoit Mosser	(Institut d'Astrophysique, Paris, France)
Rita Schulz	(Max-Planck-Institut für Aeronomie, Katlenburg-Lindau, Germany)
Richard West	(European Southern Observatory)

TIMETABLE

Jan. 15, 1995:	Deadline for submission of abstracts of contributed talks and posters to Conference Secretariat
Jan. 20, 1995:	ESO C&EE Committee allocates support for participation in Workshop; grantees are informed
Jan. 20, 1995:	Final Programme available. Participants will be informed about their proposed presentations
Feb. 13–15, 1995:	European SL-9/Jupiter Workshop at ESO HQ
Feb. 27, 1995:	Deadline for submission of manuscripts
May 1, 1995:	Publication of Proceedings

CONFERENCE SECRETARIAT

D-85748 Garching bei München, Germany	Email: ips@eso.org (Internet)
European Southern Observatory	Fax : (+49-89) 320-23-62
Elisabeth Völk (SL9-1995)	Tel : (+49-89) 320-06-276
Karl-Schwarzschild-Str. 2	Tlx : 52828222 eo d
D-85748 Garching bei München, Germany	Email: ips@eso.org (Internet)

ESO/MPA Workshop on Spiral Galaxies in the Near-IR

Garching, 7–9 June 1995

The Workshop will bring theorists and observers together to discuss what can be learned about the dynamics, populations and nuclei of spiral galaxies from the newly available array data in the near infra-red. Topics to be covered include:

- Resolved Populations
- Global Colours
- Structure of Disks and Bars
- Milky Way Structure
- Nuclei of Spirals
- Spectroscopic Population Constraints

Scientific Organizing Committee: E. Athanassoula, K. Freeman, R. Genzel, D. Minniti, A. Moorwood, M. Rieke, H.-W. Rix, S. D. M. White.

Send inquiries to: dante@eso.org or rix@mpa-garching.mpg.de

Contact Addresses:

Dante Minniti European Southern Observatory Karl-Schwarzschild-Str. 2 D-85748 Garching bei München, Germany phone: +49 89 320 06 532 fax: +49 89 320 2362	Hans-Walter Rix Max-Planck-Institut für Astrophysik Karl-Schwarzschild-Str. 1 D-85748 Garching bei München, Germany phone: +49 89 3299 323 fax: +49 89 3299 3295
--	---

The Role of Dust in the Formation of Stars

ESO, Garching, September 11–14, 1995

To keep the VLT observatory and its scientific instrumentation in phase with the evolution of astronomical research, ESO is organizing selected workshops dedicated to specialized fields of current research. The objective of this workshop is to have an exchange between observers, experimentalists and theoreticians. The discussion shall encompass the status of observations and observational techniques, laboratory experiments and theoretical research with emphasis on what observations are needed for the future to test predictions and to constrain models.

Among topics to be covered are:

- a short presentation of the VLT project
- Present observations of YSO
- Properties of dust around YSO
- Processing of dust in YSO
- Models (e.g. synthetic spectra or evolutionary scenarios)
- Dust as a catalytic agent for star formation

Scientific organization: Rolf Chini and Endrik Krügel (MPIfR, Bonn), Thomas Henning (MPG-AG Dust and Star Formation, Jena), John Mathis (Univ. Wisconsin, Madison), Antonella Natta (Oss. Astronomico Arcetri), Jean-Loup Puget (IAS, Orsay), Alexander Tielens (NASA Ames, Moffet Field), Nikolai Voshchinnikov (Astronomical Institute, St. Petersburg)

The workshop will be **organized locally** by: Hans Ulrich Käuffel (ESO, Garching) and Ralf Siebenmorgen (ESA/ESTEC, Noordwijk)

Pre-registration by: December 31, 1994

All information about this workshop is available via [www http://http.hq.eso.org/stardust.html](http://http.hq.eso.org/stardust.html)

or using the *finger* command
`finger stardust@mc6.hq.eso.org`

ESO/ST-ECF Workshop Calibrating and Understanding HST and ESO Instruments

ESO, Garching, April 26–28, 1995

Space and Ground-based Observatories have followed different approaches to the problem of monitoring, calibrating and understanding their Scientific Instruments. However, with the increasing complexity of the new Ground-based Instrumentation, this cultural and operational gap is gradually disappearing. This Workshop, starting from a review of the level and effectiveness of the calibration procedures which are currently adopted by the refurbished HST and by the ESO main Instruments, is aimed at highlighting the remaining differences and will provide guidelines for the development of operational procedures and software tools to be used in the VLT era. The core programme will include invited reviews followed by round-table discussions; a limited number of contributed papers/posters will also be selected.

Main Topics:

- HST Instruments after the M&R Mission
- ESO/La Silla Instruments
- VLT and VLTI Instruments
- Current and Future Major Observatories
- Software Environments

Scientific Organizing Committee: D. Baade (ESO), P. Benvenuti (ESO/ST-ECF), J. Bergeron (ESO), S. D'Odorico (ESO), K. Freeman (MSSSO), P. Grosbøl (ESO), H. Hensberge (Koninklijke Sterrenwacht van België), M. Mountain (NOAO), M. Rosa (ST-ECF), E. Schreier (ST Scl) H. Schwarz, (ESO Chile), J. Spyromilio (ESO), J. Wampler (ESO).

Local Organizing Committee: P. Benvenuti, R. Gilmozzi, F. Murtagh, M. Péron, B. Sjöberg, J. Spyromilio.

Further information:

WWW URL <http://http.hq.eso.org/calconf.html>

Contact address: Britt Sjöberg, European Southern Observatory, Karl-Schwarzschild-Str. 2, D-85748 Garching, Germany

Tel.: +49-89-32006-291; Fax: +49-89-32006-480;
E-mail: calconf@eso.org

Registration deadline: March 3, 1995

Registration fee: DM 80.00 payable at the workshop. The fee includes a free copy of the Proceedings published by ESO.

New ESO Scientific Preprints

October–December 1994

1037. G. Mathys: Spectropolarimetry of Magnetic Stars. III. Measurement Uncertainties. — IV. The Crossover Effect. — V. The Mean Quadratic Magnetic Field. *Astronomy and Astrophysics*.
1038. R.L.M. Corradi and H.E. Schwarz: Morphological Populations of Planetary Nebulae: Which Progenitors? I. Comparative Properties of Bipolar Nebulae. *Astronomy and Astrophysics*.
1039. G. Mathys and S. Hubrig: Magnetic Fields of the HgMn Spectroscopic Binaries χ Lup and 74 Aqr. *Astronomy and Astrophysics*.
1040. A.A. Zijlstra: Stellar Evolution and Mass Loss on the Asymptotic Giant Branch. Review talk given at Edinburgh, September 1994, "Circumstellar Matter".
1041. X.-W. Liu, M.J. Barlow, I.J. Danziger and R.E.S. Clegg: Neutral Carbon Far-Red Forbidden Line Emission from Planetary Nebulae. *M.N.R.A.S.*
1042. D. Maccagni, B. Garilli and M. Tarenghi: The Complex Structure of Abell 2151 (Hercules). *The Astronomical Journal*.

VACANCY AT LA SILLA

Staff Astronomer

A position as staff astronomer will become available at La Silla in the middle of 1995. The position is open to experienced observational astronomers with a Ph.D degree or equivalent and several years of post-doctoral experience in the area of CCD imaging and low-dispersion spectroscopy.

Astronomers at ESO in Chile are required to spend 50% of their time doing support activities and 50% of their time on research. A strong background of independent research is an essential requirement. Every three weeks ESO astronomers spend one week at La Silla doing functional work, followed by one week of compensatory leave, and then one week doing research at ESO's Institute of Astronomy at Vitacura in Santiago. ESO astronomers are based in Santiago.

The successful candidate will be responsible for the EFOSC instruments at La Silla, and is therefore expected to have knowledge and interests in CCD's and their calibration, and CCD photometry and low-dispersion grism spectroscopy. The functional work includes

- introducing visitors to the use of the instruments
- writing and updating User's Manuals
- interacting with the technical staff on modifications and updates of the instrumentation.

Staff posts are normally offered for an initial period of 3 years and may be renewed for a second period of 3 years.

Applications should be submitted to ESO **not later than March 15, 1995**. Applicants will be notified by June 1, 1995. The ESO Application Form should be used and be accompanied by a list of publications. In addition, three letters of recommendation from persons familiar with the scientific work of the applicant should be sent directly to ESO. These letters should reach ESO **not later than March 15, 1995**.

The research interests of the members of the staff in the Astronomy Support Department at La Silla include low-mass star formation, chemistry of molecular clouds, high-resolution spectroscopy of cool stars, supernovae and their remnants, the distance scale, compact groups of galaxies, and observational cosmology. Staff members and senior fellows act as co-supervisors for students of European universities who spend up to 2 years on La Silla working towards a doctoral dissertation. The staff of the Astronomy Support Department consists of about 20 astronomers including staff, post-doctoral fellows, and students. Most of the ESO scientists are from the member states of ESO (Belgium, Denmark, Germany, France, Italy, the Netherlands, Sweden and Switzerland), but several are from other countries. The research facilities at La Silla consist of 12 telescopes, including the SEST 15-m submillimetre antenna, and the 3.5-m New Technology Telescope. There are ample computing facilities in Vitacura including a number of networked SUN workstations, running MIDAS, IRAF, Supermongo, etc.

Enquiries, requests for application forms and applications should be addressed to:

European Southern Observatory
Personnel Department
Karl-Schwarzschild-Strasse 2
D-85748 Garching bei München, Germany

1043. W. Freudling: An Image Restoration Technique for the Removal of Cosmic Ray Hits from Dithered Images. *P.A.S.P.*
1044. H. Kjeldsen, T.R. Bedding, M. Viskum and S. Frandsen: Solar-Like Oscillations in η Boo. *The Astronomical Journal*.
1045. E.J. Wampler, N.N. Chugai and P. Petitjean: The Absorption Spectrum of Nuclear Gas in Q0059-2735. *Astrophysical Journal*.
1046. G. Mathys and T. Lanz: Magnetic Splitting and Identification of Spectral Lines in Ap Stars. To be published in the Proc. of the Workshop "Laboratory and High Resolution Spectra" (Brussels, Aug. 29 - Sept. 2, 1994). Eds. A.J. Sauval, R. Blomme, N. Grevesse. *Astron. Soc. Pacific Conf. Series*.
1047. W. Freudling et al.: Gas Around β Pictoris: An Upper Limit on the HI Content. *Astronomy and Astrophysics*.
1048. D. Minniti, E. Olszewski and M. Rieke: IR Photometry of M33. In Proc. of the 3rd ESO/CTIO Workshop on "The Local Group Galaxies". Eds. A. Layden and J. Storm, in press.
D. Minniti and T.R. Bedding: Resolving Distant Galaxies Into Stars. In Proc. of the ESO Workshop on "Science with the VLT", 1994. Eds. J.R. Walsh and J. Danziger, in press.
A. Zijlstra and D. Minniti: Miras in Nearby Galaxies. In Proc. of the ESO Workshop on "Science with the VLT".
1049. D. Minniti: The Helium Abundance of the Galactic Bulge. In Proc. of ESO/EIPC Workshop on "The Light Element Abundances". Ed. P. Crane, in press.
The Formation of the Galactic Bulge: Clues from Metal-Rich Globular Clusters. In "The Formation of the Milky Way". Eds. E. Alfaro and G. Tenorio-Tagle, in press.
Metallicity, Structure and Kinematics of the Milky Way's Bulge. In IAU Symp. 169 on "Unsolved Problems with the Milky Way". Ed. L. Blitz, in press.

Staff Movements

Arrivals

Europe

AMICO, Paola (I), Fellow
ANDERSEN, Torben (DK), Senior Systems Analyst/Head of System Engineering Group
BELETIC, James (USA), Head of Optical Detector Group
BÖHM, Torsten (D), Fellow
COURBIN, Frédéric (F), Student
DERIE, Frédéric (F), Student
DORN, Peter (D), Laboratory Technician (Photography)
MAYR, Stephanie (D), Junior Analyst
MICHEL, Alain (F), Optical Engineer
MONNET, Guy (F), Senior Astronomer / Physicist-Head of the Instrumentation Division
VAN KESTEREN, Arno (NL), EMC and Electrical Engineer

Chile

GUISARD, Stéphane (F), Optical Engineer
PRIETO, Eric (F), Optical Engineer
STORM, Jesper (DK), Paid Associate (changed from Fellow)

Departures

Europe

BEDDING, Timothy (Aus), Fellow
GERBIER, Alain (F), Mechanical Engineer
TINNEY, Christopher (Aus), Fellow

SUBJECT INDEX

Organizational Matters

- R. Giacconi*: Message from the Director General – Summary of a Report to the ESO Staff **76**, 1
R. Giacconi: Latest Developments Around Paranal **77**, 1
R. Giacconi: Current Status of ESO – Speech to the Staff at the ESO Garching Headquarters on December 6, 1994 **78**, 1
J. Andersen: Science on la Silla in the VLT Era **78**, 3

Telescopes and Instrumentation

- D. Baade, E. Giraud, P. Gilton, P. Graves, D. Gojak, G. Mathys, R. Rojas, J. Storm and A. Wallander*: Re-invigorating the NTT as a New Technology Telescope **75**, 1
M. Quattri: VLT Main Structure Design **75**, 5
M. Tarenghi: Beginning of Construction **75**, 5
P. Giordano: A New Approach for the In-Situ Cleaning of VLT Mirrors: the Peel-Off Technique **75**, 7
P. Giordano and A. Torrejon: In-Situ Cleaning of the NTT Main Mirror by CO₂ Snow-Flake Sweeping **75**, 9
D. Enard: Work Starts on the VLT M2 Units **76**, 2
B. Koehler: Hunting the Bad Vibes at Paranal **76**, 4
H. Zodet: Recent Photographs of Paranal **76**, 10
M. Sarazin: Site Surveys, from Pioneering Times to the VLT Era **76**, 12
M. Sarazin: Seeing Update: La Silla Back on the Track **76**, 13
S. D'Odorico: A F/5.2 Camera with a Thinned 2048² CCD at the EMMI Red Arm **76**, 15
H. Dekker, S. D'Odorico and A. Fontana: Test of an R4 Echelle Mosaic **76**, 16
J. Melnick: News from La Silla **76**, 20
The NTT Team: NTT – Bits & Pixels **76**, 21
M. Tarenghi: VLT Progress Report **77**, 2
L. Pasquini, J. Storm and H. Dekker: A New High-Resolution Holographic Grating for the Blue Arm of EMMI **77**, 5
C.M. de Oliveira, A. Gilliotte and R. Tighe: New Holographic Grating for the B&C on the ESO 1.52-m Telescope **77**, 6
A. Moorwood, G. Finger and H. Gemperlein: Test of the Upgraded IRAC1 Camera for 1–5 μm Imaging **77**, 8
The NTT Team: NTT – Bits & Pixels **77**, 11
J. Melnick: Additional News from ESO-Chile **77**, 12
H.U. Käuffl: N-Band Long-Slit Grism Spectroscopy with TIMMI at the 3.6-m Telescope **78**, 4
The NTT Team: NTT – Bits & Pixels **78**, 7

Science with the VLT

- T. Encrenaz*: Observation of Solar-System Objects with the VLT **75**, 12

- A.-M. Lagrange*: Studies of Disks Around Main-Sequence Stars with the VLT **76**, 23
F. Fusi Pecci, C. Cacciari, F.R. Ferraro, R. Gratton and L. Origlia: Globular Clusters with the VLT **77**, 14
B. Théodore, P. Petitjean and N. Hubin: Scientific Capabilities of the VLT Adaptive Optics System **77**, 20
D. Dravins: Astrophysics on Its Shortest Timescales **78**, 9

SL-9/Jupiter Encounter – Special

- R.M. West*: Comet Shoemaker-Levy 9 Collides with Jupiter – the Continuation of a Unique Experience **77**, 28
G. Chernova and K. Jockers: Imaging of Comet SL-9 in the Gunn Photometric System **77**, 32
R.M. West and O. Hainaut: Predicting the Impacts **77**, 33
H. Barwig and O. Bärbantner: Searching for SL-9 Light Echoes – a Challenge for High-Speed Multi-Channel Photometry **77**, 34
K. Jockers: Near-Infrared Imaging of Comet SL-9 and Jupiter's Atmosphere **77**, 35
H.U. Käuffl: Imaging of the Signatures of the Impact Events in the Thermal Infrared **77**, 37
Th. Encrenaz, R. Schulz, J.A. Stuewe, G. Wiedemann, P. Drossart and J. Crovisier: Near-IR Spectroscopy of Jupiter at the Times of SL-9 Impact Using NTT-IRSPEC: Emissions of CH₄, H₃⁺ and H₂ **77**, 40
N. Thomas, L. Jorda and B. Sicardy: CCD Imaging of Jupiter During the Comet Shoemaker-Levy 9 Impact Using the Danish 1.54-m Telescope at ESO **77**, 42
R. Schulz, Th. Encrenaz, J.A. Stüwe and G. Wiedemann: The Distribution of Near-IR Emissions in the Jovian Stratosphere Caused by the SL-9 Impact **77**, 44
B. Mosser: Jovian Quakes **77**, 46
F. Murtagh and M. Fendt: The SL-9/ESO Web Encounter **77**, 47
R. Albrecht: The Comet, Jupiter, and Everything: SL-9 and the Media – a Strictly Personal Impression **77**, 47

Reports from Observers

- R. Genzel, A. Eckart, R. Hofmann, A. Quirrenbach, B. Sams and L. Tacconi-Garman*: High-Resolution NIR Imaging of Galactic Nuclei **75**, 17
L. Origlia, A.F.M. Moorwood and E. Oliva: Infrared Spectroscopy of Galactic Globular Clusters **75**, 21
L.-F. Wang and E.J. Wampler: New NTT Images of SN 1987 A **75**, 22
P.O. Lagage and E. Pantin: Probing Dust Around Main-Sequence Stars with Timmi **75**, 24

- S. Ortolani, E. Bica and B. Barbuy*: NTT Observations of Obscured Globular Clusters **75**, 26
L. Reduzzi, R. Rampazzo, J.W. Sulentic and P. Prugniel: Fine Structure in the Early-Type Components in Mixed Pairs of Galaxies **75**, 28
J.L. Beuzit, B. Brandl, M. Combes, A. Eckart, M. Faucherre, M. Heydari-Malayeri, N. Hubin, O. Lai, P. Léna, C. Perrier, G. Perrin, A. Quirrenbach, D. Rouan, B. Sams and P. Thébault: Contributions of the ESO Adaptive Optics Programme to Astronomy: a First Review **75**, 33
A. Vallenari, G. Bertelli, C. Chiosi and S. Ortolani: The History of Star Formation in the Large Magellanic Cloud **76**, 30
R. Mignani, P.A. Caraveo and G.F. Bignami: Geminga, 10 Years of Optical Observations **76**, 32
M. Shaw, C. Tadhunter, N. Clark, R. Dickson, R. Morganti, R. Fosbury and R. Hook: Jet/Cloud Interactions in Southern Radio Galaxies? **76**, 34
P.E. Nissen, D.L. Lambert and V.V. Smith: The Lithium Isotope Ratio in Metal-Poor Stars **76**, 36
M. Arnaboldi, K.C. Freeman, X. Hui, M. Cappacioli and H. Ford: The Kinematics of the Planetary Nebulae in the Outer Regions of NGC 1399 **76**, 40
F. Font, D. Queloz, M. Mayor and G. Burki: Milky Way Rotation from Cepheids **76**, 45
M. Srinivasan Sahu and A. Blaauw: Interstellar Na I Absorption Towards Stars in the Region of the IRAS Vela Shell **76**, 48
M. Kürster, A.P. Hatzes, W.D. Cochran, C.E. Pulliam, K. Dennerl and S. Döbereiner: A Radial Velocity Search for Extra-Solar Planets Using an Iodine Gas Absorption Cell at the CAT + CES **76**, 51
R. Falomo: High-Resolution Imaging of the Active Galaxy PKS 0521-365 and its Optical Jet **77**, 49
R. Gredel: Molecular Hydrogen Observations Towards Herbig-Haro Objects **77**, 52
P. Saracco, A. Iovino, G. Chincarini, B. Garilli and D. Maccagni: Towards a Deep IR ESO Sample **77**, 55
A. Marconi, A.F.M. Moorwood, L. Origlia and E. Oliva: A Prominent Ionization Cone and Starburst Ring in the Nearby Circinus Galaxy **78**, 20
M. Pierre, R. Hunstead, A. Reid, G. Robertson, Y. Mellier, G. Soucail, H. Böhringer, H. Ebeling, W. Voges, C. Cesarsky, J. Oukbir, J.-L. Sauvageot and L. Vigroux: Multi-Wavelength Study of ROSAT Clusters of Galaxies **78**, 24
M. Tarenghi: The VLT Site at Paranal: September 1994 **78**, 27
R. Falomo and J.E. Pesce: The Cluster Environment of BL Lac Objects **78**, 30
E. Tessier, J. Bouvier, J.-L. Beuzit and W. Brandner: COME-ON+ Adaptive Optics Images on the Pre-Main Sequence Binary NX Pup **78**, 35

P. Andreani, H. Böhringer, R. Booth, G. Dall'Oglio, L.-A. Nyman, L. Pizzo, P. Shaver and N. Whyborn: Observations of the Zeldovich Effect Towards ROSAT Clusters with SEST and the Italian Double-Channel Photometer **78, 41**

Other Astronomical News

P. Benvenuti: The New Data Management Division at ESO **75, 38**
U. Michold: The ESO Library Information System **75, 39**
J. Breysacher: The New ESO Observing Programmes Committee **75, 43**
C. Césarsky, J. Breysacher and R. Kudritzki: Meeting on Key Programmes **75, 45**
Science Data Analysis Group: The 94May Release of ESO-MIDAS **76, 56**
The ESO Web Consortium: ESO's New On-Line Information System **76, 56**
P. Crane and J. Faulkner: The Light Element Abundances – a Light Review of the Recent ESO/EIPC Workshop **76, 58**
R.M. West: Shoemaker-Levy 9/Jupiter Collision to be Observed at ESO **76, 59**
M. Véron and E.J. Wampler: The 4th ESO/OHP Summer School – Two Weeks in

Provence; Stars, Comets, Good Food and Warm Hospitality **77, 58**
H.-M. Adorf, D. Egret, A. Heck, R. Jackson, A. Koekemoer, F. Murtagh and D. Wells: The AstroWeb Database of Internet Resources **78, 44**
M. Pierre: Producing Multi-Wavelength Overlays with MIDAS **78, 46**
Science Data Analysis Group: The 94NOV Release of ESO-MIDAS **78, 48**

Announcements

Council and Committee Members in 1994 **75, 48**
Time-Table of Council Sessions and Committee Meetings **75, 48**
Observing Programmes Approved for Period 53 **75, 48**
Postdoctoral Fellowship on La Silla **77, 54**
Announcement of ESO Workshop on "Science with the VLT" **75, 54**
Announcement of ESO Workshop on "QSO Absorption Lines" **75, 54**
New ESO Publications (December 1993–February 1994) **75, 54**
Staff Movement **75, 56**
S.R. Pottasch: Adriaan Blaauw at 80 **76, 62**
ESO Studentship Programme **76, 64**

ESO Fellowships **76, 64**
Studentships at La Silla **76, 64**
Fellowships at La Silla **76, 64**
Senior Visitor Programme at La Silla **76, 65**
New ESO Preprints (March–June 1994) **76, 65**
Announcement of ESO Workshop on "QSO Absorption Lines" **76, 65**
Staff Movements **76, 66**
F. Palma: Written-Off Items Available at ESO Headquarters **76, 66**
Observing Programmes Approved for Period 54 **77, 61**
LISA II – Library and Information Services in Astronomy II **77, 66**
Staff Movements **77, 66**
New ESO Publications (July–September 1994) **77, 67**
European SL-9/Jupiter Workshop **78, 50**
ESO/MPA Workshop on "Spiral Galaxies in the Near-IR" **78, 51**
Workshop on "The Role of Dust in the Formation of Stars" **78, 51**
ESO/ST-ECF Workshop on "Calibrating and Understanding HST and ESO Instruments" **78, 51**
New ESO Scientific Preprints (October–November 1994) **78, 51**
Staff Movements **78, 52**

AUTHOR INDEX

A

Adorf H.-M., D. Egret, A. Heck, R. Jackson, A. Koekemoer, F. Murtagh and D. Wells: The AstroWeb Database of Internet Resources **78, 44**
Albrecht R.: The Comet, Jupiter, and Everything: SL-9 and the Media – a Strictly Personal Impression **77, 47**
Andersen, J.: Science on La Silla in the VLT Era **78, 3**
Andreani P., H. Böhringer, R. Booth, G. Dall'Oglio, L.-A. Nyman, L. Pizzo, P. Shaver and N. Whyborn: Observations of the Sunyaev-Zeldovich Effect Towards ROSAT Clusters with SEST and the Italian Double-Channel Photometer **78, 41**
Arnaboldi M., K.C. Freeman, X. Hui, M. Cappacioli and H. Ford: The Kinematics of the Planetary Nebulae in the Outer Regions of NGC 1399 **76, 40**

B

Baade D., E. Giraud, P. Gitton, P. Glaves, D. Gojak, G. Mathys, R. Rojas, J. Storm and A. Wallander: Re-invigorating the NTT as a New Technology Telescope **75, 1**
Barwig H. and O. Bärbantner: Searching for SL-9 Light Echoes – a Challenge for High-Speed Multi-Channel Photometry **77, 34**
Benvenuti P.: The New Data Management Division at ESO **75, 38**
Beuzit J.L., B. Brandl, M. Combes, A. Eckart, M. Faucherre, M. Heydari-Malayeri, N. Hubin, O. Lai, P. Léna, C. Perrier, Perrin G.,

A. Quirrenbach, D. Rouan, B. Sams and P. Thébaud: Contributions of the ESO Adaptive Optics Programme to Astronomy: a First Review **75, 33**
Breysacher J.: The New ESO Observing Programmes Committee **75, 43**

C

Césarsky C., J. Breysacher and R. Kudritzki: Meeting on Key Programmes **75, 45**
Chernova G. and K. Jockers: Imaging of Comet SL-9 in the Gunn Photometric System **77, 32**
Crane P. and J. Faulkner: The Light Element Abundances – a Light Review of the Recent ESO/EIPC Workshop **76, 58**

D

D'Odorico S.: A F/5.2 Camera with a Thinned 2048² CCD at the EMMI Red Arm **76, 15**
Dekker H., S. D'Odorico and A. Fontana: Test of an R4 Echelle Mosaic **76, 16**
de Oliveira C.M., A. Gilliotte and R. Tighe: New Holographic Grating for the B&C on the ESO 1.52-m Telescope **77, 6**
Dravins D.: Astrophysics on Its Shortest Timescales **78, 9**

E

Enard D.: Work Starts on the VLT M2 Units **76, 2**
Encrenaz Th.: Observation of Solar-System Objects with the VLT **75, 12**

Encrenaz Th., R. Schulz, J.A. Stuewe, G. Wiedemann, P. Drossart and Crovisier J.: Near-IR Spectroscopy of Jupiter at the Times of SL-9 Impact Using NTT-IRSPEC: Emissions of CH₄, H₃⁺ and H₂ **77, 40**

F

Falomo R.: High-Resolution Imaging of the Active Galaxy PKS 0521-365 and its Optical Jet **77, 49**
Falomo R. and J.E. Pesce: The Cluster Environment of BL Lac Objects **78, 30**
Font F., D. Queloz, M. Mayor and G. Burki: Milky Way Rotation from Cepheids **76, 45**
Fusi Pecci F., C. Cacciari, F.R. Ferraro, R. Gratton and L. Origlia: Globular Clusters with the VLT **77, 14**

G

Genzel R., A. Eckart, R. Hofmann, A. Quirrenbach, B. Sams and L. Tacconi-Garman: High-Resolution NIR Imaging of Galactic Nuclei **75, 17**
Giacconi R.: Message from the Director General – Summary of a Report to the ESO Staff **76, 1**
Giacconi R.: Latest Developments Around Paranal **77, 1**
Giacconi R.: Current Status of ESO – Speech to the Staff at the ESO Garching Headquarters on December 6, 1994 **78, 1**
Giordano P.: A New Approach for the In-Situ Cleaning of VLT Mirrors: the Peel-Off Technique **75, 7**

- Giordano P. and A. Torrejon*: In-Situ Cleaning of the NTT Main Mirror by CO₂ Snow-Flake Sweeping **75**, 9
Greidel R.: Molecular Hydrogen Observations Towards Herbig-Haro Objects **77**, 52

J

- Jockers K.*: Near-Infrared Imaging of Comet SL-9 and Jupiter's Atmosphere **77**, 35

K

- Käuffl H.U.*: Imaging of the Signatures of the Impact Events in the Thermal Infrared **77**, 37
Käuffl H.U.: N-Band Long-Slit Grism Spectroscopy with TIMMI at the 3.6-m Telescope **78**, 4
Koehler B.: Hunting the Bad Vibes at Paranal! **76**, 4
Kürster M., A.P. Hatzes, W.D. Cochran, C.E. Pulliam, K. Dennerl and S. Döbereiner: A Radial Velocity Search for Extra-Solar Planets Using an Iodine Gas Absorption Cell at the CAT + CES **76**, 51

L

- Lagage P.O. and E. Pantin*: Probing Dust Around Main-Sequence Stars with Timmi **75**, 24
Lagrange A.-M.: Studies of Disks Around Main-Sequence Stars with the VLT **76**, 23

M

- A. Marconi, A.F.M. Moorwood, L. Origlia and E. Oliva*: A Prominent Ionization Cone and Starburst Ring in the Nearby Circinus Galaxy **78**, 20
Melnick J.: News from La Silla **76**, 20
Melnick J.: Additional News from ESO-Chile **77**, 12
Michold U.: The ESO Library Information System **75**, 39
Mignani R., P.A. Caraveo and G.F. Bignami: Geminga, 10 Years of Optical Observations **76**, 32
Moorwood A., G. Finger and H. Gemperlein: Test of the Upgraded IRAC1 Camera for 1–5 μ m Imaging **77**, 8
Mosser B.: Jovian Quakes **77**, 46
Murtagh F. and M. Fendt: The SL-9/ESO Web Encounter **77**, 47

N

- Nissen P.E., D.L. Lambert and V.V. Smith*: The Lithium Isotope Ratio in Metal-Poor Stars **76**, 36

O

- Origlia L., A.F.M. Moorwood and E. Oliva*: Infrared Spectroscopy of Galactic Globular Clusters **75**, 21
Ortolani S., E. Bica and B. Barbuy: NTT Observations of Obscured Globular Clusters **75**, 26

P

- Palma F.*: Written-Off Items Available at ESO Headquarters **76**, 66
Pasquini L., J. Storm and H. Dekker: A New High-Resolution Holographic Grating for the Blue Arm of EMMI **77**, 5
Pierre M., R. Hunstead, A. Reid, G. Robertson, Y. Mellier, G. Soucail, H. Böhringer, H. Ebeling, W. Voges, C. Cesarsky, J. Oukbir, J.-L. Sauvageot and L. Vigroux: Multi-Wavelength Study of ROSAT Clusters of Galaxies **78**, 24
Pierre M.: Producing Multi-Wavelength Overlays with MIDAS **78**, 46
Pont F., D. Queloz, M. Mayor and G. Burki: Milky Way Rotation from Cepheids **76**, 45
Pottasch S.R.: Adriaan Blaauw at 80 **76**, 62

Q

- Quattri M.*: VLT Main Structure Design **75**, 5

R

- Reduzzi L., R. Rampazzo, J.W. Sulentic and P. Prugniel*: Fine Structure in the Early-Type Components in Mixed Pairs of Galaxies **75**, 28

S

- Saracco P., A. Iovino, G. Chincarini, B. Garilli and D. Maccagni*: Towards a Deep IR ESO Sample **77**, 55
Sarazin M.: Site Surveys, from Pioneering Times to the VLT Era **76**, 12
Sarazin M.: Seeing Update: La Silla Back on the Track **76**, 13
Schulz R., Th. Encrenaz, J.A. Stüwe and G. Wiedemann: The Distribution of Near-

IR Emissions in the Jovian Stratosphere Caused by the SL-9 Impact **77**, 44

- Shaw M., C. Tadhunter, N. Clark, R. Dickson, R. Morganti, R. Fosbury and R. Hook*: Jet/Cloud Interactions in Southern Radio Galaxies? **76**, 34

Srinivasan Sahu M. and A. Blaauw: Interstellar Na I Absorption Towards Stars in the Region of the IRAS Vela Shell **76**, 48

T

- Tarengi M.*: Beginning of Construction **75**, 5
Tarengi M.: VLT Progress Report **77**, 2
Tarengi M.: The VLT Site at Paranal: September 1994 **78**, 27
Tessier E., J. Bouvier, J.-L. Beuzit and W. Brandner: COME-ON+ Adaptive Optics Images of the Pre-Main Sequence Binary NX Pub **78**, 35
Théodore B., P. Petitjean and N. Hubin: Scientific Capabilities of the VLT Adaptive Optics System **77**, 20
Thomas N., L. Jorda and B. Sicardy: CCD Imaging of Jupiter During the Comet Shoemaker-Levy 9 Impact Using the Danish 1.54-m Telescope at ESO **77**, 42

V

- Vallenari A., G. Bertelli, C. Chiosi and S. Ortolani*: The History of Star Formation in the Large Magellanic Cloud **76**, 30
Véron M. and E.J. Wampler: The 4th ESO/OHP Summer School – Two Weeks in Provence; Stars, Comets, Good Food and Warm Hospitality **77**, 58

W

- Wang L.-F. and E.J. Wampler*: New NTT Images of SN 1987 A **75**, 22
West R.M.: Shoemaker-Levy 9/Jupiter Collision to be Observed at ESO **76**, 59
West R.M.: Comet Shoemaker-Levy 9 Collides with Jupiter – the Continuation of a Unique Experience **77**, 28
West R.M. and O. Hainaut: Predicting the Impacts **77**, 33

Z

- H. Zodet*: Recent Photographs of Paranal **76**, 10

ESO, the European Southern Observatory, was created in 1962 to . . . establish and operate an astronomical observatory in the southern hemisphere, equipped with powerful instruments, with the aim of furthering and organizing collaboration in astronomy . . . It is supported by eight countries: Belgium, Denmark, France, Germany, Italy, the Netherlands, Sweden and Switzerland. It operates the La Silla observatory in the Atacama desert, 600 km north of Santiago de Chile, at 2,400 m altitude, where fourteen optical telescopes with diameters up to 3.6 m and a 15-m sub-millimetre radio telescope (SEST) are now in operation. The 3.5-m New Technology Telescope (NTT) became operational in 1990, and a giant telescope (VLT=Very Large Telescope), consisting of four 8-m telescopes (equivalent aperture = 16 m) is under construction. It will be erected on Paranal, a 2,600 m high mountain in northern Chile, approximately 130 km south of the city of Antofagasta. Eight hundred scientists make proposals each year for the use of the telescopes at La Silla. The ESO Headquarters are located in Garching, near Munich, Germany. It is the scientific-technical and administrative centre of ESO where technical development programmes are carried out to provide the La Silla observatory with the most advanced instruments. There are also extensive facilities which enable the scientists to analyze their data. In Europe ESO employs about 200 international Staff members, Fellows and Associates; at La Silla about 50 and, in addition, 150 local Staff members.

The ESO MESSENGER is published four times a year: normally in March, June, September and December. ESO also publishes Conference Proceedings, Preprints, Technical Notes and other material connected to its activities. Press Releases inform the media about particular events. For further information, contact the ESO Information Service at the following address:

EUROPEAN
SOUTHERN OBSERVATORY
Karl-Schwarzschild-Str. 2
D-85748 Garching bei München
Germany
Tel. (089) 32006-0
Telex 5-28282-0 eo d
Telefax: (089) 3202362
ips@eso.org (internet)
ESO::IPS (decnet)

The ESO Messenger:
Editor: Marie-Hélène Ulrich
Technical editor: Kurt Kjær

Printed by Universitäts-Druckerei
Dr. C. Wolf & Sohn
Heidemannstraße 166
80939 München 45
Germany

ISSN 0722-6691

Contents

R. Giacconi: Current Status of ESO – Speech to the Staff at the ESO Garching Headquarters on December 6, 1994	1
J. Andersen: Science on La Silla in the VLT Era	3

TELESCOPES AND INSTRUMENTATION

H.U. Käuffl: N-Band Long-Slit Grism Spectroscopy with TIMMI at the 3.6-m Telescope	4
NTT Bits and Pixels	7

SCIENCE WITH THE VLT

D. Dravins: Astrophysics on Its Shortest Timescales	9
---	---

REPORTS FROM OBSERVERS

A. Marconi, A.F.M. Moorwood, L. Origlia and E. Oliva: A Prominent Ionization Cone and Starburst Ring in the Nearby Circinus Galaxy	20
M. Pierre, R. Hunstead, A. Reid, G. Robertson, Y. Mellier, G. Soucail, H. Böhringer, H. Ebeling, W. Voges, C. Cesarsky, J. Oukbir, J.-L. Sauvageot and L. Vigroux: Multi-Wavelength Study of ROSAT Clusters of Galaxies	24
M. Tareghi: The VLT Site at Paranal: September 1994	27
R. Falomo and J.E. Pesce: The Cluster Environment of BL Lac Objects	30
E. Tessier, J. Bouvier, J.-L. Beuzit and W. Brandner: COME-ON+ Adaptive Optics Images of the Pre-Main Sequence Binary NX Pup	35
P. Andreani, H. Böhringer, R. Booth, G. Dall'Oglio, L.-A. Nyman, L. Pizzo, P. Shaver and N. Whyborn: Observations of the Sunyaev-Zeldovich Effect Towards ROSAT Clusters with SEST and the Italian Double-Channel Photometer	41

OTHER ASTRONOMICAL NEWS

H.-M. Adorf, D. Egret, A. Heck, R. Jackson, A. Koekemoer, F. Murtagh and D. Wells: The AstroWeb Database of Internet Resources	44
M. Pierre: Producing Multi-Wavelength Overlays with MIDAS	46
Science Data Analysis Group: The 94NOV Release of ESO-MIDAS	48

ANNOUNCEMENTS

European SL-9/Jupiter Workshop	50
ESO/MPA Workshop on "Spiral Galaxies in the Near-IR"	51
Workshop on "The Role of Dust in the Formation of Stars"	51
ESO/ST-ECF Workshop on "Calibrating and Understanding HST and ESO Instruments	51
New ESO Scientific Preprints (October–November 1994)	51
Staff Movements	52

MESSENGER INDEX 1994 (Nos. 75–78)	53
---	----